2007

OPTIMIZATION OF A DUAL-MODE SURFACE PLASMON RESONANCE SENSOR

Prasanth Bathae Kumaresh

University of Kentucky, prasanth.bk@gmail.com

ABSTRACT OF THESIS

OPTIMIZATION OF A DUAL-MODE SURFACE PLASMON RESONANCE SENSOR

Surface plasmon waves are TM polarized charge density waves that propagate at the interface of two media with real dielectric constants of opposite sign (i.e. liquid dielectric and certain metals). Surface plasmon resonance (SPR) sensors use these waves to detect refractive index changes adjacent to the metal layer. Refractive index changes arise from the binding of an analyte (e.g. a target molecule, protein, or bacterium) to the functionalized metal layer or from interfering effects such as changes in solution index. Standard, single channel SPR sensors cannot differentiate these two effects as their design allows only one mode to be coupled. This novel self-referencing technique employs two surface plasmon modes to simultaneously measure surface binding and solution refractive index.

Dual surface plasmon modes are achieved by matching the refractive indices on either side of the metal film. The two modes generated - symmetric, long-range surface plasmon (LRSP) and anti-symmetric, short-range surface plasmon (SRSP) - have different field profiles and hence assist in differentiating solution refractive index changes from surface layer formation. Amorphous Teflon, with a refractive index close to water, is chosen as the buffer layer and gold is chosen as the metal layer. Magnesium fluoride, with a higher index than Teflon, is used as the buffer layer when using ethanol as the base solution.

The sensor operation was optimized through simulations to yield higher sensitivity, lower reflectivity and resonances within the spectrometer's range. Optimization results showed good performance over a wide range for Teflon, MgF_2 and gold thicknesses which helped in the fabrication of the sensor. Demonstration of self-referencing operation was done through two different sets of experiments: (1) formation of an alkanethiol self-assembled monolayer on gold in the presence of ethanol and methanol solutions having different refractive indices and (2) streptavidin-biotin binding with solutions of different NaCl concentration and thus different refractive indices. In both these experiments, the resonance wavelengths were accurately predicted, reflectivity varied by 10-15% and sensitivity by 25% from that of the simulated values.

KEYWORDS: Surface Plasmon Resonance, Dual Mode SPR Sensor, Biosensor, Optical sensor, ODT

Prasanth Bathae Kumaresh

Author's Signature

03/20/2007

Date

OPTIMIZATION OF A DUAL-MODE SURFACE PLASMON RESONANCE SENSOR

By

Prasanth Bathae Kumaresh

Dr. Todd Hastings

Director of Thesis

Dr. YuMing Zhang

Director of Graduate Studies

3/20/2007

RULES FOR THE USE OF THESES

Unpublished theses submitted for the Master's degree and deposited in the University of Kentucky Library are as a rule open for inspection, but are to be used only with due regard to the rights of the authors. Bibliographical references may be noted, but quotations or summaries of parts may be published only with the usual scholarly acknowledgements.

Extensive copying or publication of the dissertation in whole or in part also requires the consent of the Dean of the Graduate School of the University of Kentucky.

A library that borrows this project for use by its patrons is expected to secure the signature of each user.

Name Date

_____

_____

_____

_____

_____

_____

THESIS

Prasanth Bathae Kumaresh

The Graduate School

University of Kentucky

2007

OPTIMIZATION OF A DUAL-MODE SURFACE PLASMON RESONANCE SENSOR

THESIS

A thesis submitted in partial fulfillment of the requirements for the degree of Master of Science in the College of Engineering at the University of Kentucky

By

Prasanth Bathae Kumaresh

Lexington, Kentucky

Director: Dr. Todd Hastings, Assistant Professor of Electrical Engineering

Lexington, Kentucky

2007

MASTER'S THESIS RELEASE

Prasanth Bathae Kumaresh

3/20/2007

ACKNOWLEDGMENTS

This thesis would not have been possible without the support of Dr. Todd Hastings. Dr. Todd Hastings provided me with constant guidance to help me complete this thesis work.

I would like to thank

a) Dr. Janet Lumpp and Dr. Laurence Hassebrook for taking time and being in my defense committee.

b) George Spiggle for helping me learn all the processes required in my thesis work.

c) my fellow lab mates for their help throughout my research. Donnie Keathley helped me by designing a flow cell used in this work. My scientific discussions with Jing Guo helped me have a better understanding of the project. Silpa Nagari, Yugu Yang, Harish Srinivasan and Akil Matcheswala helped me in asking interesting questions regarding the project.

d) my parents for their constant support throughout my master's program.

e) Last but not the least; I would like to thank the Almighty for being with me all the time and help me my master's degree.

TABLE OF CONTENTS

TABLE OF FIGURES

TABLE OF TABLES

LIST OF FILES

1. PrasanthBathaeKumaresh_MSThesis.pdf

1 CHAPTER 1 – INTRODUCTION

1.1 Background

Surface plasmon resonance (SPR) has become a widely accepted optical technique for characterizing and quantifying bio-molecular interactions. Ever since the potential of Surface Plasmon Resonance (SPR) for the characterization of thin films [1] and monitoring processes at metal interfaces [2] was recognized, the field of SPR sensing has been growing and receiving constant attention from the scientific community. This largely started with the usage of SPR for gas detection and bio-sensing [3-5] in the early 1980s. Surface plasmon resonance technology has been commercialized by several companies and hence has become a leading technology in the field of direct label-free real-time observation of bio-molecular interactions [6].

SP waves are electron charge-density waves produced at the surface of the metal film under certain specific conditions. When light is passed from a higher refractive index media to a lower refractive index media, part of the light will be reflected and the other part refracted. Above a particular angle, referred to as the "critical angle", entire incident light is totally internally reflected (TIR). When TIR occurs, there exists an evanescent field which has its field intensity exponentially decreasing with its penetration depth in the lower refractive index medium (dielectric). When the TIR surface is coated with a conducting material of a suitable thickness, the TM-polarized incident light can penetrate the metal layer and excite the free electrons in the metal leading to the generation of surface plasmon (SP) waves. This resonant transfer of energy from photons to plasmons, during which both energy and momentum are conserved, is deduced by a reduction in the reflected light. Because of the concentration of the electric field near the metal surface, the conditions for resonance are sensitive to the refractive index changes occurring near the gold surface.

Refractive index can be changed by selective adsorption on the gold layer, which is the index change due to surface binding, referred to as a specific effect. Refractive index near

the metal surface can also be varied by changing the solution flowing on top of the sensor, which is the bulk index change, representing a non-specific effect.

1.2 Conventional SPR sensor

The conventional SPR sensor employs one mode and hence differentiating bulk index changes from surface binding reactions is impossible. Figure 1.1 denotes a single-mode SPR sensor's reflectivity spectrum for a bulk index change of 0.001. Figure 1.2 is the reflectivity spectrum for a single-mode SPR sensor with a surface layer change of 2nm. Figure 1.3 is the overlap of Figure 1.1 and Figure 1.2.

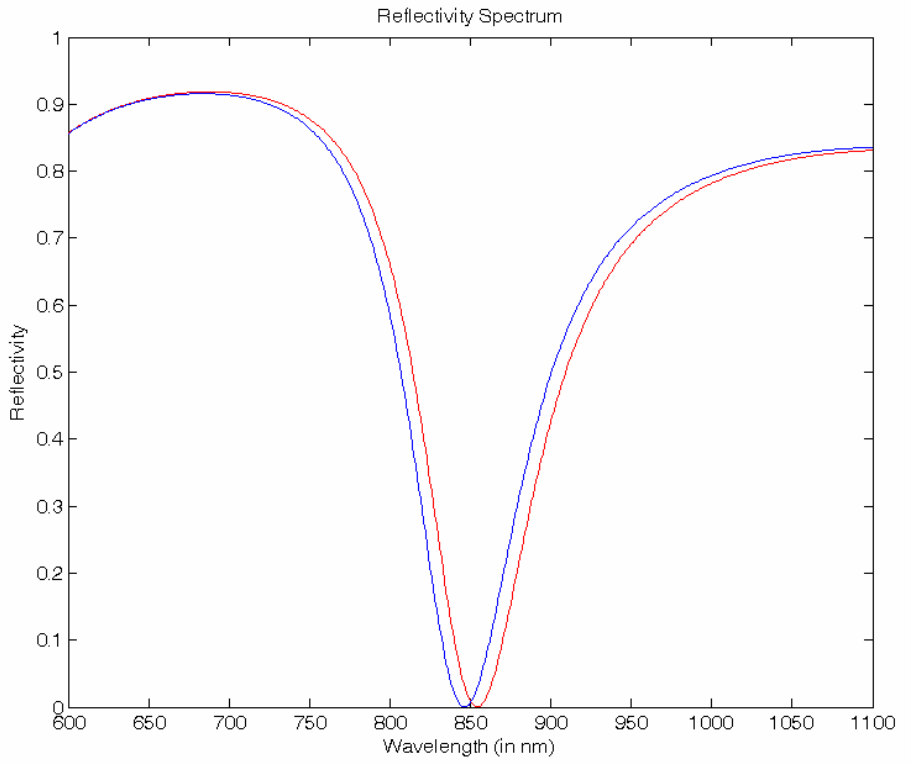

Figure 1.1 Reflectivity spectrum for a single-mode SPR sensor having θ = 65.6° and gold = 50nm using water as the solution . The shift in resonance wavelength due to a bulk index change is shown: blue for n0 and red for n0+0.001

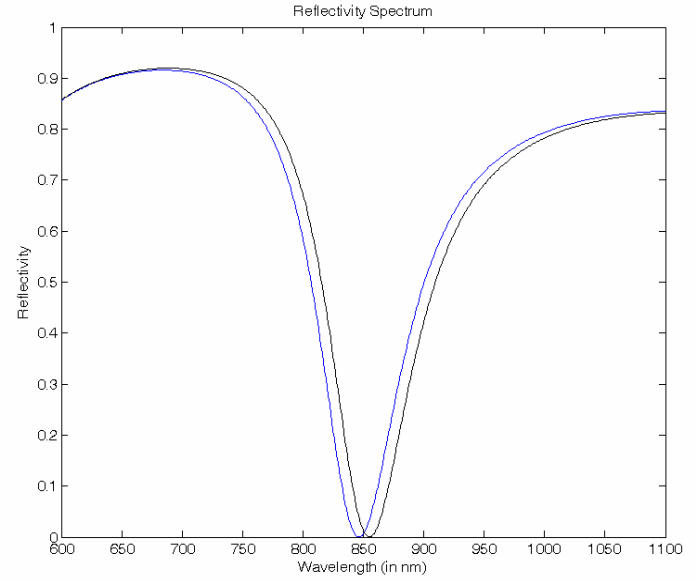

Figure 1.2 Reflectivity spectrum for a single-mode SPR sensor having θ = 65.6° and gold = 50nm using water as the solution. The shift in resonance wavelength for surface layer thickness change is shown - blue for t=0nm and black for t=2nm

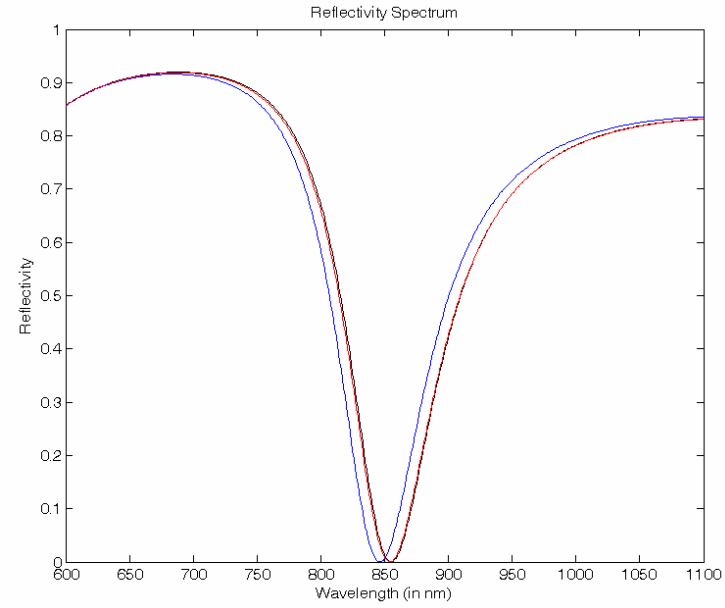

Figure 1.3 Reflectivity spectrum for a single-mode SPR sensor with θ = 65.6° and gold = 50nm using water as the solution. The color of the line indicates the condition for the sensor: blue for n=n0 and t=0nm, red for n=n0+0.001 and t=0nm and black for n=n0 and t=2nm. Note that the formation of a 2nm surface layer cannot be distinguished from a background index change of 0.001.

As seen in Figure 1.3, differentiating between a bulk index change and a surface layer thickness and its associated index changes is not possible. When presented with a spectrum as in Figure 1.1 or Figure 1.2, we cannot conclude whether bulk index change or surface layer index change is responsible for the shift in the resonance wavelength because both changes cause the same amount of shift as indicated in Figure 1.3 . Hence there is a need to differentiate between the two changes.

1.2.1 Different SPR sensor configurations to differentiate bulk and surface changes

Different methods exist to differentiate bulk index changes from surface layer index changes for SPR sensors using wavelength interrogation technique: using multi-channel sensing with WDM [7], A more sophisticated method uses a special light-pipe which excites two surface plasmons with different penetration depths at two different spots on the sensor [8]. Functionalizing one part of the sensor will help to differentiate surface and bulk index changes, though the channels have their responses from different locations. Another method uses multi-channel devices containing sensing channels with bio-molecular recognition elements for sensing and reference channels responding only to non-specific effects [9]. In this method, two separate readouts are needed and both channels are spatially separated. Another effective approach to differentiate the two effects employ a high index dielectric layer covering a part of the sensing area [10]. In this method, the sensing and reference channels are adjacent to one another but there is a spatial separation. When extended to multi-channels, this sensor could also compensate for non-specific binding [11]. Other multi-channel configurations [12, 13] also differentiate between bulk and surface changes. All multi-channel sensors have a spatial difference in their sensing and reference channels where identical conditions cannot be guaranteed. In addition, all previous multi-channel sensors have relied on different surface materials that interact differently with the target analyte. This makes calibration of the sensor particularly difficult.

1.3 Dual mode SPR sensor

Instead of employing different channels and compromising on their spatial separation, we present an alternative method of self referencing. Differentiating two effects can be performed by generating two surface plasmon modes at the same spot [14, 15]. By properly designing the sensor and using a single beam of light, without the usage of a dielectric over layer, we can generate two surface plasmon modes at a single location and optimally change the response of the two modes, long range surface plasmon (LRSP) and short range surface plasmon (SRSP) mode, to differentiate surface binding reactions from bulk index variations.

1.4 Applications of SPR sensors

SPR sensors are used for label-free and dynamic observation of bio-molecular interactions. SPR sensors are used for real-time monitoring of the ligand-analyte (most often antigen - antibody) binding to determine the association and dissociation of the molecules involved. The shift in resonance wavelength is dependent upon the refractive index change and not on the nature of the bio-molecules. The refractive indices for most common target molecules (proteins and nucleic acids) are similar [16]; hence SPR sensors can be used to sense different analytes by appropriate functionalization on the sensor surface. SPR sensors find usage in the areas of environmental protection (e.g. herbicides [17]), biotechnology, medical diagnostics (e.g. DNA [18], hormones [19]), drug screening, food safety (e.g. protein toxins [20], bacteria [21]) and security [7, 22]. Apart from biosensing, SPR sensors are used for chemical sensing [6]. They are also used for the measurement of physical quantities [6] such as displacement [23] and angular position [24] or physical phenomenon such as humidity [25, 26] and temperature [27].

2 CHAPTER 2 - PRINCIPLES OF SPR SENSORS

In the 1960s optical excitation of surface plasmons using attenuated total reflection (ATR) method [28, 29] started the interest in surface plasmon resonance (SPR). Since then SPR and its properties have been extensively studied [30-34] which helped in better understanding and improved usage of SP waves in multitude of applications.

Surface plasmon waves are charge-density waves produced at the interface of materials having real dielectric constants of opposite signs. This condition exists at certain optical wavelengths and energy and momentum can be transferred from TM polarized light to the free electrons present in the metal. Most often this resonance condition is identified by a reduction in the reflected light, which is observed at a specific angle when illuminated with a fixed wavelength or at a specific wavelength when illuminated at a fixed angle. In general, some means of phase matching between the SP wave and the incident light must be provided, and this can take the form of a prism, a diffraction grating, or simply a roughened surface.

The propagation constant of the SP wave is sensitive to refractive index changes on either side of the metal surface, and thus the reflected spectrum changes with changing refractive index [16]. When used for sensing purposes, the refractive index can be changed by adsorption of a thin film on the gold surface. If the surface is functionalized so that only a target analyte binds, we refer to this as specific binding. However, index changes also occur due to the change in the background solution index which is an interfering event or non-specific effect.

The refractive index of a material is a temperature dependent quantity. The sensor and the solutions used for sensing operation had to be kept at a uniform temperature to avoid variations in index due to temperature change. Hence in the experiments which follow, all the solutions are kept at a constant temperature to avoid index variations due to temperature.

2.1 ATR configuration

The propagation constant of a surface plasmon wave is higher than an optical wave propagating in free space for a given wavelength. Thus the excitation of a SP wave directly by an optical wave is impossible [6]. To increase the momentum of the incident wave attenuated total reflection (ATR) with a prism coupler is commonly employed.[28, 29] Other methods to excite surface plasmon wave include the use of optical waveguides and diffraction gratings [22]. In this thesis, the ATR configuration is used to generate surface plasmon waves.

The ATR configuration to excite the surface plasmon waves is shown in Figure 2.1.

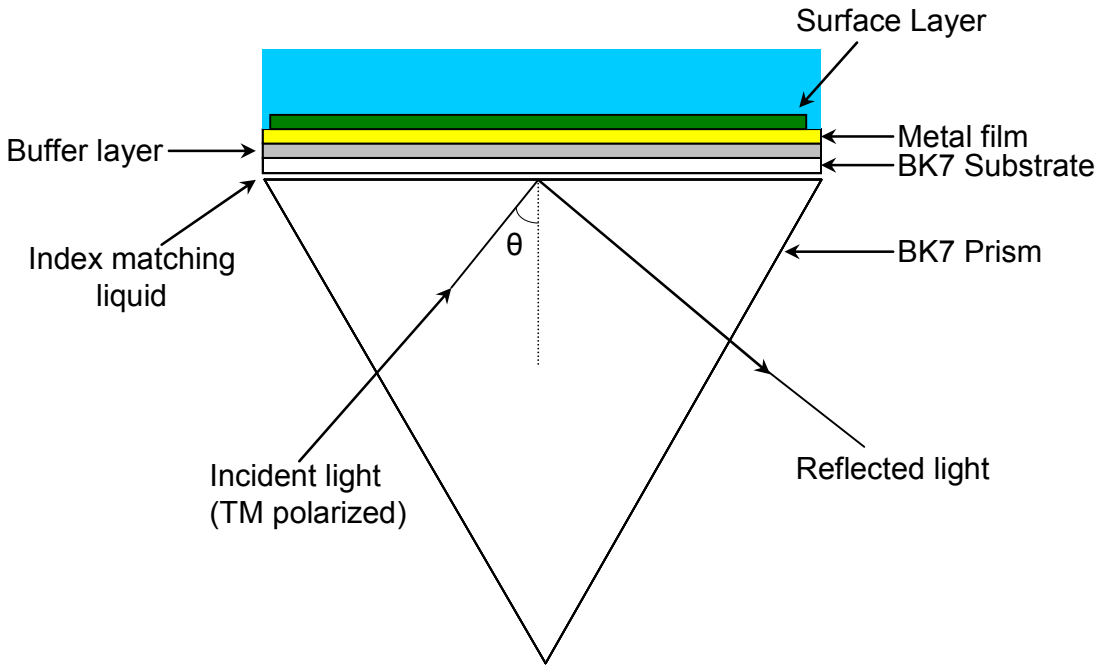

Figure 2.1 ATR configuration used to excite surface plasmon waves

2.2 Selection of gold as the metal layer

The metals that can be used to obtain surface plasmon resonance must have their conducting band electrons capable of resonating at the wavelength of the incident light. In addition, the metals must also be environmentally stable and should be free of oxides, sulphides and should not react with atmosphere or with commonly used experimental liquids like water, alcohols, etc [35]. This property is best satisfied by gold and silver. Silver oxidizes in air and hence it is environmentally unstable. Hence, Gold with its higher environmental stability, wider compatibility with various chemicals and lower reactivity (or) chemical inertness toward solutions and solutes used in bio-molecular interactions make it an ideal choice for the metal layer in SPR sensors.

2.3 Selection of Teflon as the buffer layer

In order to excite two surface plasmon waves, there is a need to have same refractive index on either side of the metal. Since most of the analytes of interest are in aqueous solutions, there is a need to have a substance having refractive index close to water which is 1.33 at room temperature (25°C). Selection of a material based on refractive index is limited and Teflon AF having its refractive index [36] closer to water and possessing better optical properties is used as the buffer layer.

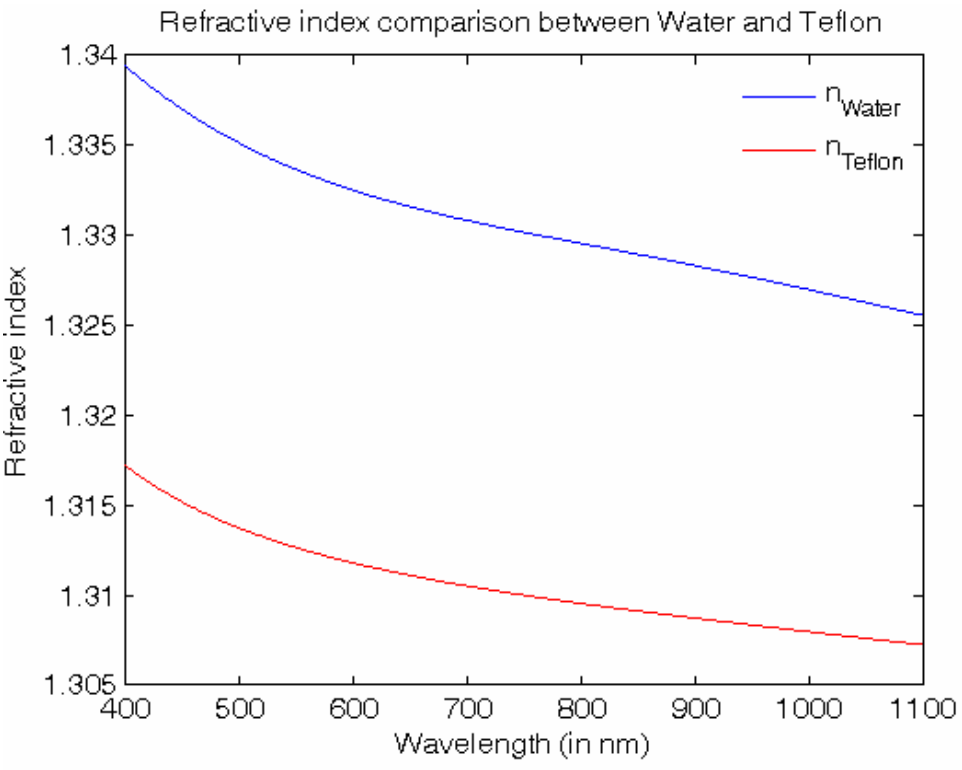

Figure 2.2 Refractive index comparison between Water and Teflon

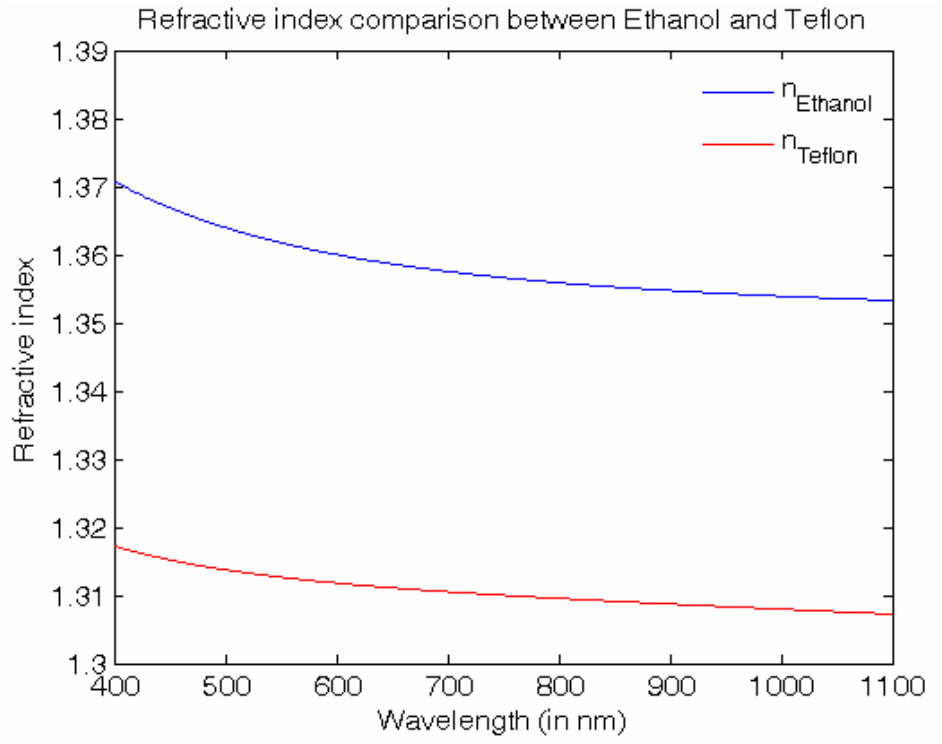

Figure 2.3 Refractive index comparison between Ethanol and Teflon

2.4 Selection of magnesium fluoride as the buffer layer

Magnesium fluoride can also be used as the buffer layer to provide better index matching to higher refractive index liquids such as ethanol. The higher index of magnesium fluoride helps in achieving a better index matching with ethanol (with its refractive index in the range of 1.371 to 1.3535 for the range of wavelength values considered) than using Teflon. As seen in Figure 2.4, the index of ethanol matches better with magnesium fluoride than Teflon.

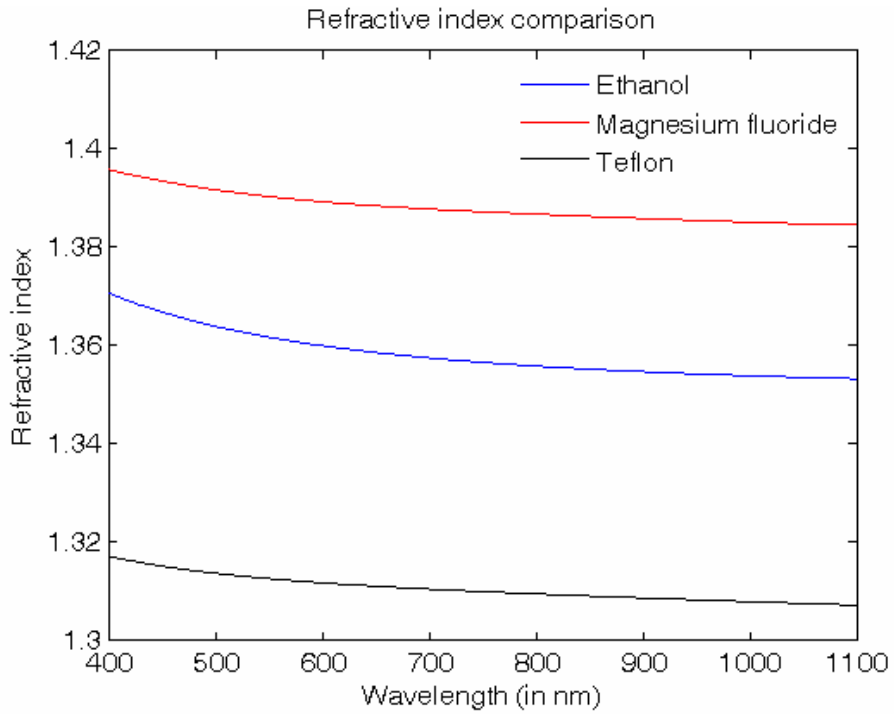

Figure 2.4 Comparison of refractive indices between ethanol, magnesium fluoride and Teflon

2.5 Interrogation techniques

The two widely employed SPR configurations are angular interrogation and spectral interrogation technique. Angular interrogation involves measuring the change in resonance angle for refractive index changes using a fixed wavelength light source. Spectral interrogation employs a light source at a fixed angle and the index changes are

indicated by the change in the resonance wavelength. In both cases the resonance is indicated as a dip in the reflectivity spectrum [6]. A deeper dip in reflectivity yields higher accuracy which results in higher resolution [37].

The sensor discussed in this work uses the method of spectral interrogation to determine the refractive index changes occurring near the metal surface.

2.6 Generation of Surface plasmon waves

As mentioned earlier, the condition for the generation of Surface plasmon wave is satisfied when $re(\varepsilon_m) < re(\varepsilon_d)$ for TM polarized incident light. The magnetic field is perpendicular to the direction of propagation and is parallel to the plane of incidence. The electric field has the same magnitude as the magnetic field but is perpendicular to it.

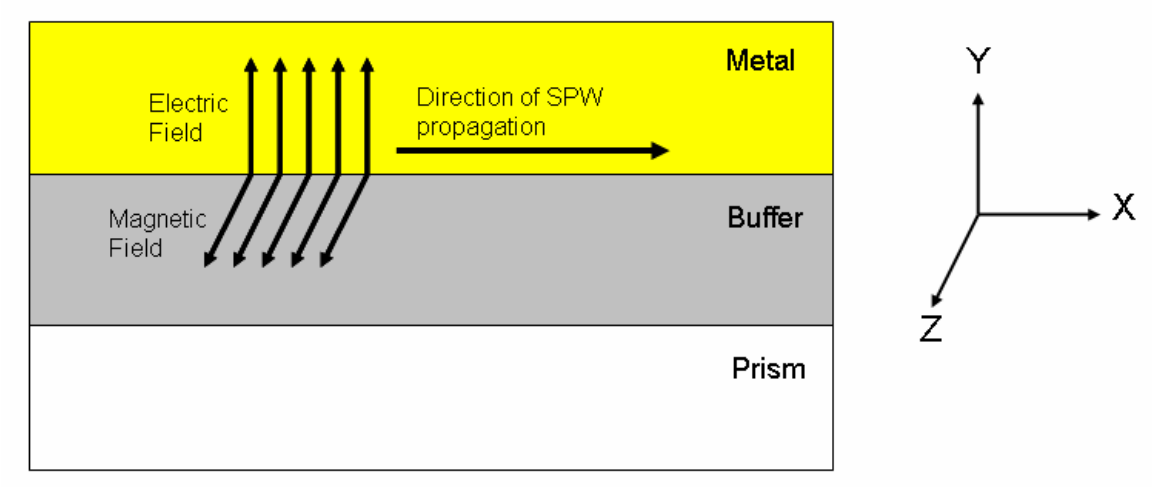

Figure 2.5 SPR structure showing the fields involved and the direction of SPR wave propagation

Since the SP waves are confined to the metal surface, the wavevector of the SP wave is matched by the wavevector of the incident light parallel to the surface. These two wavevectors are equal in magnitude and direction, for the same wavelength of the incident light. The direction of the generated SP wave is the same as the incident

wavevector and the magnitude depends on the refractive indices of all the materials which interact with its electromagnetic field [16].

The magnitude of the wavevector parallel to the conducting surface, k_X is given by

$$k_x = \left(\frac{2*\pi}{\lambda}\right) * n_{prism} * \sin\theta \qquad (2.1)$$

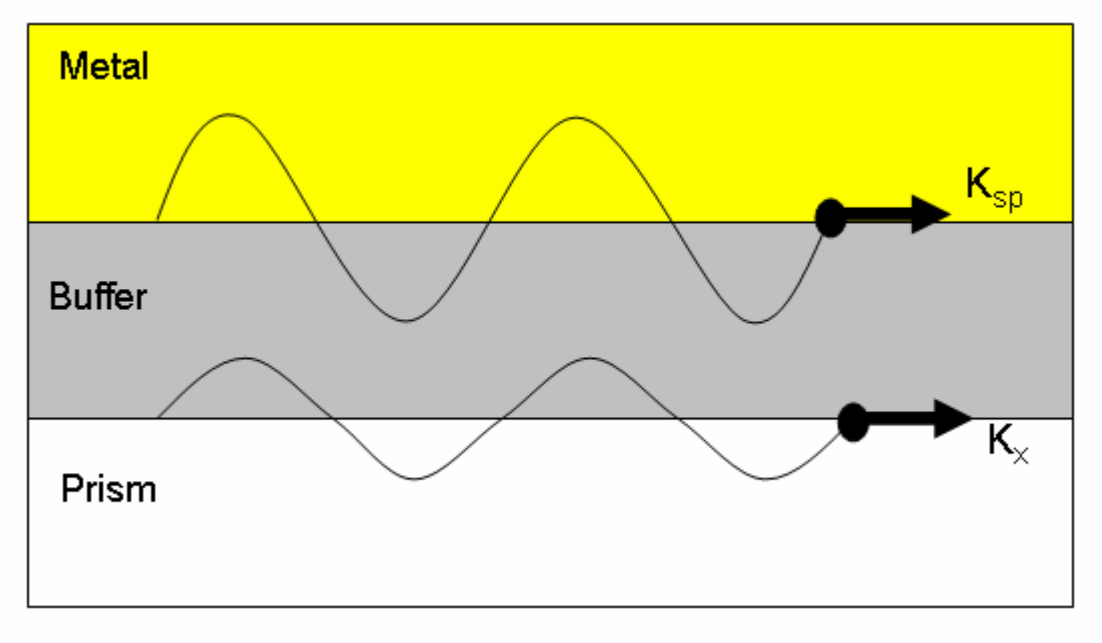

Figure 2.6 SPR structure indicating the wavevectors

The wavevector of the SP wave depends on the refractive indices of the gold (n_m) and the layers surrounding it, i.e., dielectric (buffer) layer and the solution flowing over the gold surface, collectively referred as n_d. The magnitude of the wavevector of the SP wave, k_{SP} at the semi-infinite metal dielectric interface [6] is given by

$$k_{SP} = \left(\frac{2*\pi}{\lambda}\right) * \sqrt{\frac{n_m^2 * n_d^2}{(n_m^2 + n_d^2)}} \qquad (2.2)$$

or, in terms of dielectric constant,

$$k_{SP} = \left(\frac{2*\pi}{\lambda}\right) * \sqrt{\frac{\varepsilon_m * \varepsilon_d}{(\varepsilon_m + \varepsilon_d)}} \tag{2.3}$$

$$k_{SP} = k_0 * \sqrt{\frac{\varepsilon_m * \varepsilon_d}{(\varepsilon_m + \varepsilon_d)}} \tag{2.4}$$

where

$k_0 = \frac{2*\pi}{\lambda}$, is the free space wave vector

ε_m = dielectric constant of the metal

ε_d = dielectric constant of buffer layer and solution

n_m = refractive index of the metal

n_d = refractive index of the buffer layer and solution

λ = free space wavelength

When these two wavevectors match, there is a resonant transfer of energy through the evanescent wave causing surface plasmon excitation. This is indicated by a drop in the reflected light at certain wavelengths as shown in Figure 2.7. During this resonant transfer from photons to plasmons, both energy and momentum are conserved.

From Eqn.(2.4), we see k_{SP} depends on k_0, ε_m and ε_d , and from Eqn.(2.1), k_X depends on k_0, n_{prism} and the angle of incidence, θ. The metal layer, the buffer layer, prism and the angle of incidence (since we are using spectral interrogation) does not change over the course of an experiment and hence any change in the background solution's index and/or a surface layer thickness, changes k_{SP}, which is matched by k_X at an another wavelength resulting in a change in resonance wavelength.

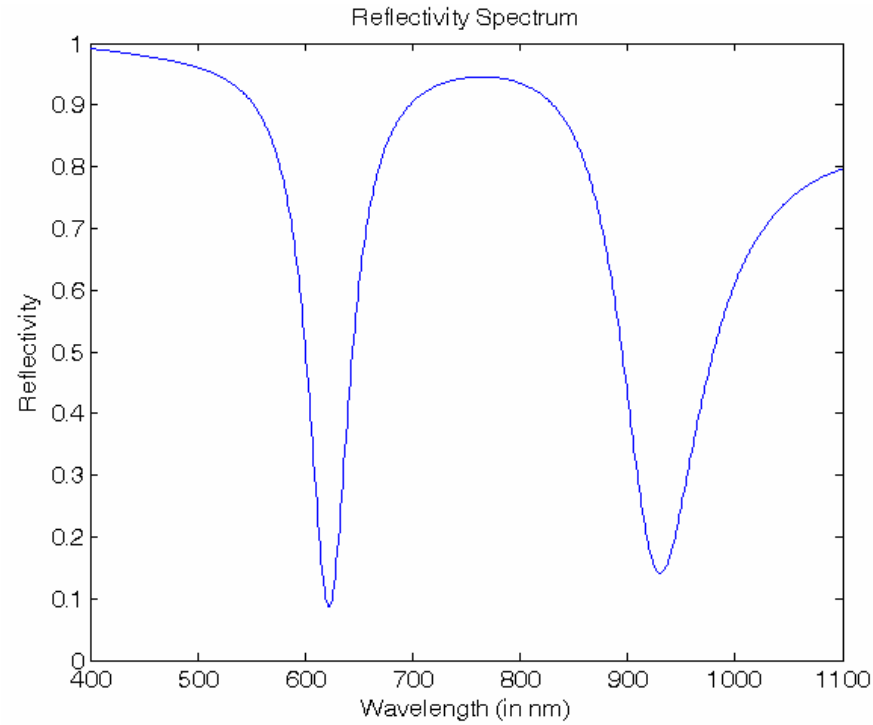

Figure 2.7 Spectrum of a dual mode SPR sensor using ethanol for θ = 68° and Teflon = 400nm and gold = 55nm

When the metal layer is placed between dielectrics of similar refractive index, two surface plasmon modes are excited. They are the long-range surface plasmon (LRSP) mode and the short-range surface plasmon (SRSP) mode. These names arise from their propagation lengths [38]. The electric field of the short range mode is more strongly concentrated in the metal; thus, the SRSP is more strongly absorbed and propagates a shorter distance. The electric field of the long-range mode overlaps less with the metal and thus propagates a longer distance. Because both modes have different penetration depths in the dielectric, the LRSP is expected to be less sensitive to surface binding than the SRSP. Thus, the two modes can be used to differentiate surface and bulk effects.

2.7 Dispersion relationship

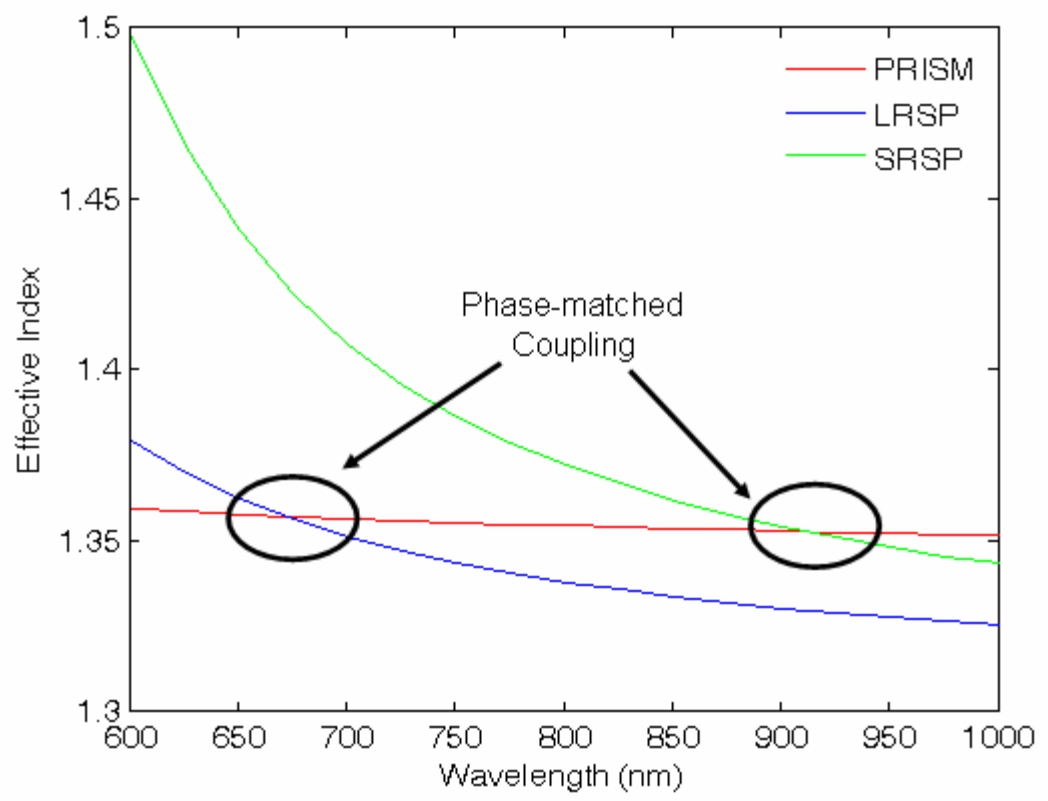

Figure 2.8 Dispersion relations of LRSP, SRSP and prism for a 55nm thick gold layer surrounded by symmetrical refractive indices of Teflon-AF on both sides

Figure 2.8 shows the dispersion relationship of the two modes [39] along with that of the prism. The straight line indicates the effective index corresponding to the tangential wavevector of the light inside the prism. This index is less than the index of the prism due to the incidence of light at an angle. If the light incident is parallel to the normal, then the index of the light is equal to the index of the prism. In all other cases, it is the cosine of the incident angle times the index of the prism.

$$\text{Effective index of light inside the prism} = \cos\theta * n_{prism}$$

where θ is the incident angle

The dispersion relationship of LRSP and SRSP's effective index depends on

n_{buffer}, n_{metal}, $n_{solution}$ and the thickness of the metal layer. The dispersion relations of LRSP and SRSP do not take into account the index of the prism and the index of the surface layer (if and when formed). These exclusions do not strongly affect the overall dispersion pattern and even when the indices are added, there is only a slight increase in the LRSP and SRSP's effective indices.

As seen in Figure 2.8, the SRSP is better matched with the index of the prism than the LRSP which produces higher sensitivity for the SRSP over the LRSP. If the SP's dispersion relation is closely matched (ideally parallel) with that of the light inside the prism, high sensitivity is achieved. However, the width of the resonance is very wide making estimation of the resonance wavelength less precise. On the other hand, if the SP's dispersion relation is not matched with the incident light (ideally perpendicular), the width of the resonance is smaller, but the disadvantage in this type of matching is the low sensitivity achieved. Hence, there has to be a tradeoff to achieve optimum performance from the two modes.

2.8 Magnetic field profile

Figure 2.9 shows the magnetic field profile for both LRSP and SRSP at 650 and 900 nm respectively when a 55nm gold layer is sandwiched between same refractive index material, Teflon-AF in this case. If the fields were plotted for each mode at the same wavelength we would observe that the long-range mode penetrates much deeper into the dielectric than the short range mode. However, this effect is mitigated somewhat by the fact that the long-range mode is excited at a shorter wavelength and thus the fields decay more rapidly. As a result, the long-range mode penetrates only slightly farther into the dielectric than the short range mode. A sensor design that minimizes this problem is discussed in chapter 7.

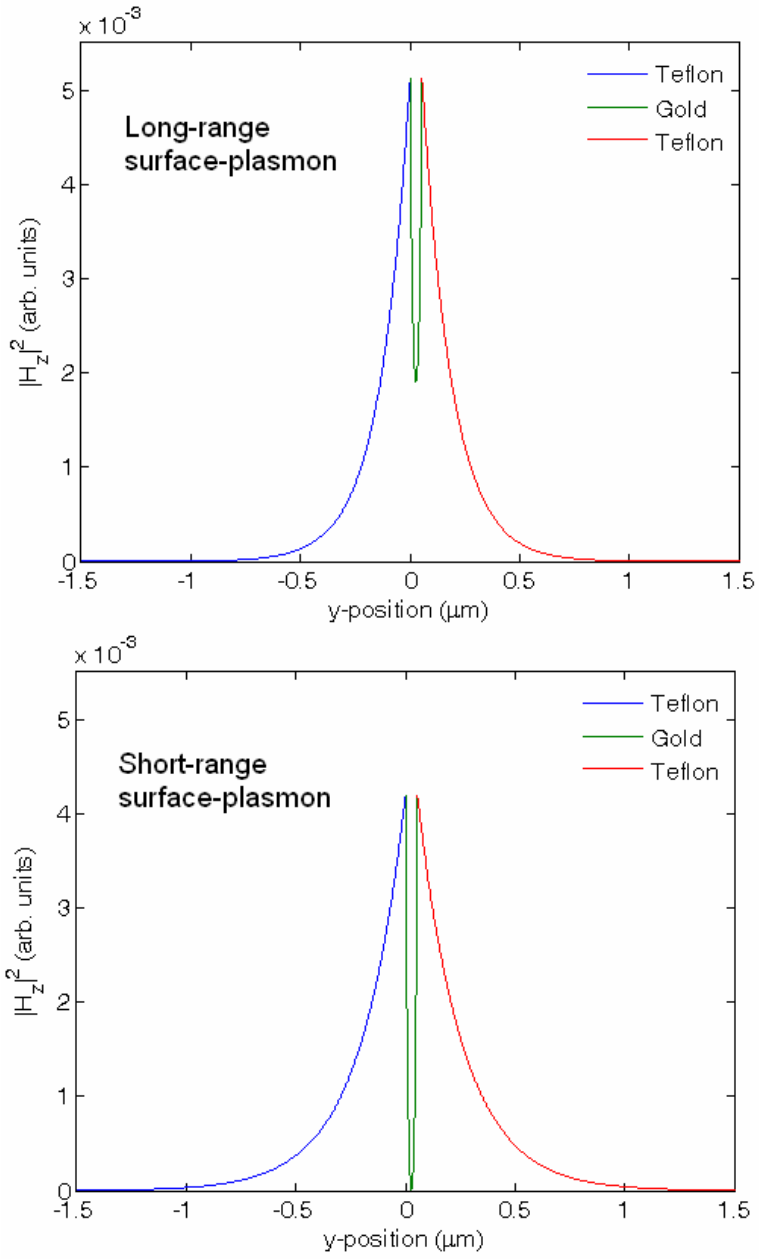

Figure 2.9 Magnetic field profile of LRSP at 650nm and SRSP at 900nm for a 55nm gold layer between Teflon-AF and Teflon-AF

If the indices on both sides of the gold layer are not the same (which will be the case in all practical applications), the symmetry of both modes seen in Figure 2.9 is lost and one mode extends into the higher index material and the lower mode into lower index material, which is further evidenced in the next plots.

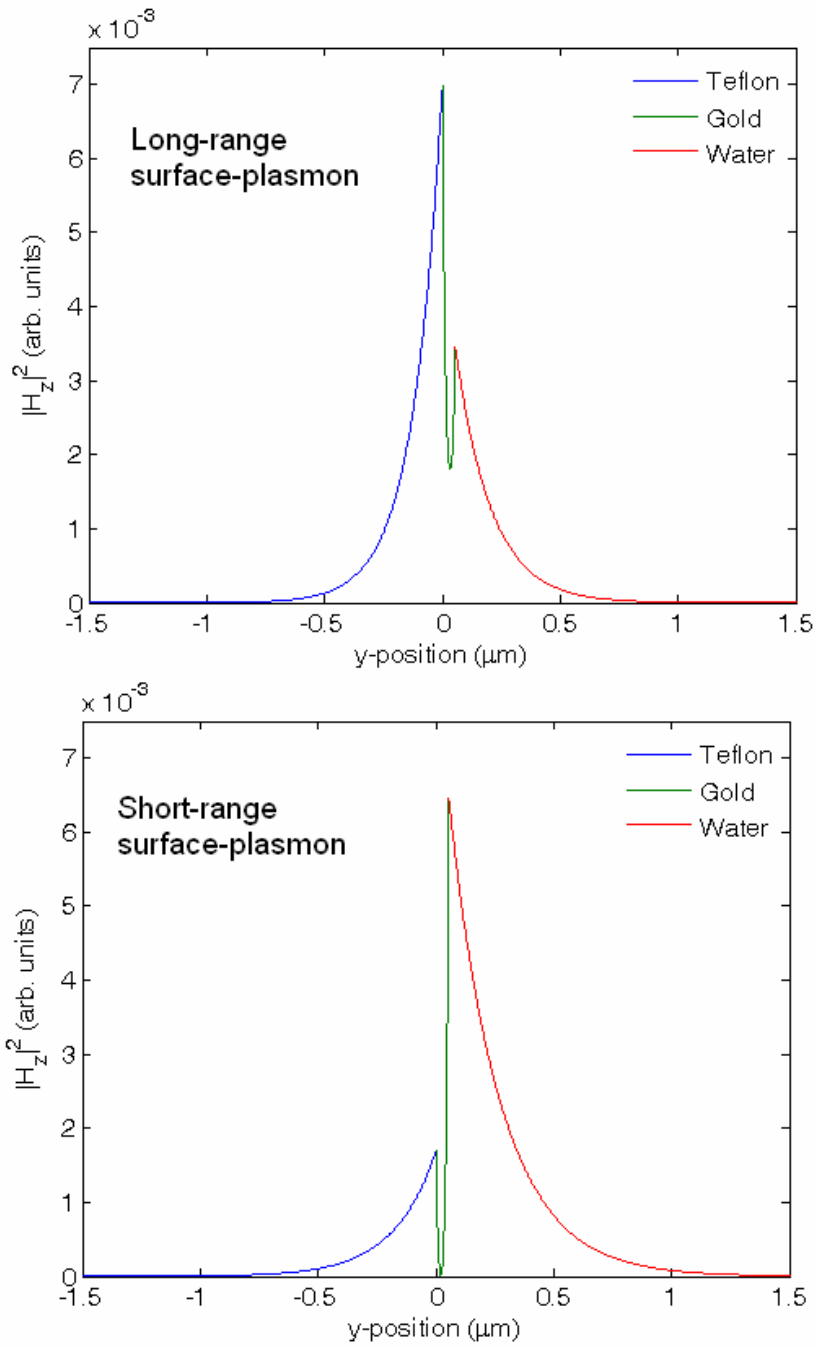

Figure 2.10 Magnetic field profile of LRSP at 650nm and SRSP at 900nm for a 55nm gold layer between Teflon-AF and water

Figure 2.10 and Figure 2.11 show the field profile of a dual-mode SPR sensor employing a 55nm gold surface sandwiched between Teflon-AF and water and ethanol, respectively. As seen in both the figures, the short-range's field is more into the solution than into the buffer. The stronger SRSP field in the solution along with better matching of SRSP's

index with that of prism than LRSP's index (refer Figure 2.8), yields better sensitivities for SRSP than LRSP as indicated in Table 3.1 and Table 3.6.

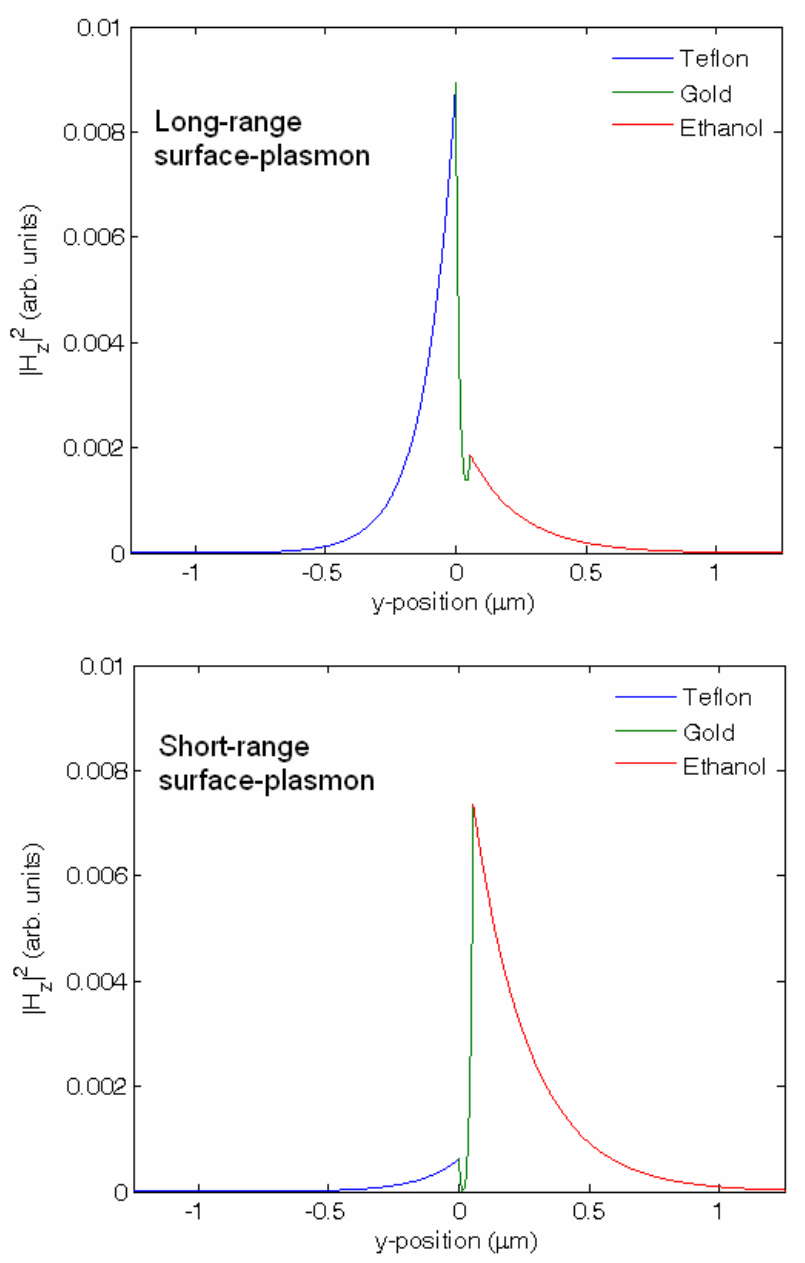

Figure 2.11 Magnetic field profile of LRSP at 650nm and SRSP at 900nm for a 55nm gold layer between Teflon-AF and ethanol

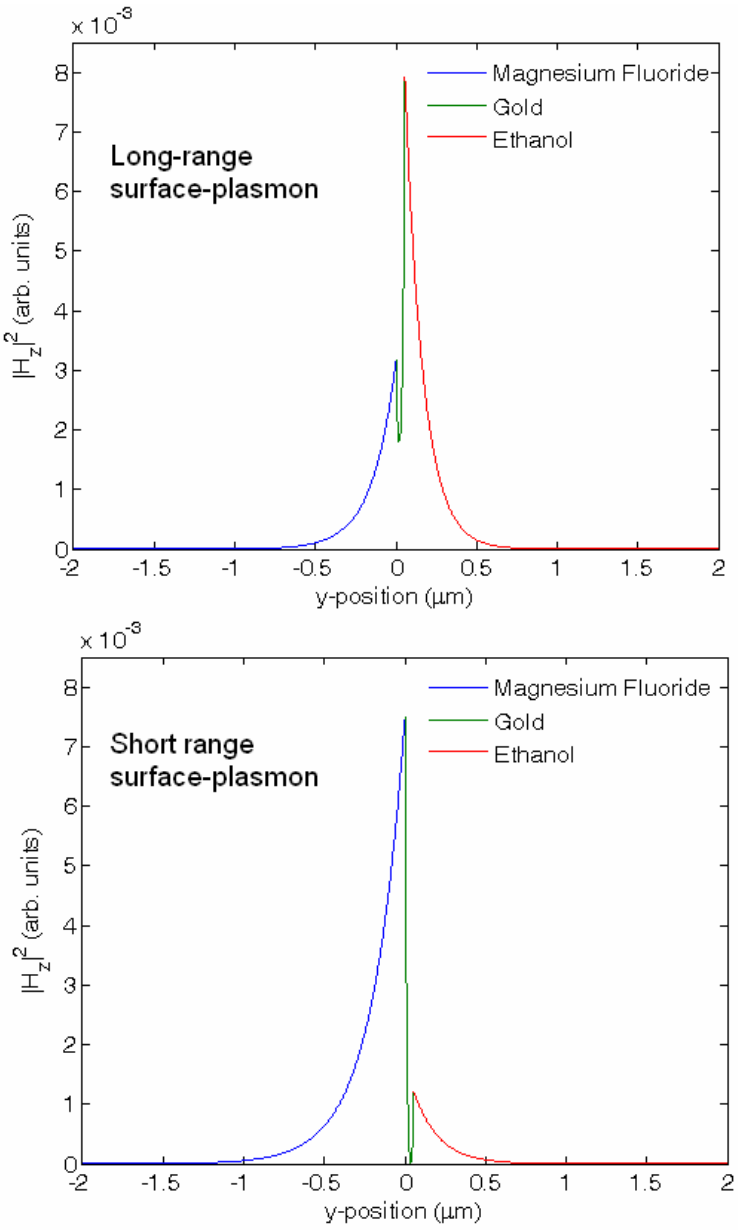

Figure 2.12 Magnetic field profile of LRSP at 650nm and SRSP at 900nm for a 55nm gold layer between magnesium fluoride and ethanol

Using magnesium fluoride as the buffer layer instead of Teflon-AF and using Ethanol as the base solution, the magnetic profile of the both modes is shown in Figure 2.12. The field profiles appear distinctly different than when using Teflon-AF, due to increased index of magnesium fluoride. Difference in their field profiles change the bulk and surface sensitivities of both modes than using Teflon-AF as the buffer layer as indicated in Table 3.11.

2.9 Model employed – Linear model

Sensitivity is determined by measuring the change in the resonance wavelength ($\Delta\lambda$) due to a change in background index and/or due to a change in surface layer binding. The two surface plasmon resonance modes (LRSP and SRSP) behave differently for changes due to bulk index variation and also due to surface layer thickness changes. These variations in their sensitivities help to differentiate between the two effects and provide self-referencing capability.

In order to predict the bulk and surface sensitivity, we assume the linear model. This model assumes that the responses due to variations in surface layer thickness and bulk index change are linear. Change in long range resonance wavelength ($\Delta\lambda_{LR}$) and the short range wavelength ($\Delta\lambda_{SR}$) are given by

$$\Delta\lambda_{\mathrm{LR}} = S_{\mathrm{S\text{-}LR}}\Delta t + S_{\mathrm{B\text{-}LR}}\Delta n_B \tag{2.5}$$

$$\Delta\lambda_{\mathrm{SR}} = S_{\mathrm{S\text{-}SR}}\Delta t + S_{\mathrm{B\text{-}SR}}\Delta n_B \tag{2.6}$$

Where

$\Delta\lambda_{LR}$ = change in long range resonance wavelength

$\Delta\lambda_{SR}$ = change in short range resonance wavelength

S_{S-LR} = Surface sensitivity of LRSP

S_{S-SR} = Surface sensitivity of SRSP

S_{B-LR} = Bulk sensitivity of LRSP

S_{B-SR} = Bulk sensitivity of SRSP

Δt = change in the adsorbed surface layer thickness

Δn_B = change in the bulk refractive index

In the experimental section, bulk and surface sensitivities of a self-referencing sensor were calculated using predetermined Δt and Δn values and measuring their corresponding resonance wavelength changes. The bulk index change is achieved by using

a) different molar solutions of methanol in ethanol for experiments using ethanol as the medium ($\Delta n = 7.76*10^{-4}$)
b) different molar solutions of Glycerol in salt water for experiments using water as the medium ($\Delta n = 5.65*10^{-4}$)

In both the cases, the change in the index is predetermined and not very large thus eliminating non-linearity in our calculations.

The surface layer thickness formed is also predetermined using ODT as surface binding layer having thickness of 2nm [40]

The general form of Eqn. (2.5) and (2.6) involving resonance wavelength, sensitivity and changes in index or thickness is

$$(\Delta\lambda)_{matrix} = (\Delta t \Delta n)_{matrix} * (sensitivity)_{matrix} \tag{2.7}$$

(i.e.)

$$\begin{pmatrix} \lambda_{n0t0} \\ \lambda_{n1t0} \\ \lambda_{n0t1} \\ \lambda_{n1t1} \end{pmatrix} = \begin{pmatrix} 1 & 0 & 0 \\ 1 & \Delta n & 0 \\ 1 & 0 & \Delta t \\ 1 & \Delta n & \Delta t \end{pmatrix} \begin{pmatrix} \lambda_{n0t0} \\ S_B \\ S_S \end{pmatrix} \tag{2.8}$$

Where

n0 = initial background refractive index

n1 = change in the background index $(n_1 = n_0 + \Delta n)$

t0 = initial surface layer thickness

t1 = change in the surface layer thickness $(t_1 = t_0 + \Delta t)$

The last row of the matrix in eqn.(2.8) is included as a check on the linearities of the surface and bulk sensitivities. In general, Eqn. (2.8) does not have an exact solution and must be solved using a least-squares method.

From Eqn(2.7),

$$\text{Sensitivity} = (\Delta t \Delta n)_{\text{matrix}} \backslash (\Delta\lambda)_{\text{matrix}} \tag{2.9}$$

Eqn(2.9) helps to find S_B and S_S for LRSP and SRSP, which then forms the basis for future measurements using the same sensor. These calculated sensitivities were later used to differentiate between bulk index changes from surface layer thickness changes. Using these sensitivity values, unknown surface layer thickness and bulk index changes can be calculated using Eqns. (2.10) and (2.11)

$$\Delta t = \frac{S_{B-SR}\Delta\lambda_{LR} - S_{B-LR}\Delta\lambda_{SR}}{S_{S-LR}S_{B-SR} - S_{S-LR}S_{B-LR}} \tag{2.10}$$

$$\Delta n_B = \frac{S_{S-SR}\Delta\lambda_{LR} - S_{S-LR}\Delta\lambda_{SR}}{S_{B-LR}S_{S-SR} - S_{B-LR}S_{S-LR}} \tag{2.11}$$

2.10 Cross-sensitivity

The resonance wavelength of the spectrally interrogated SPR sensor depends on

a) angle of incidence
b) properties of the metal film
c) refractive index of the layers adjoining the metal layers

With the incidence angle fixed during the experiment, only changes due to variations in the surface layer thickness and background solutions affect the resonance wavelength.

The main aim of this sensor is to differentiate both effects. Because of their difference in their field profile, LRSP and SRSP respond differently to background index and surface binding changes. This difference in their response forms the basis for self-referencing operation. When there is a change in the bulk index, the two modes have their shift in resonance wavelength to different effects, which should not be the same for changes due to surface-binding. In other words, cross-sensitivity (sensitivity between bulk and surface changes) should be different, i.e.

$$\left(\frac{Sensitivity_{SRSP}}{Sensitivity_{LRSP}}\right)_{Bulk} \neq \left(\frac{Sensitivity_{SRSP}}{Sensitivity_{LRSP}}\right)_{Surface}$$

When this condition is achieved, the two modes have their resonance wavelength shift to different values due to changes in the sensor, which can be the result of bulk index change or surface layer binding. Because of their differential response, bulk index changes can be differentiated from surface layer binding.

2.11 Calculation of the angle inside the prism

The incident angle at the sample is calculated from the angle of incidence at the air — prism interface.

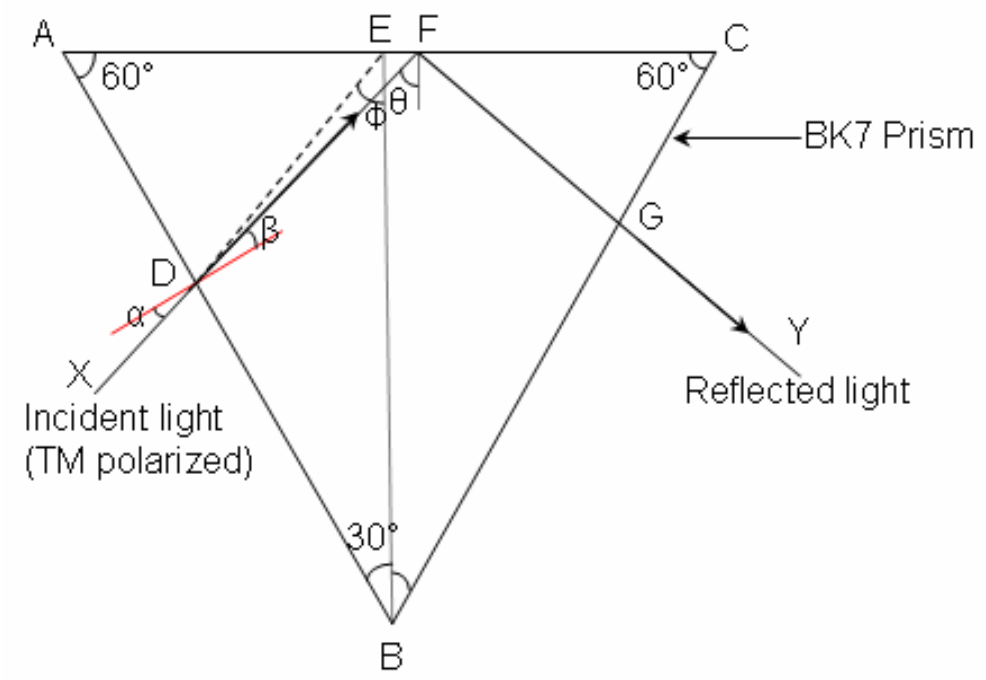

Figure 2.13 Calculation of the incident angle

Figure 2.13 shows the refraction and reflection of the incident light in the prism. XD represents the incident ray and FY the reflected ray from the prism. DF is the refracted

light ray whereas DE indicates the light ray without refraction. The red line indicates a line normal to plane AB.

Calculating θ, the angle of incidence inside the prism is as follows:

From Δ AFD,

$$60^\circ + (90 - \theta) + (90 - \beta) = 180^\circ$$

$$\Rightarrow \theta = 60^\circ - \beta \tag{2.12}$$

According to Snell's law,

$$n_1 \sin\theta_1 = n_2 \sin\theta_2$$

where,

n_1 = refractive index of air (which is 1)

n_2 = refractive index of the prism (n_p)

θ_1 = incident angle (α)

θ_2 = refracted angle (β)

=> $\sin\alpha = n_p \sin\beta$

$$\Rightarrow \beta = \sin^{-1}\left(\frac{\sin\alpha}{n_p}\right) \tag{2.13}$$

From Δ DEB,

$$\phi + 30^\circ + (90^\circ + \alpha) = 180^\circ$$

$$\Rightarrow \alpha = 60^\circ - \phi \tag{2.14}$$

From Eqns.(2.13) and (2.14)

$$\beta = \sin^{-1}\left(\frac{\sin(60^\circ - \phi)}{n_p}\right) \tag{2.15}$$

Therefore, from Eqns.(2.12) and (2.15)

$$\theta = 60^\circ - \sin^{-1}\left(\frac{\sin(60^\circ - \phi)}{n_p}\right) \quad \text{(or)}$$

$$\theta = 60^\circ + \sin^{-1}\left(\frac{\sin(\phi + 60^\circ)}{n_p}\right) \tag{2.16}$$

Since the refractive index of the prism (n_p) is dependent on the wavelength, incidence angle θ, is also dependent on the wavelength. Assuming the resonance wavelength at 650nm, Figure 2.14 shows the variations of θ with Φ.

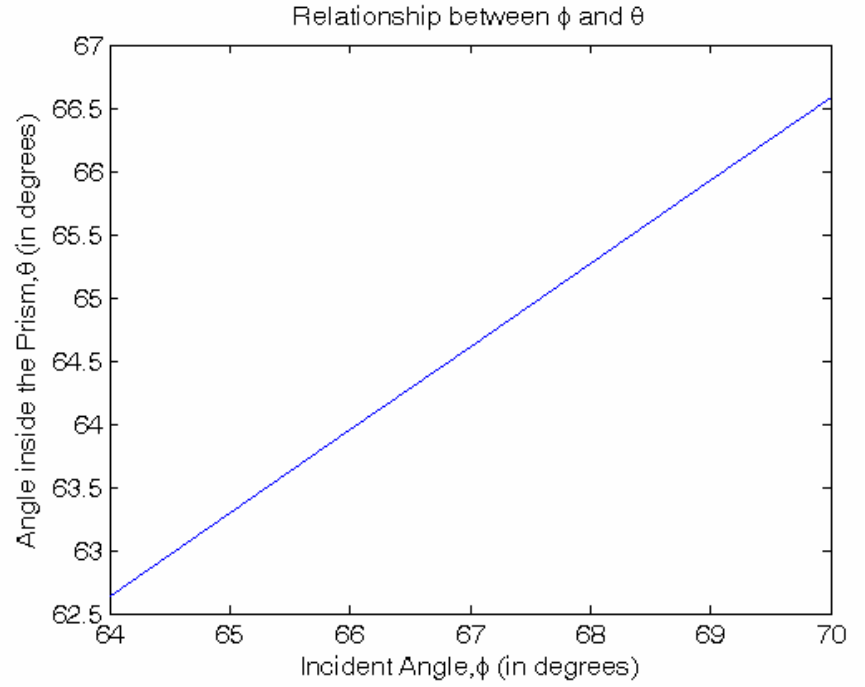

Figure 2.14 Relationship between incident angle, ϕ and the angle inside the prism, θ with the resonance at 650nm

2.12 Reflectivity calculation

2.12.1 Transmission matrix calculation

Theoretical analysis of light propagation in this configuration is based on transfer matrix method, Fresnel's formulae and multiple-reflection theory [41]. The Fresnel equations for the reflected and transmitted electric fields in p-polarization (TM) [42] are given by

$$\text{Reflection Coefficient, r} = \left(\frac{E_r}{E_t}\right)_{11} = \frac{n_2 \cos\theta_1 - n_1 \cos\theta_2}{n_1 \cos\theta_2 + n_2 \cos\theta_1} \tag{2.17}$$

$$\text{Transmission Coefficient, t} = \left(\frac{E_t}{E_t}\right)_{11} = \frac{2n_1 \cos\theta_1}{n_1 \cos\theta_2 + n_2 \cos\theta_1} \tag{2.18}$$

The power reflection, R and transmission, T coefficients are determined by calculating the ratio of either reflected or transmitted intensity to the intensity of the incident light.

$$R \equiv \frac{I_r}{I_i} = \left(\frac{E_r}{E_i}\right)^2 \tag{2.19}$$

$$T \equiv \frac{I_t}{I_i} = \frac{n_2 \cos\theta_2}{n_1 \cos\theta_1}\left(\frac{E_t}{E_i}\right)^2 \tag{2.20}$$

Where intensity, $I \propto nE^2$

We used transmission matrix (T-matrix) [43] to calculate the net reflection and transmission. The main advantage of using T-matrices is the modeling of complex structures by simply performing matrix multiplication of individual components.

For an interface between two layers of different indices, T-matrix is given by

$$T = \begin{pmatrix} \frac{1}{t} & \frac{r}{t} \\ \frac{r}{t} & \frac{1}{t} \end{pmatrix} \tag{2.21}$$

If the wave has to travel a distance of L in the second medium, the T-matrix is given by

$$T = \begin{pmatrix} e^{j\beta L} & 0 \\ 0 & e^{-j\beta L} \end{pmatrix} \tag{2.22}$$

Where β is the component of the wavevector normal to layer

For a dielectric block of length, L, the resultant T-Matrix is obtained by multiplying (2.21) and (2.22),

$$T = \begin{pmatrix} e^{\frac{j\beta L}{t}} & 0 \\ 0 & e^{\frac{-j\beta L}{t}} \end{pmatrix} \tag{2.23}$$

From eqns. (2.22) and (2.23), the overall transmission matrix depends on

a) the wave vector normal to the layer(β),
b) length or thickness of the medium (L),
c) reflection coefficient (r) and
d) transmission coefficient (t).

The reflection and transmission coefficients, in turn depend on the refractive indices of the two media and the incident angles in them, as seen in eqns. (2.17), (2.18) and (2.21).

2.12.2 Snell's law

When light travels through medium with different refractive index, part of the light is reflected and other part refracted. To calculate the relationship between incident angle and refracted angle, Snell's law is used.

According to Snell's law,

$$n_1 \sin\theta_1 = n_2 \sin\theta_2 \tag{2.24}$$

Where n_1 and n_2 are two media with different refractive indices with θ_1 and θ_2, the incident and refracted angle respectively.

Before the light is totally internally reflected in the prism, it propagates through media with different indices in the following order: prism, buffer, metal, adsorbed layer (if any)

and finally solution. The refractive indices of all the layers and the incident angle are known, which helps in calculation the incident angle at each interface using Snell's law.

From (2.24),

$$\theta_2 = \sin^{-1}\left(\frac{n_1}{n_2}\sin\theta_1\right) \tag{2.25}$$

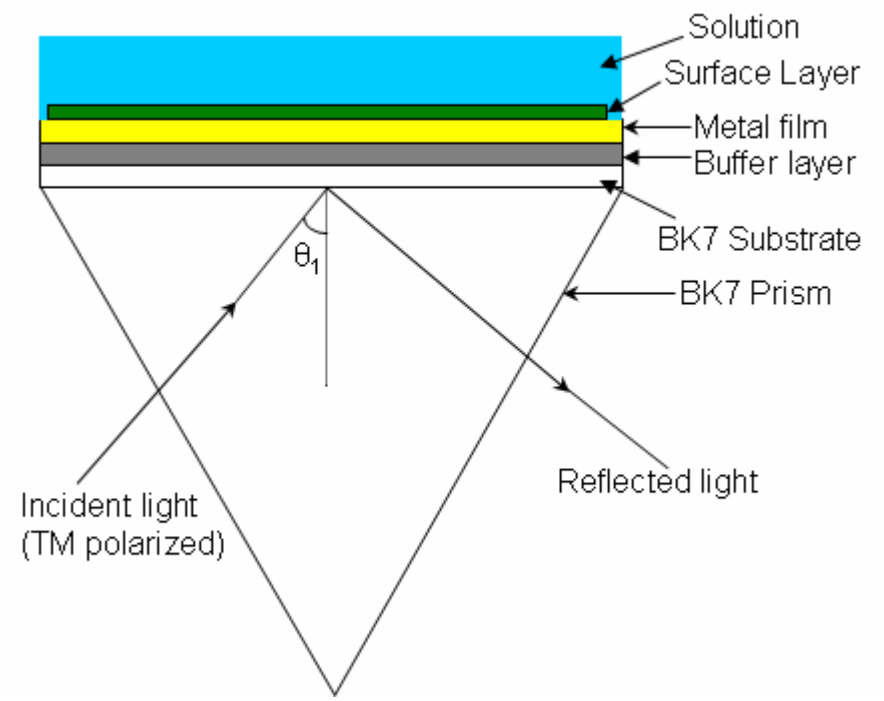

Figure 2.15 SPR configuration.

Note that in the presence of evanescent waves, the angles become complex and account for the attenuation of the fields in the medium.

2.12.3 Calculation of incident angle and propagation constant

Light travels in the following order:

Prism → buffer → metal → surface layer → solution

Let the incident angles in each layer (from prism to solution) be

$$\theta_1 \rightarrow \theta_2 \rightarrow \theta_3 \rightarrow \theta_4 \rightarrow \theta_5$$

Let the propagation constants at different interfaces be

$$k_1 \rightarrow k_2 \rightarrow k_3 \rightarrow k_4 \rightarrow k_5$$

If θ_1 is the incident angle inside the prism, then the other incident angles inside the prism are calculated from eqn.(2.25), as follows:

$$\theta_2 = \sin^{-1}\left(\frac{n_{prism}}{n_{buffer}}\sin\theta_1\right)$$

$$\theta_3 = \sin^{-1}\left(\frac{n_{buffer}}{n_{metal}}\sin\theta_2\right)$$

$$\theta_4 = \sin^{-1}\left(\frac{n_{metal}}{n_{layer}}\sin\theta_3\right)$$

$$\theta_5 = \sin^{-1}\left(\frac{n_{layer}}{n_{solution}}\sin\theta_4\right)$$

The normal wavevector in each medium is calculated as

$$k_i = \frac{2\pi n_i}{\lambda}\cos\theta_i$$

where the subscript *i* indexes each layer in the structure.

2.12.4 Reflectivity

The net transmission matrix for the whole setup is given by

$$T = T(n_{prism}, n_{buffer}, \theta_2, \theta_1) \; * \; T(n_{buffer}, n_{metal}, \theta_3, \theta_2, k_2, t_{buffer}) \\ * \; T(n_{metal}, n_{layer}, \theta_4, \theta_3, k_3, t_{metal}) * \; T(n_{layer}, n_{solution}, \theta_5, \theta_4, k_4, t_{layer}) \\ * \begin{pmatrix} 1 \\ 0 \end{pmatrix} \tag{2.26}$$

The coefficient of reflection is given by

$$r = \frac{T(2)}{T(1)} \tag{2.27}$$

The coefficient of transmission is given by

$$t = \frac{1}{T(1)} \tag{2.28}$$

Reflectivity (the % of reflection) is given by

$$R = |\, r \,|^2 \tag{2.29}$$

3 CHAPTER 3 - OPTIMIZATION OF THE SENSOR

In order to achieve a better performance from the SPR sensor, the thicknesses of the buffer and the metal layer had to be optimized.

The main goals considered for optimization were as follows:

Higher sensitivity – The Sensor should have its resonance wavelength shift as much as possible for a small change in either the background solution's refractive index or in the thickness of the layer formed. In other words, there should be maximum output change for a minimum input change.

Lower Reflection – when coupling into the surface plasmon modes occur, ideally 100% of light is expected to couple into those two modes. But since ideal coupling is impossible, there is a need to have maximal coupling which implies the need to have lower reflectivity.

Limit of the Resonance wavelengths – The coupling wavelength for LRSP and SRSP were limited to visible and near IR regions (500-1000nm), as the spectrometer used was reliable only in those regions.

Simulations were performed with the thickness of gold ranging from 39.5-69 nm and the thickness of Teflon-AF or magnesium fluoride varying from 200-1000nm. The wavelength ranged from 400 to 1100nm with 1nm increments.

3.1 Selection of wavelength incremental value

The incremental value used for changing the wavelength step, was employed to get data with more/less resolution. In the simulations discussed below, an incremental value of 1nm was used. Incremental values of 0.5nm and 0.25nm can be used to get closer data points with their respective simulations taking two and four times longer time than for simulations performed with 1nm increments. Using increments smaller than 1nm only improved the estimation of the resonance wavelength by 25%, so 1nm increments were used throughout the simulation runs.

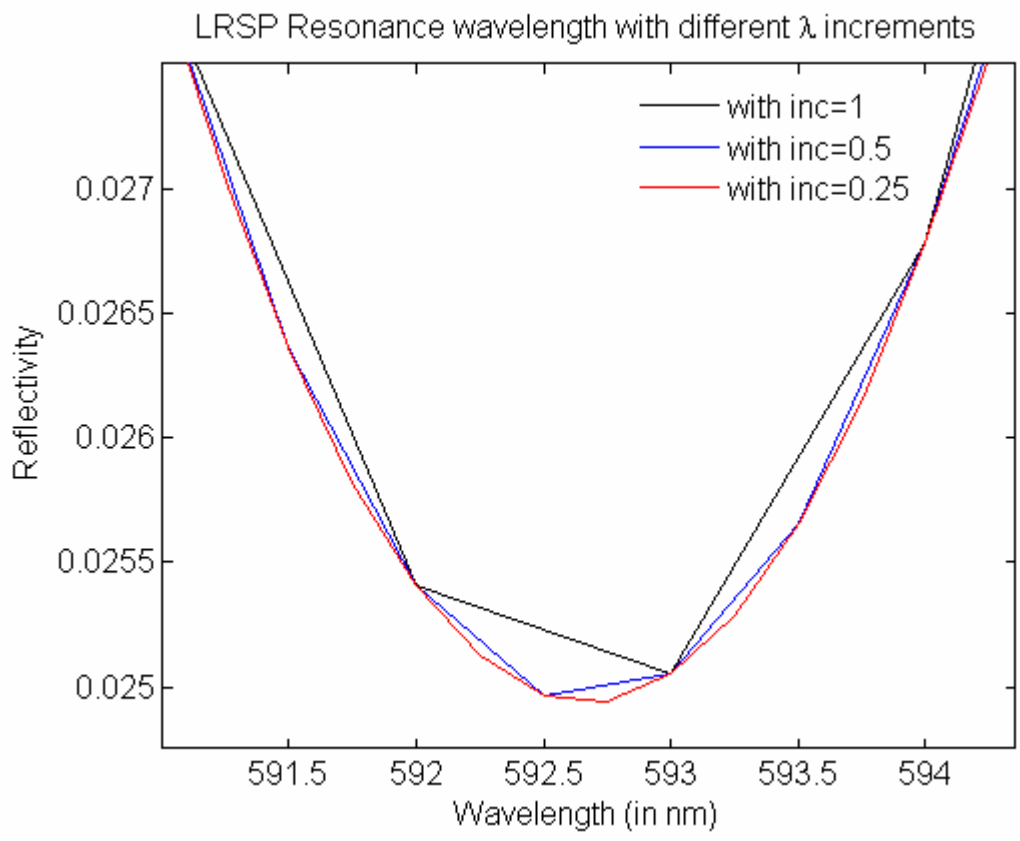

Figure 3.1 LRSP resonance wavelength for θ = 69°, gold = 50nm and Teflon = 300 nm with three different wavelength increments using ethanol as the base solution

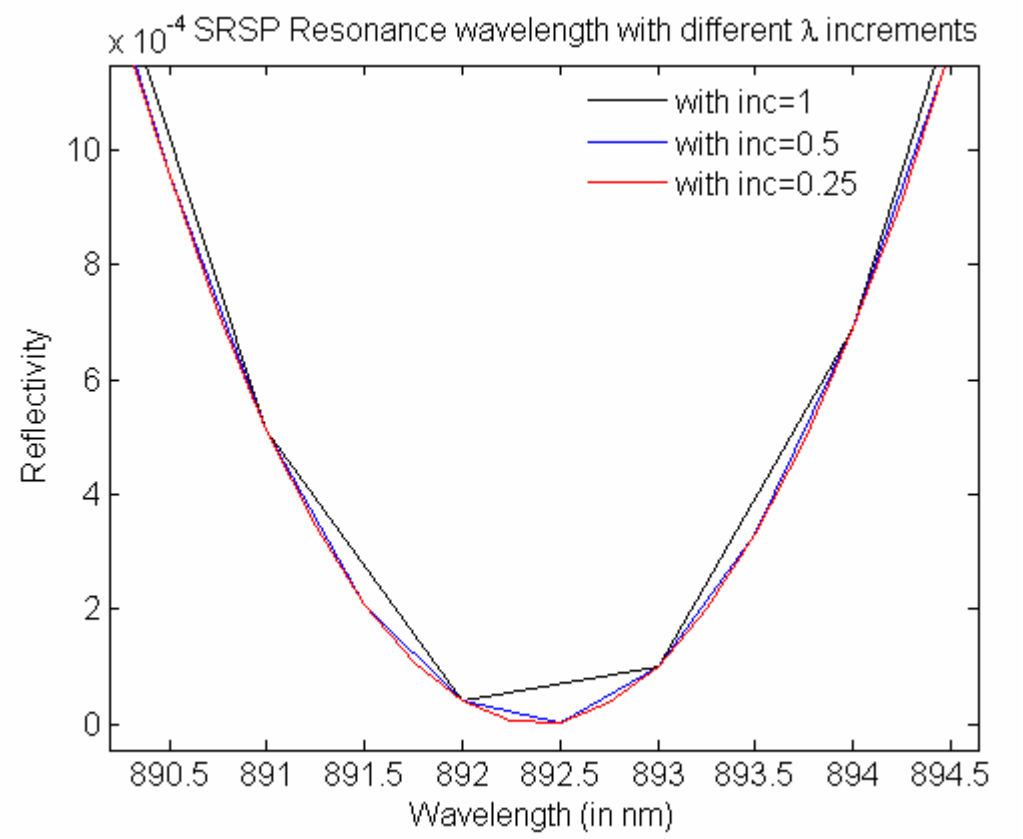

Figure 3.2 SRSP resonance wavelength for θ = 69°, gold = 50nm and Teflon = 300 nm with three different wavelength increments (in nm) using ethanol as the base solution

Figure 3.1 and Figure 3.2 show the zoomed-in LRSP and SRSP resonance wavelengths with different wavelength increments. The calculation of exact wavelength minima is performed by fitting a parabola to the approximate resonance wavelength using MATLAB's *polyfit* function. Hence the calculation of the approximate resonance wavelength is not very critical. Hence "1" is used as the incremental value.

3.2 Selection of Gold thickness range

3.2.1 Selection of Minimum gold thickness

Gold thinner than 39.5nm placed the coupling to the SRSP at wavelengths greater than 1000nm — the region where the spectrometer was unacceptably noisy in its operation.

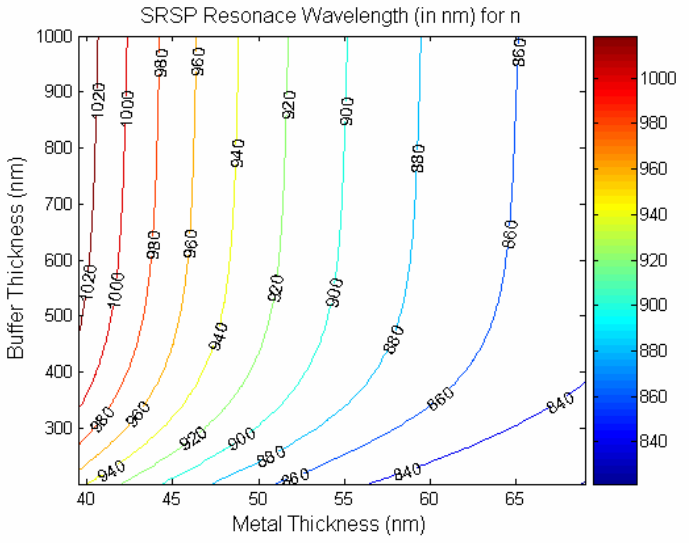

Figure 3.3 SRSP resonance wavelength for different gold and Teflon thicknesses for θ = 66° with water as the base solution

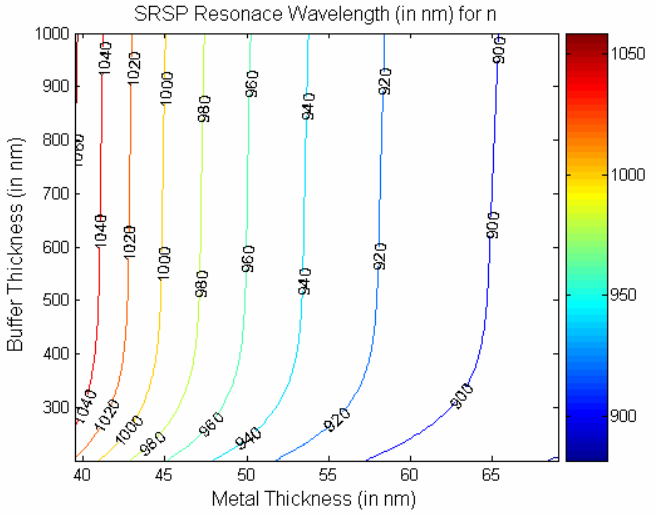

Figure 3.4 SRSP resonance wavelength for different gold and Teflon thicknesses for θ = 68° with ethanol as the base solution

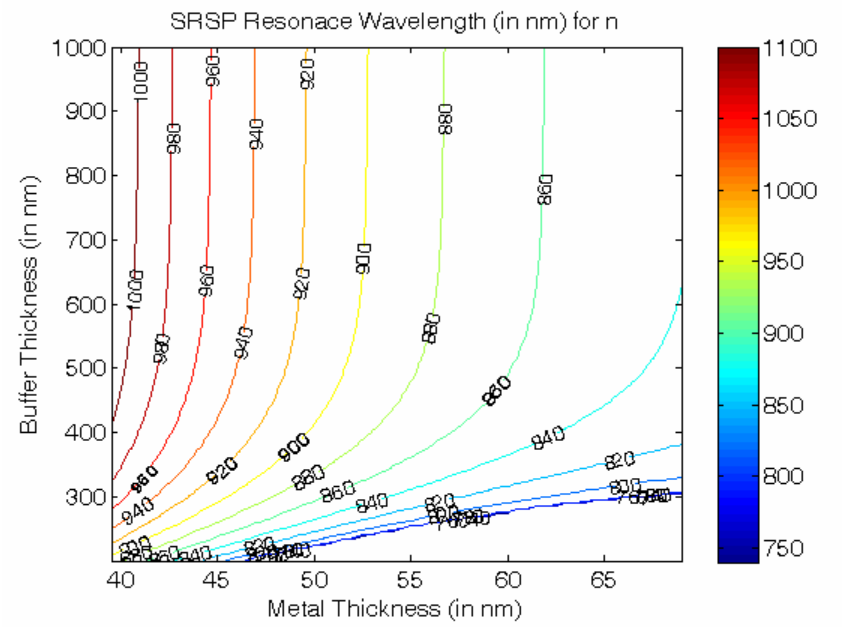

Figure 3.5 SRSP resonance wavelength for different gold and magnesium fluoride thicknesses for θ = 73° with ethanol as the base solution

Thinner gold placed the coupling to the LRSP at wavelengths around 550nm — the region where the dielectric constant of gold starts to increase toward more positive values, shown in Figure 3.9.

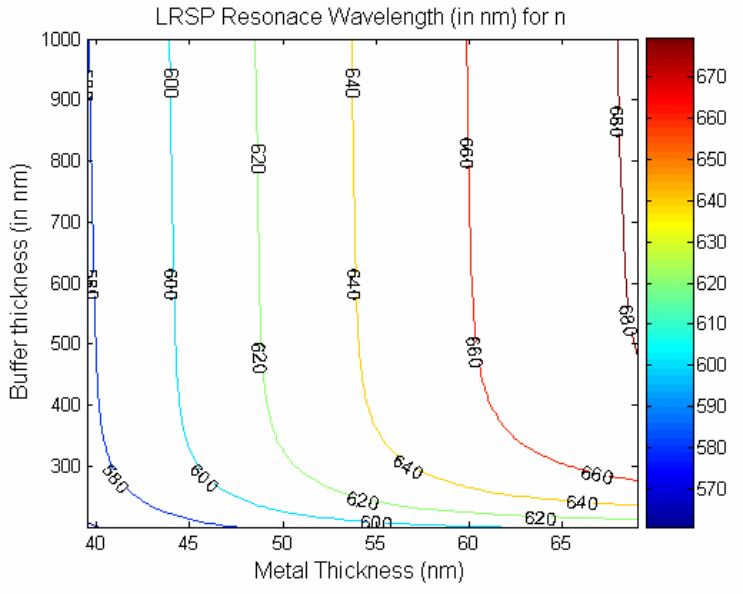

Figure 3.6 LRSP resonance wavelength for different gold and Teflon thicknesses for θ = 66° with water as the base solution

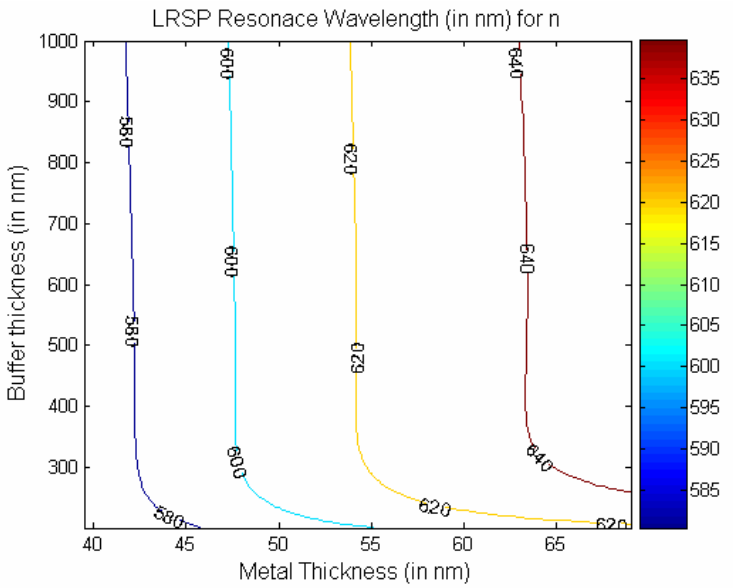

Figure 3.7 LRSP resonance wavelength for different gold and Teflon thicknesses for θ = 68° with ethanol as the base solution

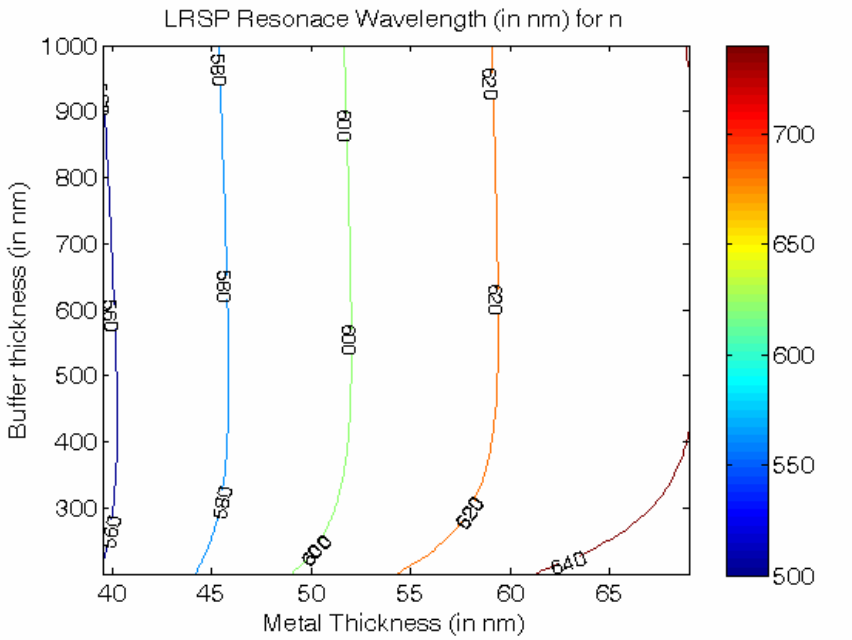

Figure 3.8 LRSP resonance wavelength for different gold and magnesium fluoride thicknesses for θ = 68° with ethanol as the base solution

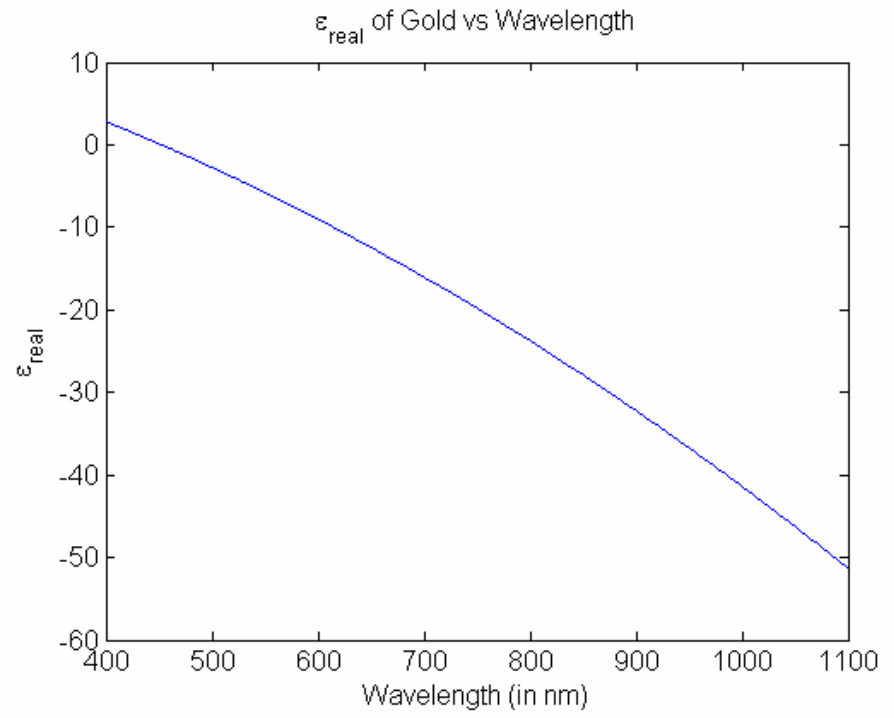

Figure 3.9 Variation of the real part of Gold's dielectric constant with wavelength

Hence thinner gold causes

a) Coupling to the SRSP mode beyond 1000nm where silicon detectors are unsuitable for use.
b) Coupling to the LRSP mode around 550 nm, a region where the dielectric constant of gold starts to become positive and a surface-plasmon wave is no longer supported.

3.2.2 Selection of maximum gold thickness

Gold thicker than 69nm made both bulk and surface sensitivities of LRSP decrease as indicated in Figure 3.10 and Figure 3.11.

(a) (b)

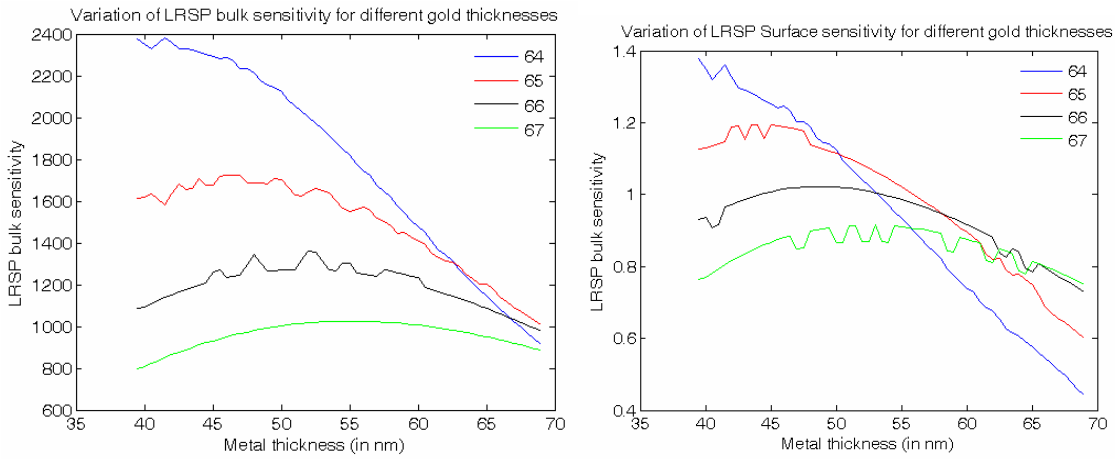

Figure 3.10 Variation of (a) LRSP bulk sensitivity and (b) LRSP surface sensitivity for different metal thickness using water as the base solution and Teflon thickness = 500nm with different incident angles. The ripples in the calculated sensitivities are due to rounding errors in interpolating the refractive index of water.

(a) (b)

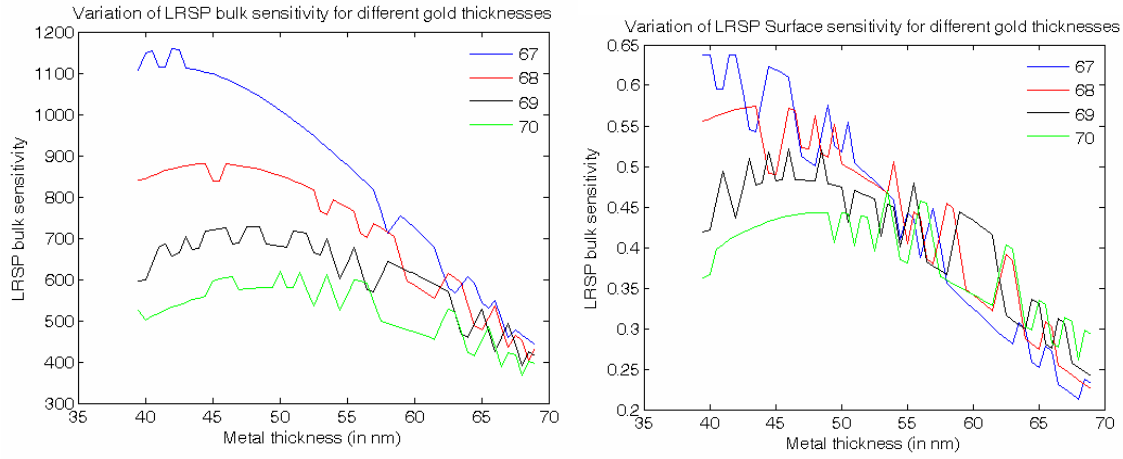

Figure 3.11 Variation of (a) LRSP bulk sensitivity and (b) LRSP surface sensitivity for different metal thickness using ethanol as the base solution and Teflon thickness = 500nm with different incident angles

Figure 3.12 and Figure 3.13 illustrate the difference in resonance wavelength between LRSP and SRSP for various gold and Teflon thickness combinations with different incident angles for water and ethanol respectively.

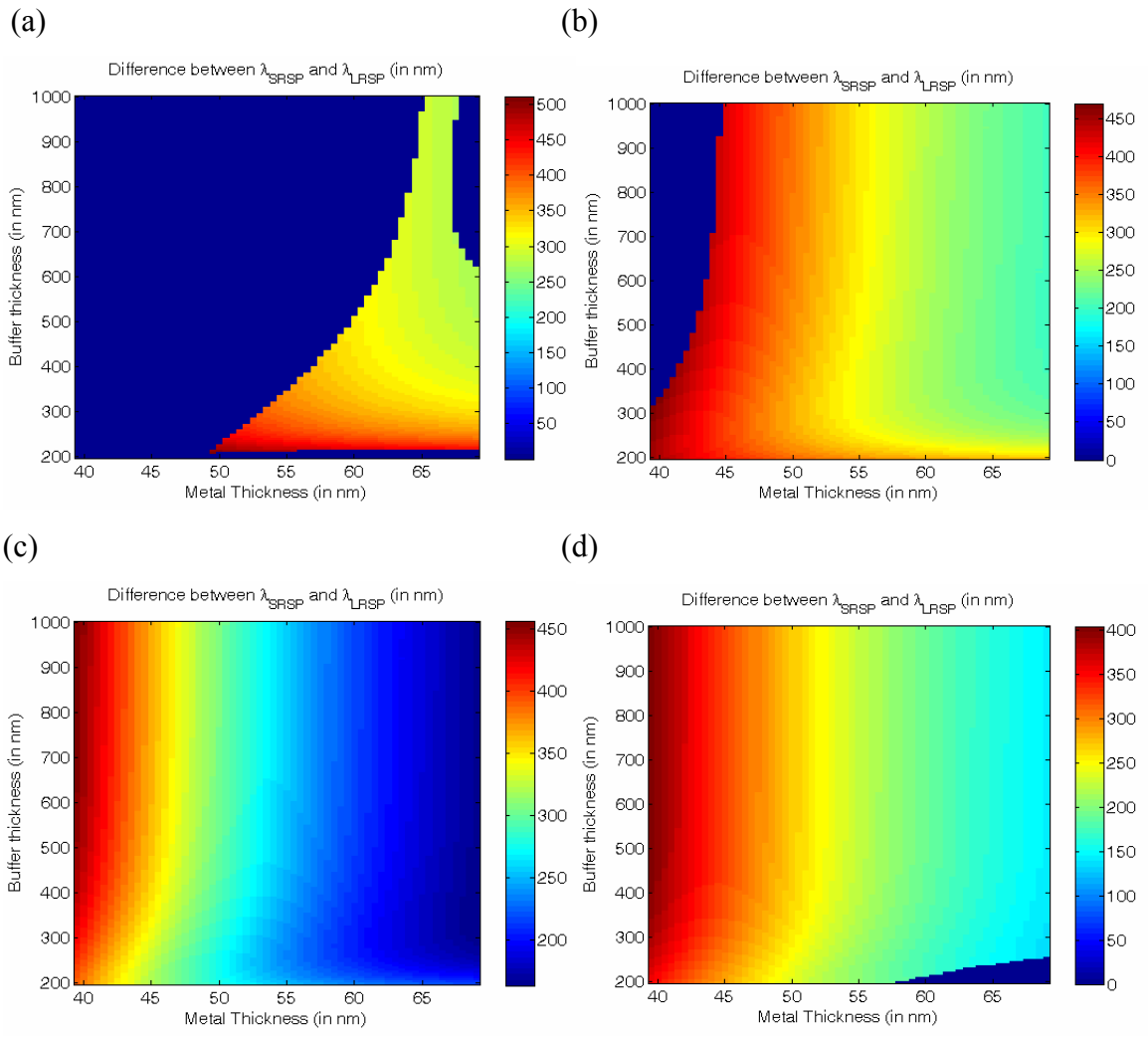

Figure 3.12 Difference in resonance wavelengths between SRSP and LRSP for (a) θ = 64°, (b) θ = 65°, (c) θ = 66° and (d) θ = 67° using water as the base solution for different gold and Teflon thicknesses

If the resonance wavelength of LRSP and/or SRSP is outside the range of the spectrometer, then the difference between λ_{SRSP} and λ_{LRSP} is assigned "0"

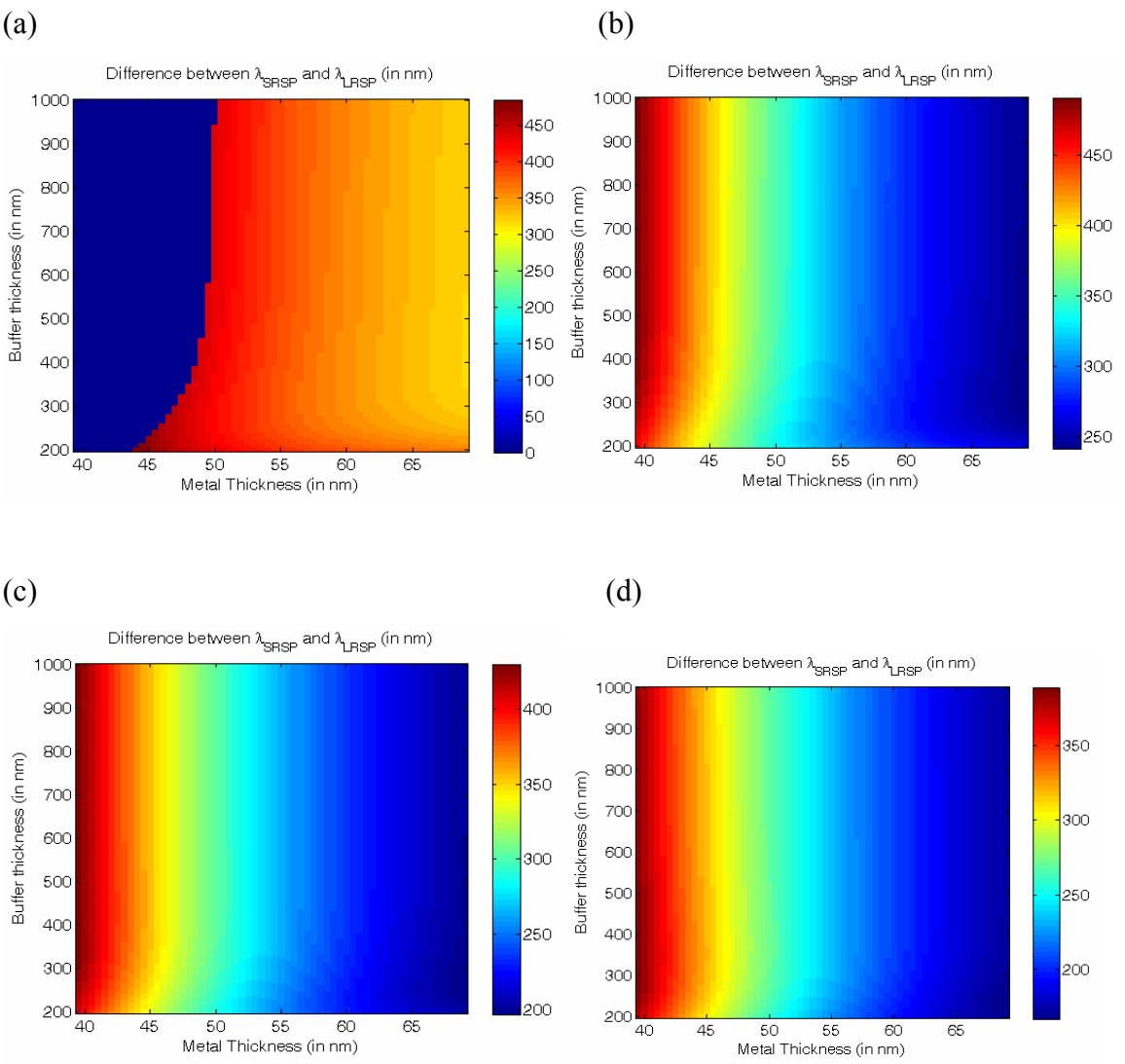

Figure 3.13 Difference in resonance wavelengths between SRSP and LRSP for (a) θ = 67°, (b) θ = 68°, (c) θ = 69° and (d) θ = 70° using ethanol as the base solution for different gold and Teflon thicknesses

Figure 3.12 and Figure 3.13 indicate a decrease in the difference between LRSP and SRSP resonance wavelengths with increasing gold thickness and with increasing incident angles using Teflon as the buffer layer.

If the resonance wavelength of LRSP and/or SRSP is outside the range of the spectrometer, then the difference between λ_{SRSP} and λ_{LRSP} is assigned "0"

Figure 3.14 and Figure 3.15 show the simulated reflectivity spectrum for a constant incident angle, constant Teflon thickness but with varying metal thicknesses using water and ethanol as the base solution respectively.

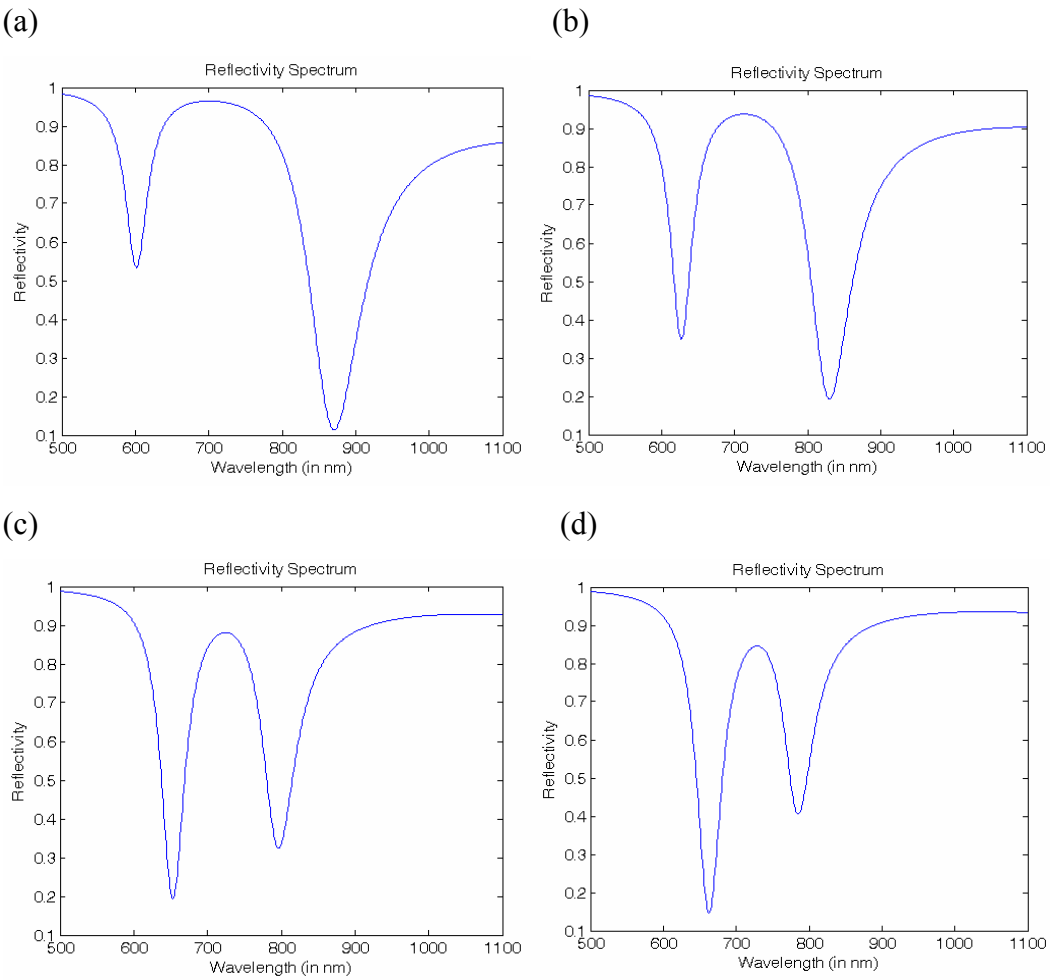

Figure 3.14 Reflectivity Spectrum indicating both Long range and Short range coupling for θ=67°, Teflon = 500nm using water as the base solution for different gold thicknesses (a) gold = 50nm, (b) gold = 58nm, (c) gold = 69nm and (d) gold = 75nm

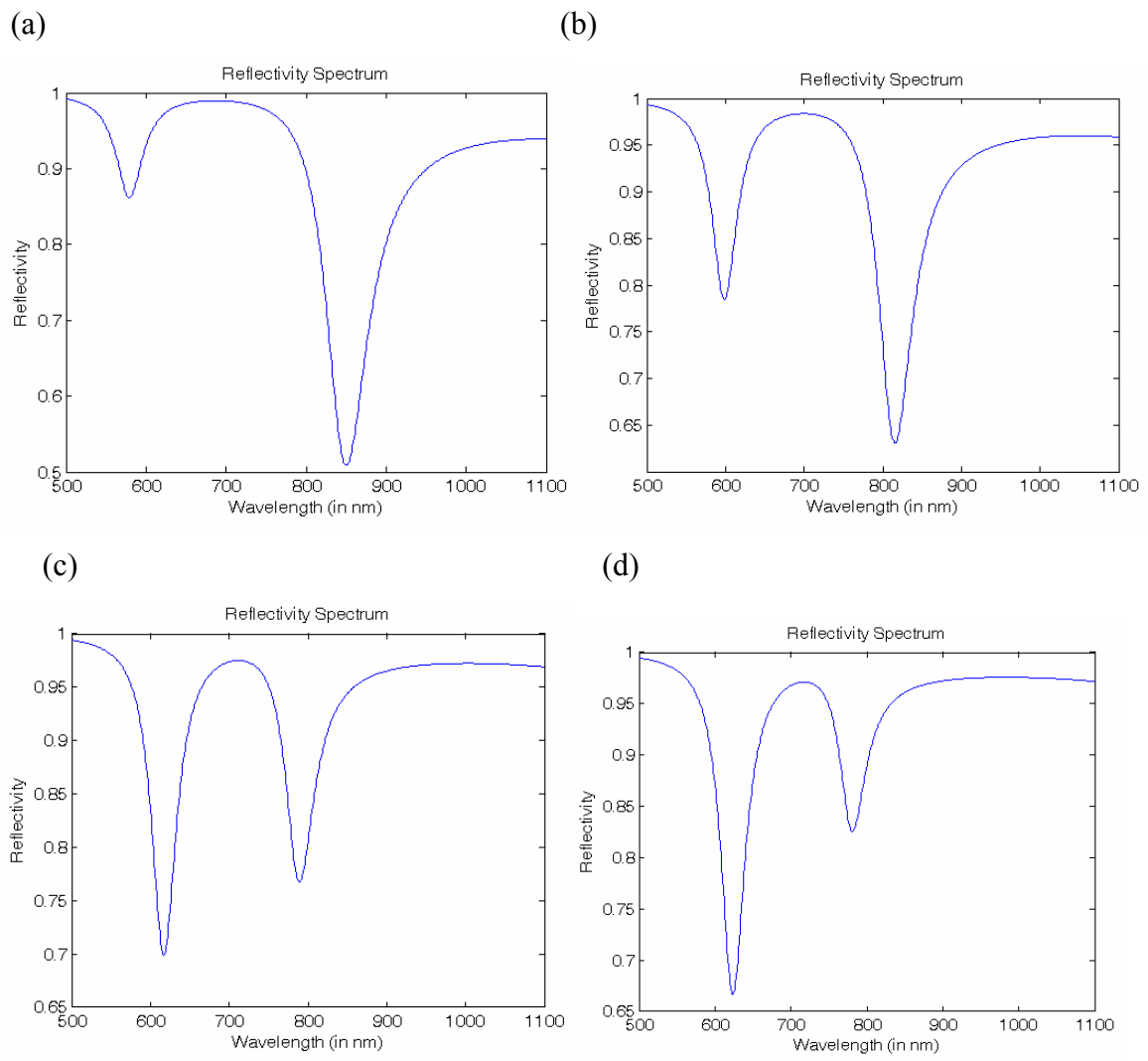

Figure 3.15 Reflectivity Spectrum indicating both Long range and Short range coupling for θ = 70°, Teflon = 500nm using Ethanol as the base solution for different gold thicknesses (a) gold = 50nm, (b) gold = 58nm, (c) gold = 69nm and (d) gold = 75nm

From Figure 3.14 and Figure 3.15, it is clear that as the resonance wavelength difference decreases, the two modes come closer to each other. This proximity in the resonance wavelengths causes difficulty in differentiating between the two modes which hinders in accurately finding the actual resonance wavelength.

Figure 3.14 and Figure 3.15 also indicate an increase in reflectivity in the Short range (SRSP) mode for thicker gold surfaces, indicating a relatively lower level of light coupling into the SRSP mode

Hence, thicker gold causes

a) Increase in the SRSP reflectivity,
b) decrease in LRSP sensitivity
c) SRSP and LRSP modes to interfere with one another as indicated by the decrease in the difference between the SRSP and the LRSP wavelengths.

From the above observations, the gold should be thick enough to allow the propagation of the two modes within the noise-free zone of the spectrometer (500-1000nm) and thin enough to avoid the interference between the two modes.

Hence, the range of Gold thickness for performing simulations was selected to vary between 39.5 and 69nm.

3.3 Selection of Teflon thickness range

Teflon is deposited on the sensor to achieve index matching on either side of the Gold layer, which allows for the propagation of two surface plasmon modes.

3.3.1 Selection of minimum Teflon thickness

Figure 3.16 and Figure 3.17 indicate the range of gold and Teflon thickness values for which the resonance wavelengths for both the LRSP and SRSP lie within the range of the spectrometer (indicated by areas in red).

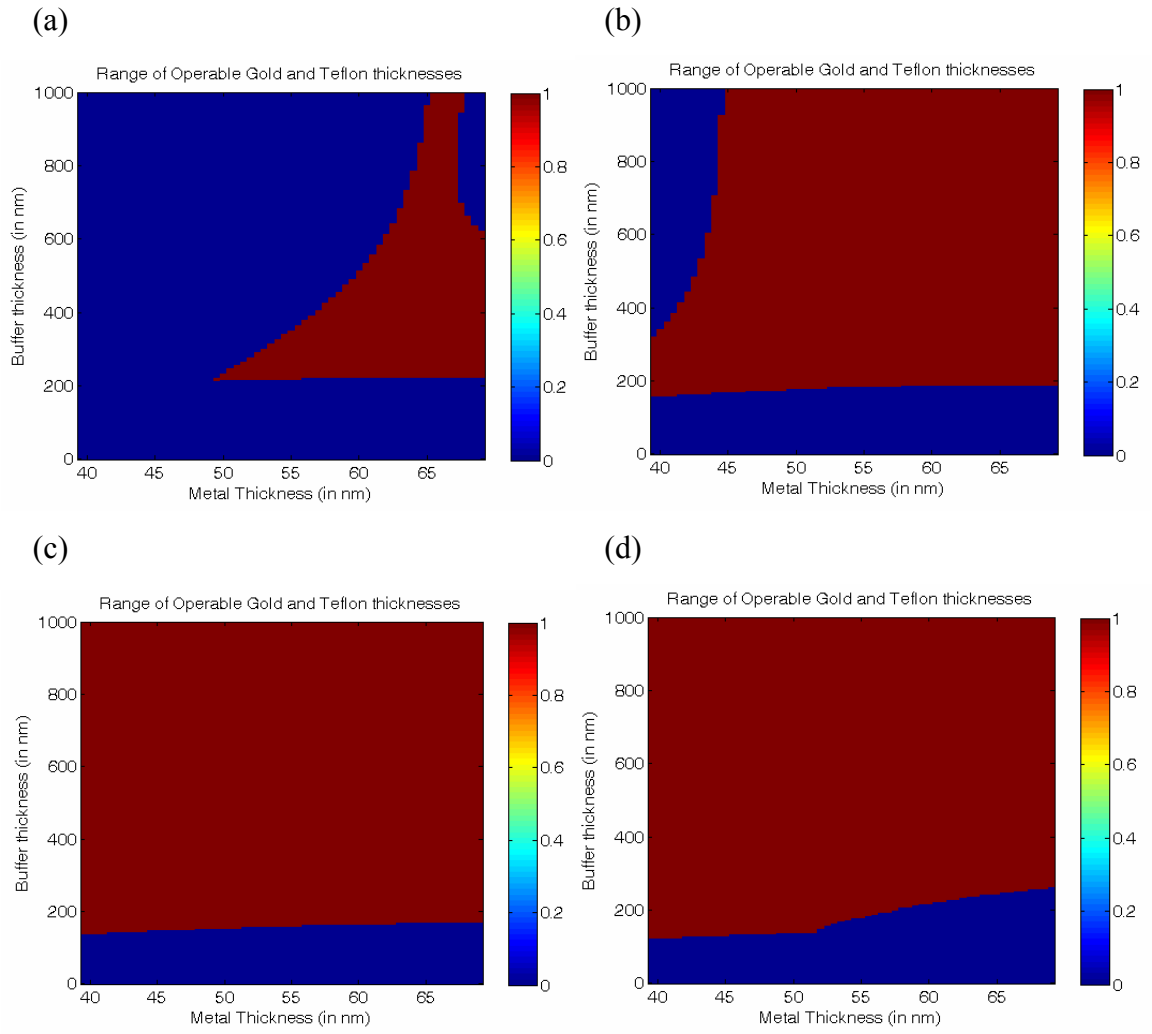

Figure 3.16 Range of gold and Teflon thicknesses for which both LRSP and SRSP wavelengths lie within the operating range using water as the base solution for (a) θ = 64°, (b) θ = 65°, (c) θ = 66° and (d) θ = 67°

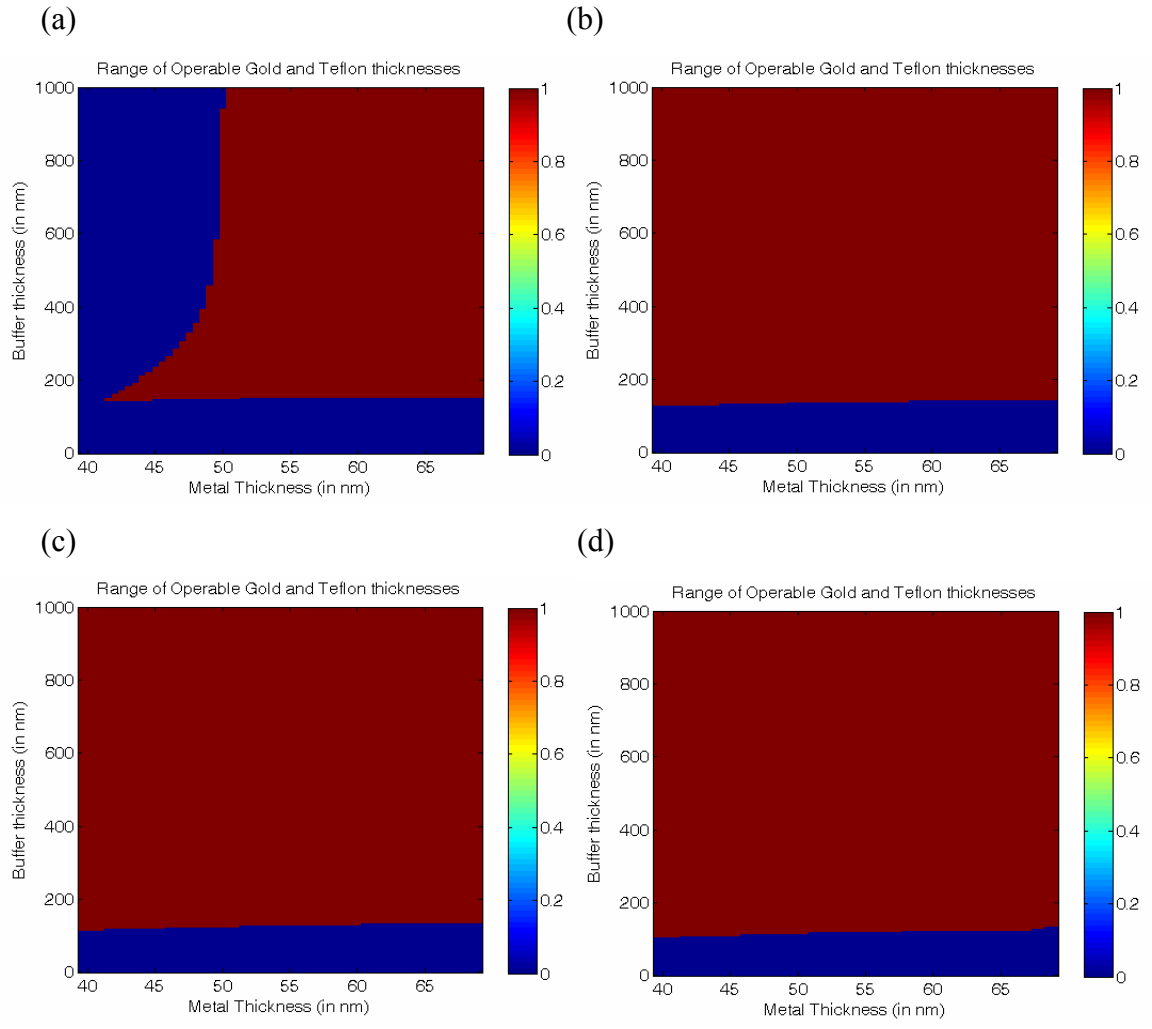

Figure 3.17 Range of gold and Teflon thicknesses for which both LRSP and SRSP wavelengths lie within the operating range using ethanol as the base solution for (a) θ = 67°, (b) θ = 68°, (c) θ = 69° and (d) θ = 70°

From the two figures, it is clear that for Teflon thickness greater than 200nm, both modes lie within the operable range of the spectrometer. Hence 200nm was chosen as the minimum Teflon thickness.

3.3.2 Selection of maximum Teflon thickness

Reflectivity of LRSP and SRSP increases as the Teflon layer gets thicker. This increase in reflectivity is illustrated in Figure 3.18 and Figure 3.19 for different combinations of gold and Teflon thicknesses using water or ethanol as the base solution for different incident angles.

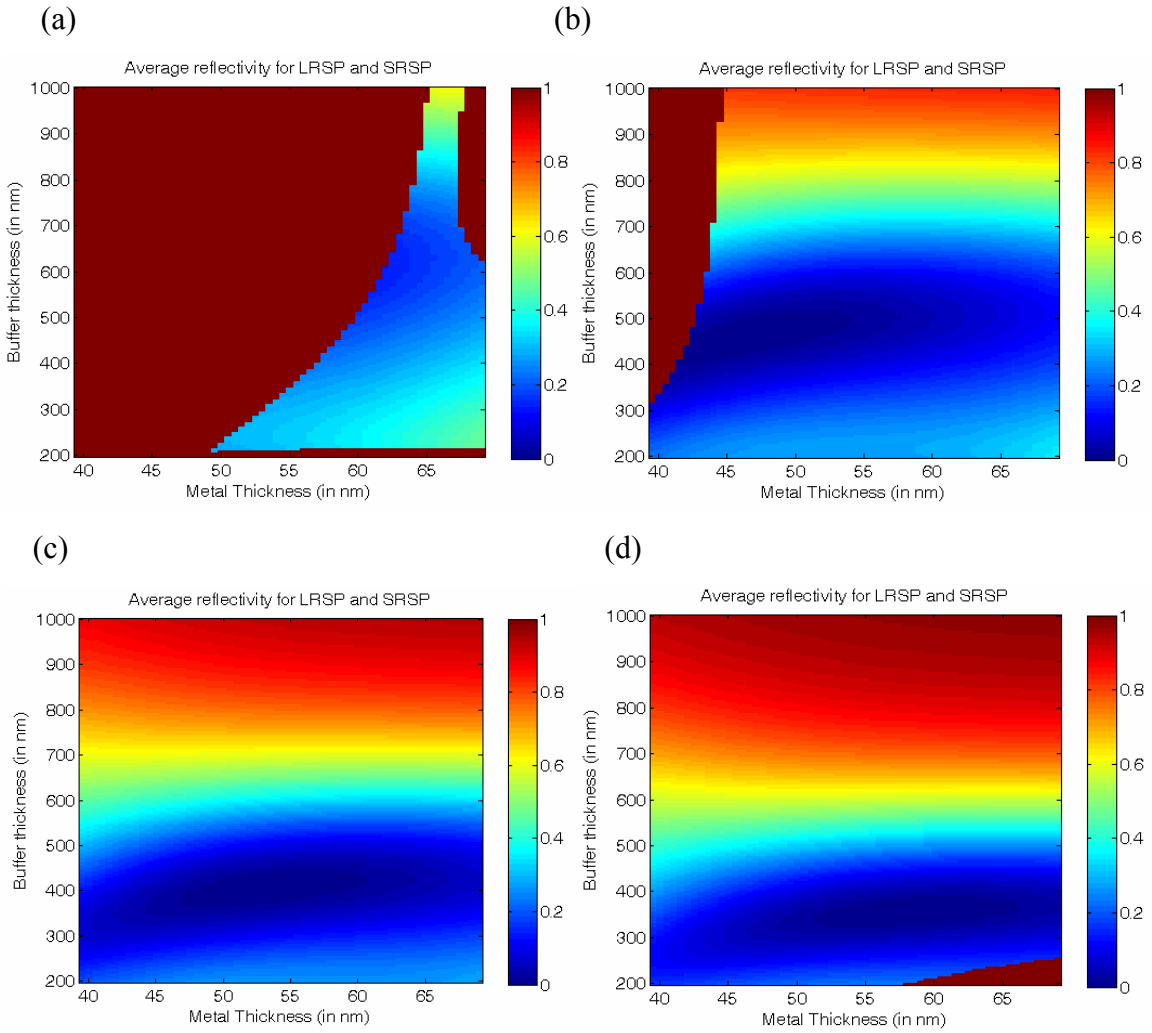

Figure 3.18 Average reflectivity of LRSP and SRSP for (a) θ = 64°, (b) θ = 65°, (c) θ = 66° and (d) θ = 67° for different gold and Teflon thicknesses using water as the solution

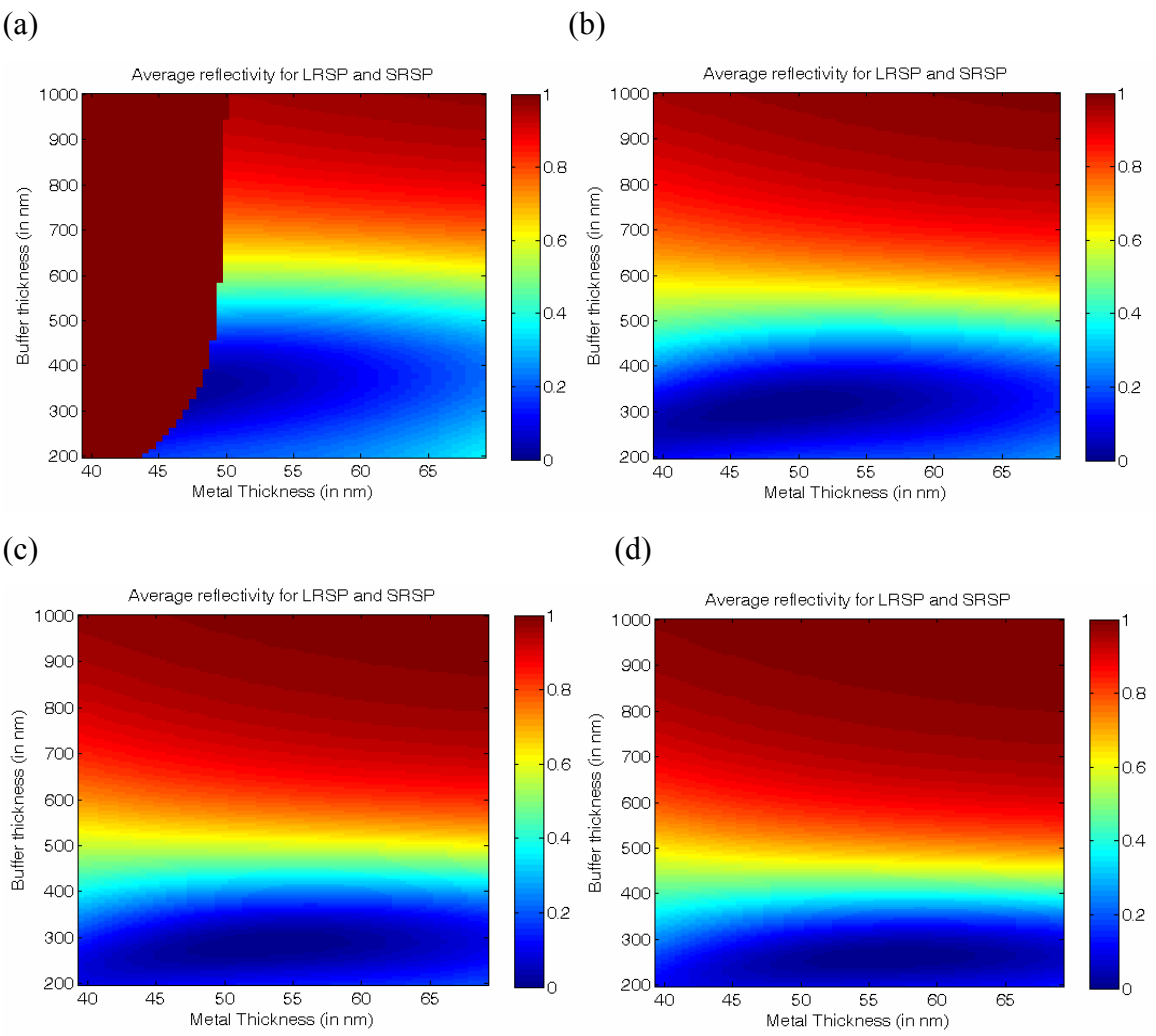

Figure 3.19 Average reflectivity of LRSP and SRSP for θ = 67°, (b) θ = 68°, (c) θ = 69° and (d) θ = 70° for different gold and Teflon thicknesses using ethanol as the solution

From Figure 3.16 — Figure 3.19, it is understood that Teflon should be thick enough to allow the propagation of the two modes within the operable range of the spectrometer and thin enough to achieve minimum reflectivity, so that maximum coupling into both surface plasmon waves is achieved.

Hence the range of Teflon thickness selected to perform simulations was varied between 200nm and 1000nm.

3.4 Selection of magnesium fluoride as the buffer layer

Magnesium fluoride is used as the buffer layer to provide better index matching when ethanol is used as the solution.

The thickness of magnesium fluoride is varied from 200-1000 nm, the same range as that of Teflon. The higher index of magnesium fluoride helps in achieving a better index matching than Teflon, when using ethanol as the solution. As seen in Figure 3.20, the index of ethanol matches better with magnesium fluoride than with Teflon.

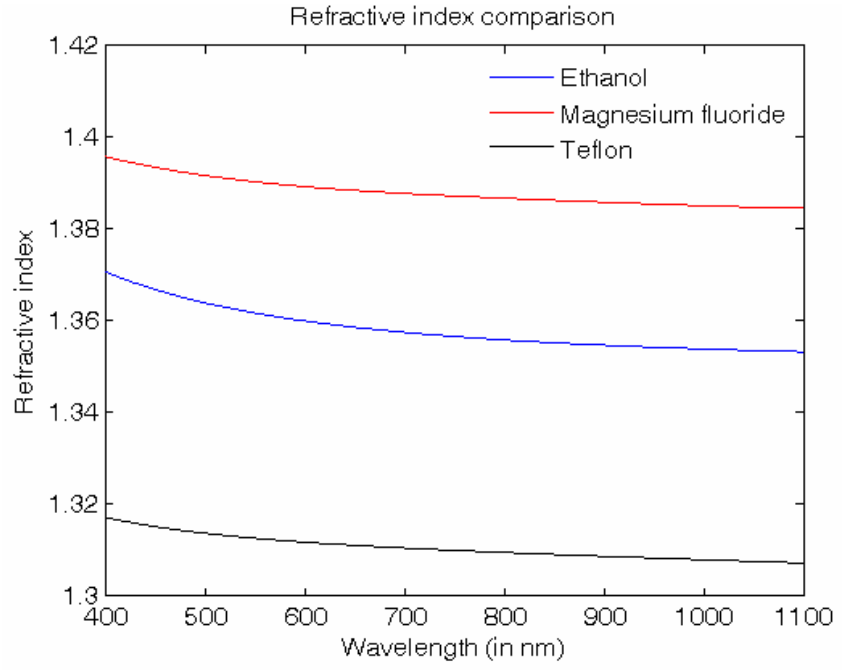

Figure 3.20 Comparison of refractive indices between ethanol, magnesium fluoride and Teflon

3.5 Algorithms

The algorithms used for optimizing the sensor performance were divided into two categories based on

1. Changes in the background solution index
2. Changes in the thickness of the layer binding to the sensor surface

Optimization was achieved by varying the thicknesses of the metal and the buffer layer and determining the corresponding sensitivity, reflectivity and the resonance wavelength.

3.5.1 Algorithm for determining the background solution index change for two surface plasmon modes, LRSP and SRSP

1. Input the following data:
    a) The wavelength range and its incremental value
    b) Angle of incident light
    c) Thickness range for buffer and metal layers
    d) Change in the background refractive index
    e) The operating wavelength range for a particular mode
    (ex) 500-750 nm for LRSP and 750-1075 nm for SRSP

2. Calculate the dielectric constant, refractive index, the incident angle and the propagation constant for the prism, buffer, metal, layer (if any) and solution in that order.

3. The transmission and the reflection matrices were calculated for each design.

4. From the reflectivity values, the approximate minimum was determined.

5. If the approximate resonance wavelength lies within the range resolved by the spectrometer, the steps (6)-(8) were taken, else
    a) Reflectivity = 1
    b) Resonance wavelength = 0

6. The exact minimum value of the reflectivity (i.e., the point at which the the incident light couples most strongly to the surface plasmon wave) was determined by fitting a parabola. The parabola was fitted around the approximate resonance wavelength. This fitting was done by taking a user assigned range of wavelengths on either side of the resonance and calculating the exact number of points based on the wavelength increment.

A parabola was then fitted using MATLAB's *polyfit* function with the approximate resonance wavelength as the midpoint of the fitting.

7. From this fitted parabola, the actual reflectivity minimal point was determined.

8. The minimum reflectivity ($refl_n$) and the resonance wavelength (λ_n) were stored for that particular design.

9. For a background index change of Δn ("deln"), the corresponding refractive index, theta, and the propagation constant were determined.

10. Steps (3)-(6) were repeated for an index change of Δn.

11. The minimum reflectivity ($refl_{n0}$) and resonance wavelength (λ_{n0}) corresponding to a Δn index change was stored for that particular design.

    a) Sensitivity was calculated based on the following conditions
    b) Both the resonance wavelengths were not zero
    c) $\lambda_{n0} > \lambda_n$ was true (assuming positive sensitivity)

12. If the conditions in step (11.a)) were true, Sensitivity = $(\lambda_n - \lambda_{n0})/ \Delta n$

    Where Δn was the change in the background (or) bulk layer index change

If the conditions were false, Sensitivity = 0

13. In the event of the reflectivity minimum occurring outside the spectrometer range,

    a) Sensitivity = 0
    b) Reflectivity = 1
    c) Resonance Wavelength = 0

3.5.2 Algorithm for determining the surface layer thickness change for two surface plasmon modes, LRSP and SRSP

1. Input the following data:
    a) The wavelength range and its incremental value
    b) Angle of incidence of the light
    c) Thickness of the buffer, metal and surface layer
    d) The operating wavelength range for a particular mode
       (ex) 500-750 nm for LRSP and 750-1075 nm for SRSP

2. Calculate the dielectric constant, refractive index, the incident angle and the propagation constant for the prism, buffer, metal, layer (if any) and solution in that order.

3. The transmission and the reflection matrices were calculated for each design.

4. From the reflectivity values, the approximate minimum was determined.

5. If the approximate resonance wavelength lies within the range resolved by the spectrometer, the steps (6)-(8) were taken, else
    a) Reflectivity = 1
    b) Resonance wavelength = 0

6. The exact minimum value of the reflectivity (i.e., the point at which the incident light couples most strongly to the surface plasmon wave) was determined by fitting a parabola. The parabola was fitted around the approximate resonance wavelength. This fitting was done by taking a user assigned range of wavelengths on either side of the resonance and calculating the exact number of points based on the wavelength increment. A parabola was then fitted using MATLAB's *polyfit* function with the approximate resonance wavelength as the midpoint of fitting

7. From this fitted parabola, the actual reflectivity minimal point was determined.

8. The minimum reflectivity ($refl_n$) and the resonance wavelength (λ_n) were stored for that particular design.

9. Steps (3) – (7) were performed for a change in the surface layer thickness and the corresponding minimum reflectivity ($refl_{t1}$) and wavelength (λ_{t1}) were determined.

10. Sensitivity was calculated based on the following conditions
    a) More than one layer thickness, i.e., the surface layer thickness varies

b) Both the resonance wavelengths values were not zero

c) $\lambda_{t1}>\lambda_{t0}$ was true

11. If the conditions in step(10) were true,

Sensitivity = $(\lambda_{t1}-\lambda_{t0})/(t1-t0)$

Where ‘t1’ and ‘t0’ were the surface layer thicknesses

If the conditions were false,

Sensitivity = 0

12. In the event of the reflectivity minimum occurring outside the spectrometer range,

a) Sensitivity = 0

b) Reflectivity = 1

c) Resonance Wavelength = 0

3.6 Optimization results

To get better performance from the fabricated sensor, we need to optimize the thickness of the metal (gold) and buffer (Teflon/MgF2) layers. For an optimized performance, the sensor should have

a) high sensitivity
b) low reflectivity
c) Resonance wavelengths lying within the low noise region of the spectrometer,
d) well separated resonance wavelengths

In general we will find that

a) sensitivity is determined by the thickness of the gold layer
b) reflectivity is determined by the thickness of the Teflon layer and
c) the distance between the resonance wavelengths is determined by the thickness of the gold layer

The goal is to obtain optimized gold and Teflon thickness is by finding

1. theta (angle inside the prism) values for which the two modes have their resonance wavelength within the range of the spectrometer
2. maximum bulk and surface sensitivities at each angle
3. range of metal and buffer thicknesses to obtain maximum sensitivity
4. range of buffer thickness to obtain minimum reflectivity (metal thickness does not significantly affect reflectivity)
5. range of metal and buffer thickness to obtain minimum reflectivity and maximum sensitivity for the two modes, LRSP and SRSP, considered separately. In other words, the thickness ranges of LRSP and SRSP are independent of one another.
6. range of metal and buffer thickness to obtain minimum reflectivity and maximum sensitivity for the two modes, LRSP and SRSP, considered together, implying the thickness ranges obtained from the previous step is slightly increased or decreased to accommodate the performance from the other mode.

3.6.1 Using water as the base solution

Optimization using water as the base solution and gold (metal) thickness varying from 39.5 to 69 nm and the Teflon (buffer) thickness varying from 200 to 1000nm provided the following results:

a) Only for theta ranging from 64° to 67°, the resonance wavelength was within the range resolved by the spectrometer. ("theta" indicates the angle of the light hitting the sensor inside the prism)
b) The maximum sensitivity for both LRSP and SRSP decreases as the value of "theta" increases, as shown in Table 3.1

	Max. Bulk Sensitivity (nm/RIU)		Max. Surface Sensitivity (nm/nm)	
Theta	LRSP	SRSP	LRSP	SRSP
64	2500	16000	1.5	5.5
65	1800	9000	1.25	4.5
66	1300	6600	1.1	3.9
67	1100	4500	0.9	3

Table 3.1 Maximum bulk and surface sensitivity for LRSP and SRSP using water as the base solution and Teflon-AF as the buffer layer for different incident angles

Figure 3.21 through Figure 3.24 illustrate the simulated bulk and surface sensitivity for LRSP and SRSP over the entire range of gold and Teflon thicknesses

(a) (b)

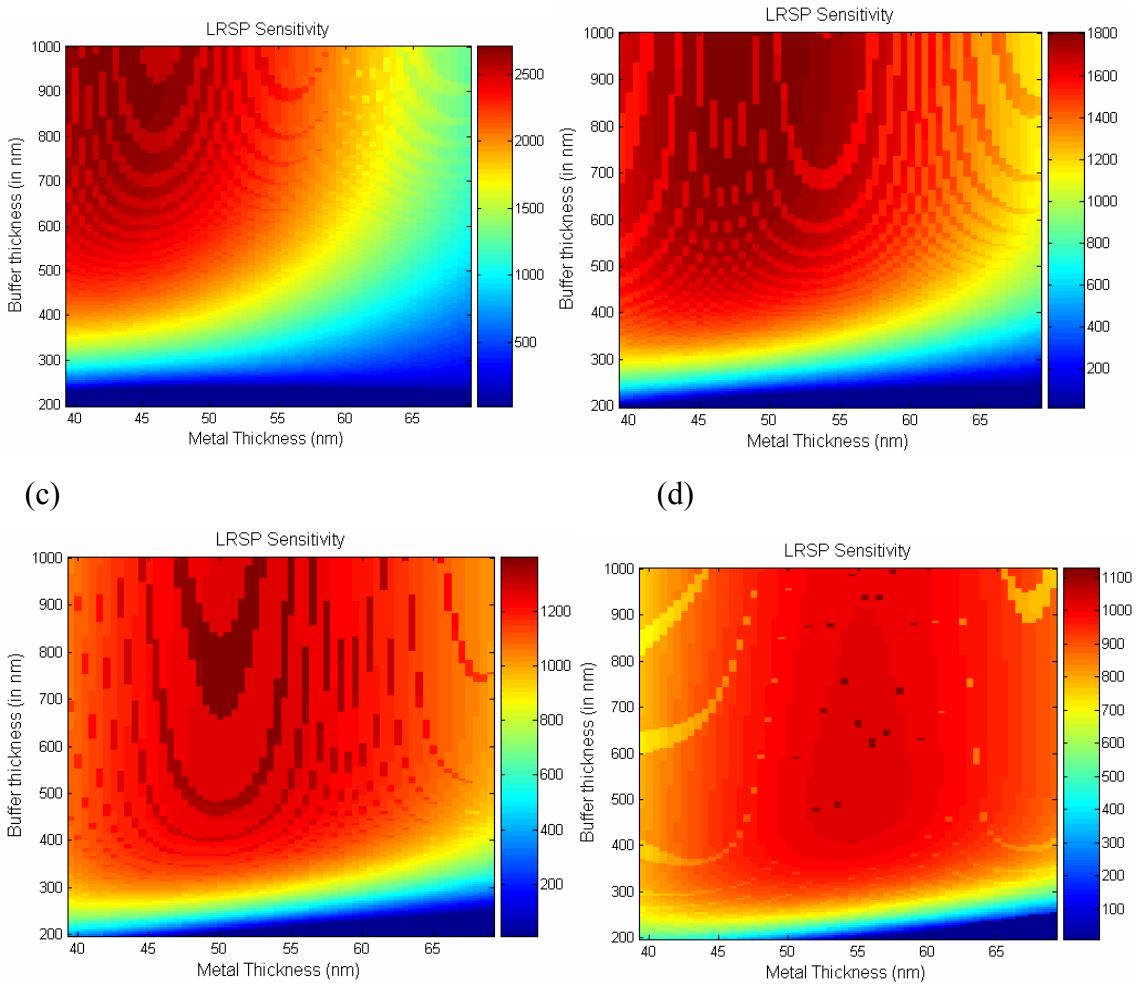

Figure 3.21 LRSP bulk sensitivity for different gold and Teflon thicknesses for different angles using water as the base solution – (a) θ = 64°, (b) θ = 65°, (c) θ = 66° and (d) θ = 67°

If the resonance wavelength of any design is outside the range of the spectrometer, then the sensitivity, the reflectivity and the resonance wavelength were assigned a predefined value, i.e, Sensitivity = 0, Reflectivity = 1, Resonance wavelength = 0

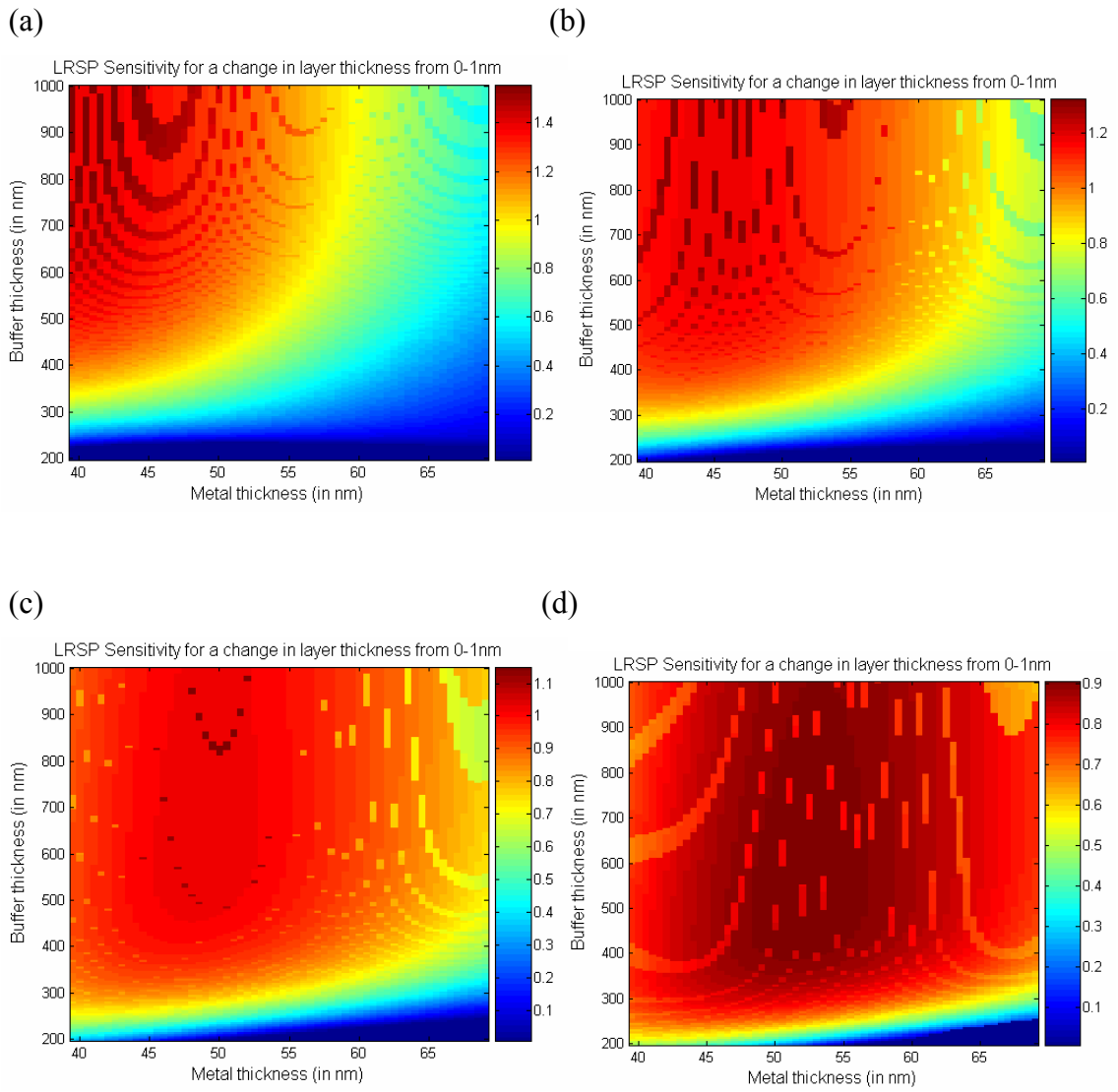

Figure 3.22 LRSP surface sensitivity for different gold and Teflon thicknesses for different angles using water as the base solution – (a) θ = 64°, (b) θ = 65°, (c) θ = 66° and (d) θ = 67°

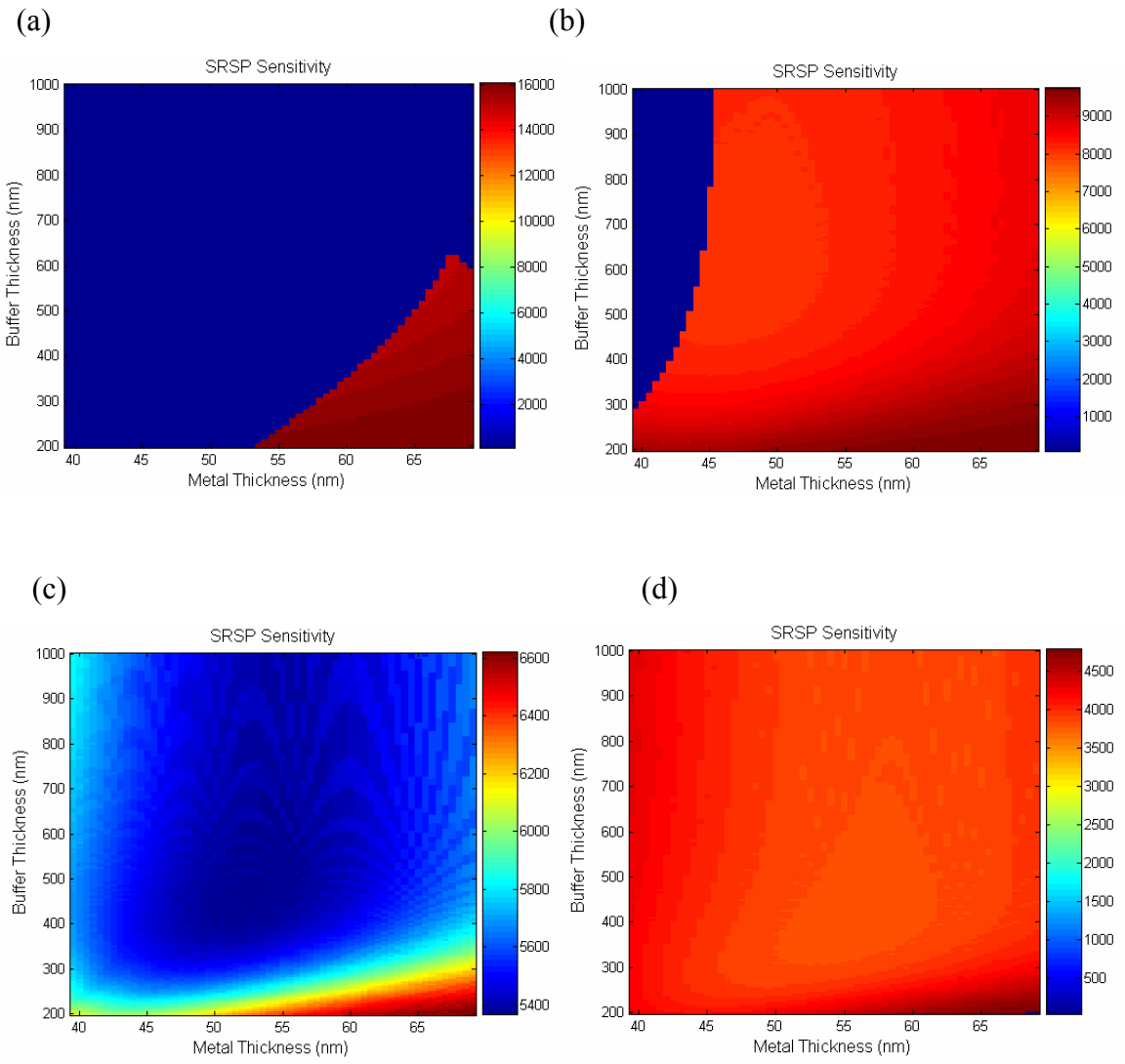

Figure 3.23 SRSP bulk sensitivity for different gold and Teflon thicknesses for different angles using water as the base solution – (a) θ = 64°, (b) θ = 65°, (c) θ = 66 ° and (d) θ = 67°

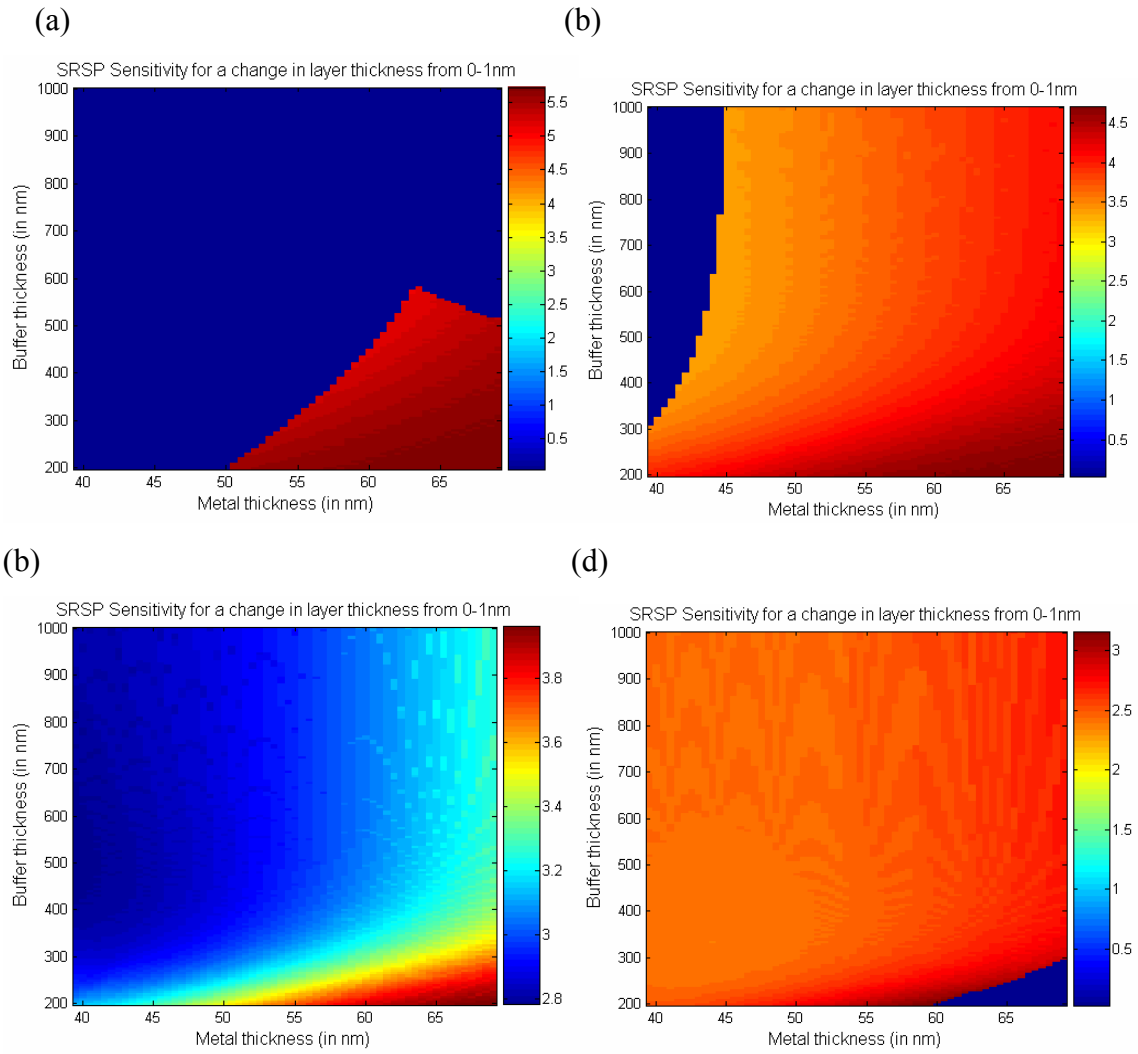

Figure 3.24 SRSP Surface sensitivity for different gold and Teflon thicknesses for different angles using water as the base solution – (a) θ = 64°, (b) θ = 65°, (c) θ = 66° and (d) θ = 67°

From these simulations we can make several general observations:

1. The SRSP bulk and surface sensitivities are fairly constant over the entire range of gold and Teflon thicknesses for the four different angles. In addition, the LRSP bulk and surface sensitivities are close to their highest values over a broad range of design parameters. The range of gold and Teflon thicknesses needed to achieve high sensitivity (bulk and surface) is given in Table 3.2

	LRSP		SRSP	
	Thickness range (in nm)		Thickness range (in nm)	
Theta	Teflon	Gold	Teflon	Gold
64	400-1000	39.5-55	200-600	55-69
65	350-1000	39.5-60	200-1000	39.5-69
66	300-1000	39.5-60	200-275	55-69
67	250-1000	45-69	200-1000	39.5-69

Table 3.2 Range of gold and Teflon thicknesses needed to achieve high bulk sensitivity for LRSP and SRSP using water as the base solution for different incident angles

2. From the simulated data, the sensitivity of SRSP remained relatively constant for the entire range of gold and Teflon layer thicknesses (for $\theta = 64$, data was out of range for other thickness values and for $\theta = 66$, the range of SRSP sensitivities is not large and the thickness range indicated is for the maximum. possible sensitivity) and hence reflectivity became major factor in determining the operating range of gold and Teflon thicknesses as far as SRSP is concerned.

3. The range of Teflon thicknesses having minimum reflectivity (<0.4) for the four different angles and for the entire range of gold thickness (as gold thickness does not strongly affect the reflectivity) is shown in Table 3.3

	Teflon thickness range (in nm)	
Theta	LRSP	SRSP
64	450-700	200-600
65	300-550	200-700
66	250-450	200-600
67	200-400	200-500

Table 3.3 Range of Teflon thickness needed to achieve minimum reflectivity for LRSP and SRSP using water as the base solution for different incident angles

LRSP and SRSP reflectivity for the entire range of gold and Teflon thickness is given in Figure 3.25 and Figure 3.26.

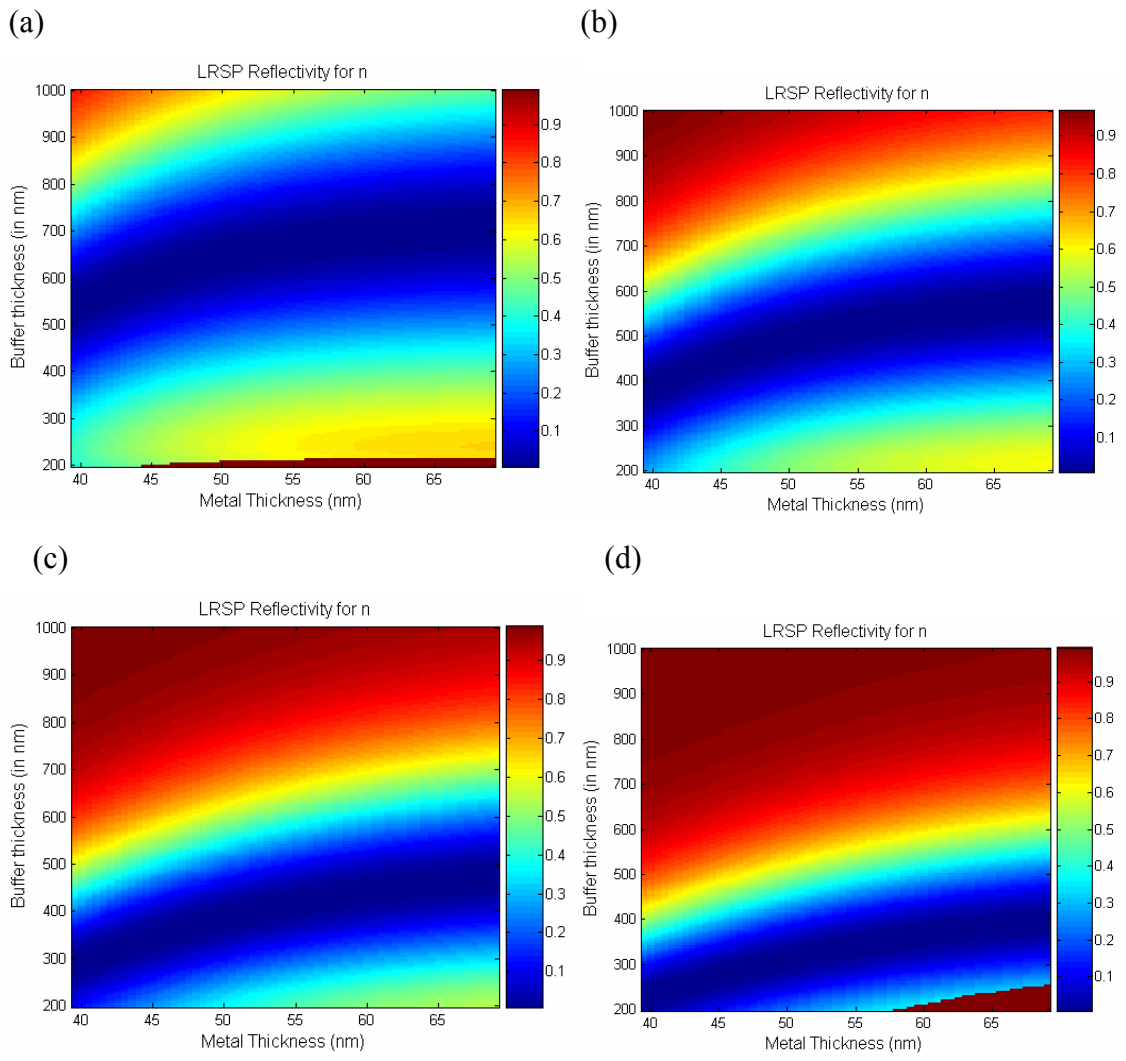

Figure 3.25 LRSP reflectivity for different gold and Teflon thicknesses for different angles using water as the base solution – (a) θ = 64°, (b) θ = 65°, (c) θ = 66° and (d) θ = 67°

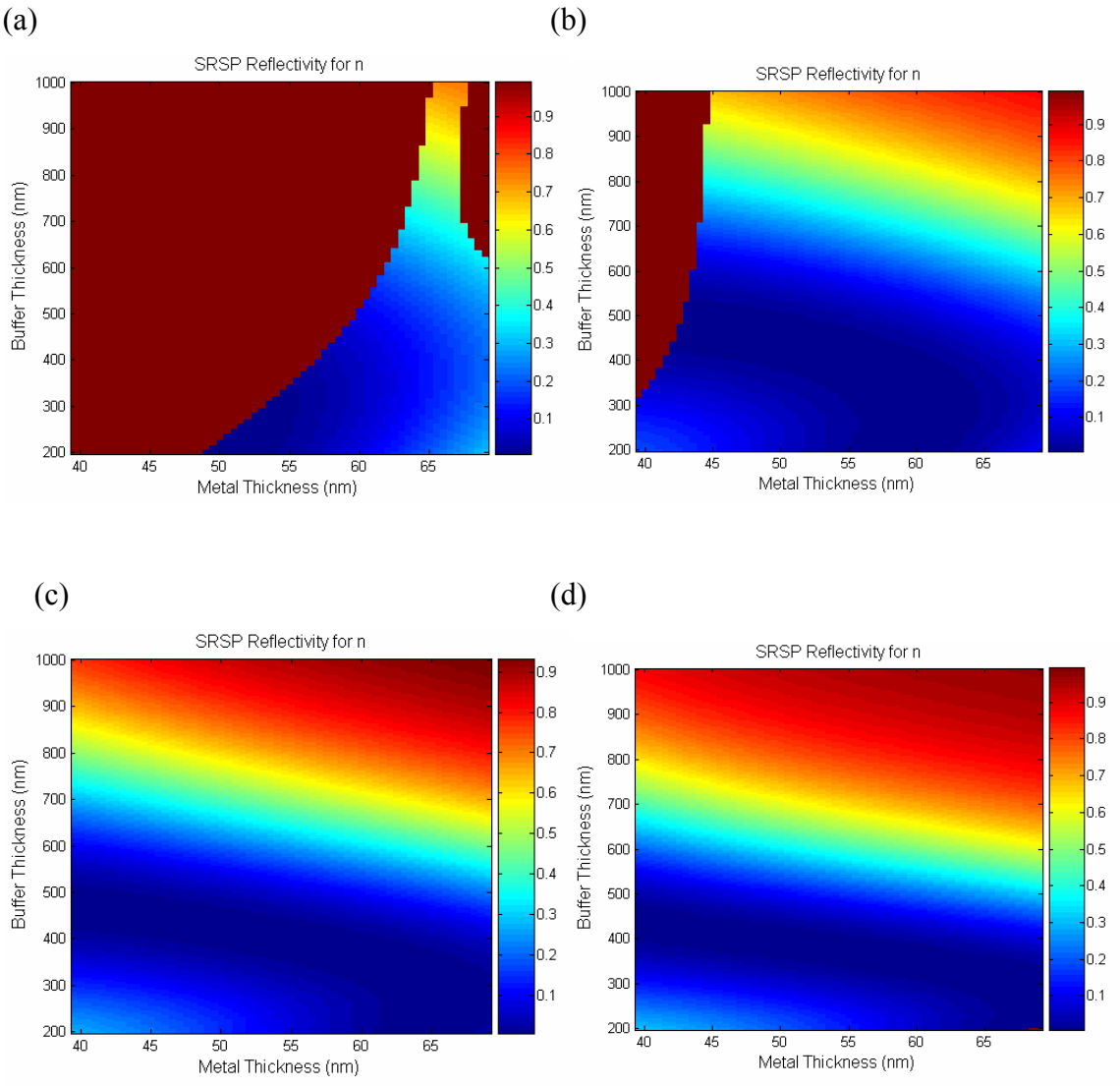

Figure 3.26 SRSP reflectivity for different gold and Teflon thicknesses for different angles using water as the base solution – (a) θ = 64°, (b) θ = 65°, (c) θ = 66° and (d) θ = 67°

To achieve high sensitivity and low reflectivity, we need the following range of gold and Teflon thicknesses for the four different incident angles. The data in Table 3.4 is obtained by taking the sensitivity and the reflectivity of each mode individually.

	LRSP		SRSP	
	Thickness range (in nm)		Thickness range (in nm)	
Theta	Teflon	Gold	Teflon	Gold
64	400-750	39.5-55	200-600	55-69
65	300-600	39.5-60	200-600	39.5-69
66	300-550	39.5-63	200-600	39.5-69
67	300-450	45-69	200-550	39.5-69

Table 3.4 Range of gold and Teflon thickness to achieve high sensitivity and low reflectivity using water as the base solution with the two modes considered separately

From Table 3.4, we can see that the range of thickness needed to achieve optimal performance for LRSP and SRSP modes are different. This difference necessitates us to further modify the thickness ranges so that both the modes have optimal performance simultaneously.

	Thickness Range (in nm)		Reflectivity		Resonance wavelength Range (in nm)		
Theta	Teflon	Gold	LRSP	SRSP	LRSP	SRSP	Diff in λ
64	375-600	55-69	0.4-0	0-0.3	700-765	1060-1030	360-265
65	300-600	39.5-69	0.4-0.2	0-0.2	600-710	1040-920	440-210
66	300-550	39.5-69	0-0.4	0-0.2	580-680	1020-840	440-160
67	300-450	45-69	0-0.35	0-0.15	565-650	900-800	335-150

Table 3.5 Range of gold and Teflon thicknesses along with LRSP and SRSP reflectivity and resonance wavelength range for optimal performance using water as the base solution with the two modes considered simultaneously

The optimized thickness range when the two modes are considered simultaneously is shown in Table 3.5. This table also provides reflectivity, resonance wavelength range and the difference in the resonance wavelengths between LRSP and SRSP for the four different angles for the range of thicknesses considered.

From Table 3.5, the range of Teflon thickness varies approximately from 300-600 nm and the thickness of gold from 39.5-69 nm (for some angles), which is the entire range of gold thickness used in the simulations. Therefore, the determining factor in selecting the thickness of the gold is the resonance wavelength of the two modes.

LRSP resonance wavelengths range from 565-765 nm and hence the resonance wavelength is approaching the positive dielectric constant range of gold (refer Figure 3.9). Gold layers thicker than 39.5nm move λ_{LRSP} into higher wavelengths, as shown in Figure 3.27 .

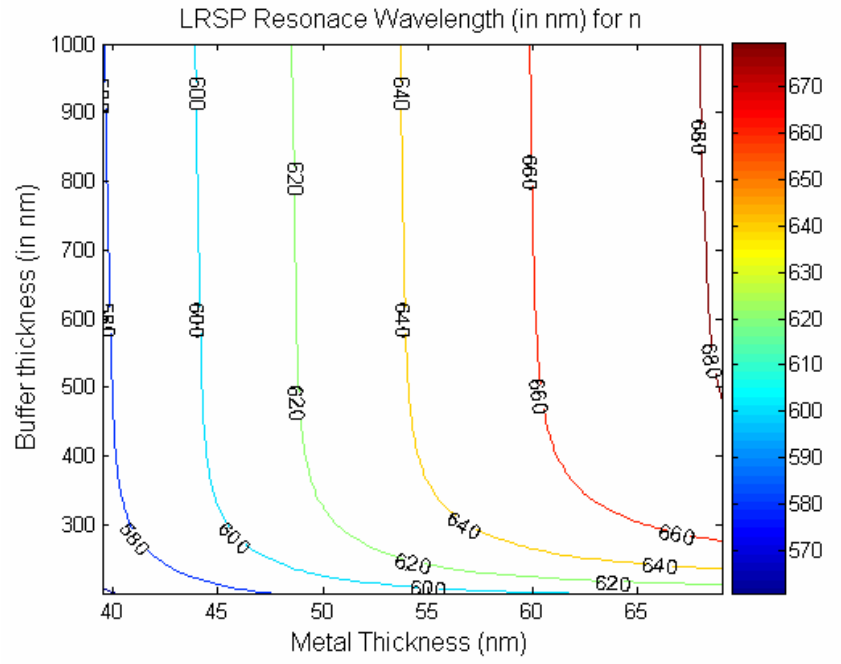

Figure 3.27 Resonance wavelength range for LRSP for θ = 66° using water as the base solution

SRSP resonance wavelengths range from 800-1060 nm, the higher end of which lies in the noisy part of the spectrometer. To get λ_{SRSP} within the low noise wavelength range of the spectrometer, gold layers thinner than 69nm had to be employed. Gold layers thinner than 69nm helped to move λ_{SRSP} into shorter wavelengths, as shown in Figure 3.28 .

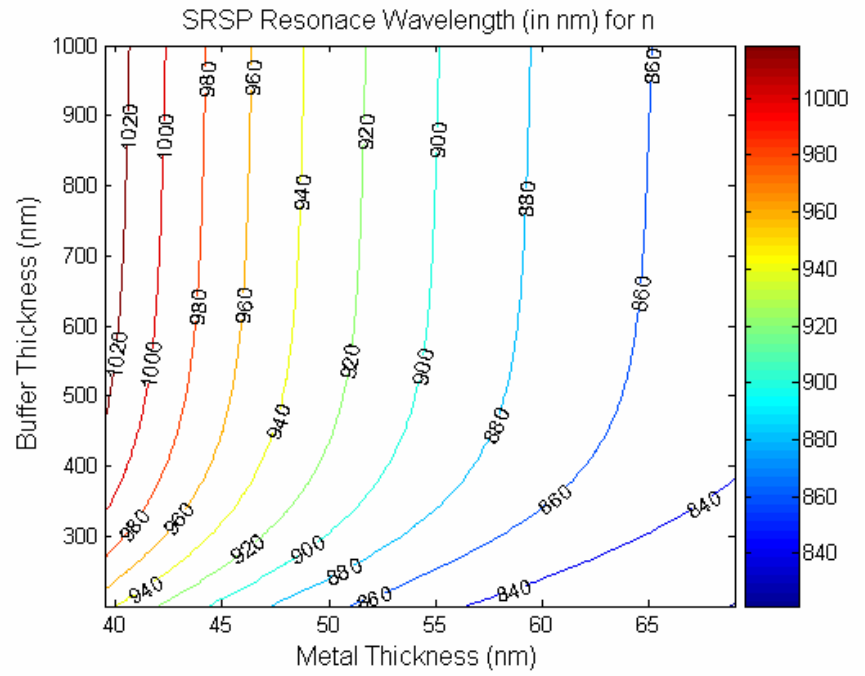

Figure 3.28 Resonance wavelength range for SRSP for θ = 66° using water as the base solution

3.6.1.1 Optimized thickness range for Teflon and gold

Based on the above results, a Teflon thickness around 500nm and gold thickness around 55nm was employed for optimized operation of achieving high sensitivity, low reflectivity and resonance wavelength at the low noise zone of the spectrometer

3.6.2 Using Ethanol as the base solution

The optimization results using ethanol as the base solution and the gold (metal) varying from 39.5 to 69 nm and the Teflon (buffer) thickness varying from 200 to 1000nm provided the following results:

a) Only for theta = 67°, 68°, 69°, 70°, the resonance wavelength was within the range resolved by the spectrometer. ("theta" indicates the angle of the light hitting the sensor inside the prism)
b) The maximum sensitivity for both LRSP and SRSP decreases as the value of "theta" increases as shown in Table 3.6.

	Max. Bulk Sensitivity (nm/RIU)		Max. Surface Sensitivity (nm/nm)	
Theta	LRSP	SRSP	LRSP	SRSP
67	1200	13000	0.6	4.5
68	850	8500	0.55	3.5
69	700	6200	0.5	3
70	625	4650	0.45	2.5

Table 3.6 Maximum bulk and surface sensitivity for LRSP and SRSP using ethanol as the base solution and Teflon-AF as the buffer layer for different incident angles

Figure 3.29 – Figure 3.32 illustrate the bulk and surface sensitivity for LRSP and SRSP over the entire range of gold and Teflon thickness

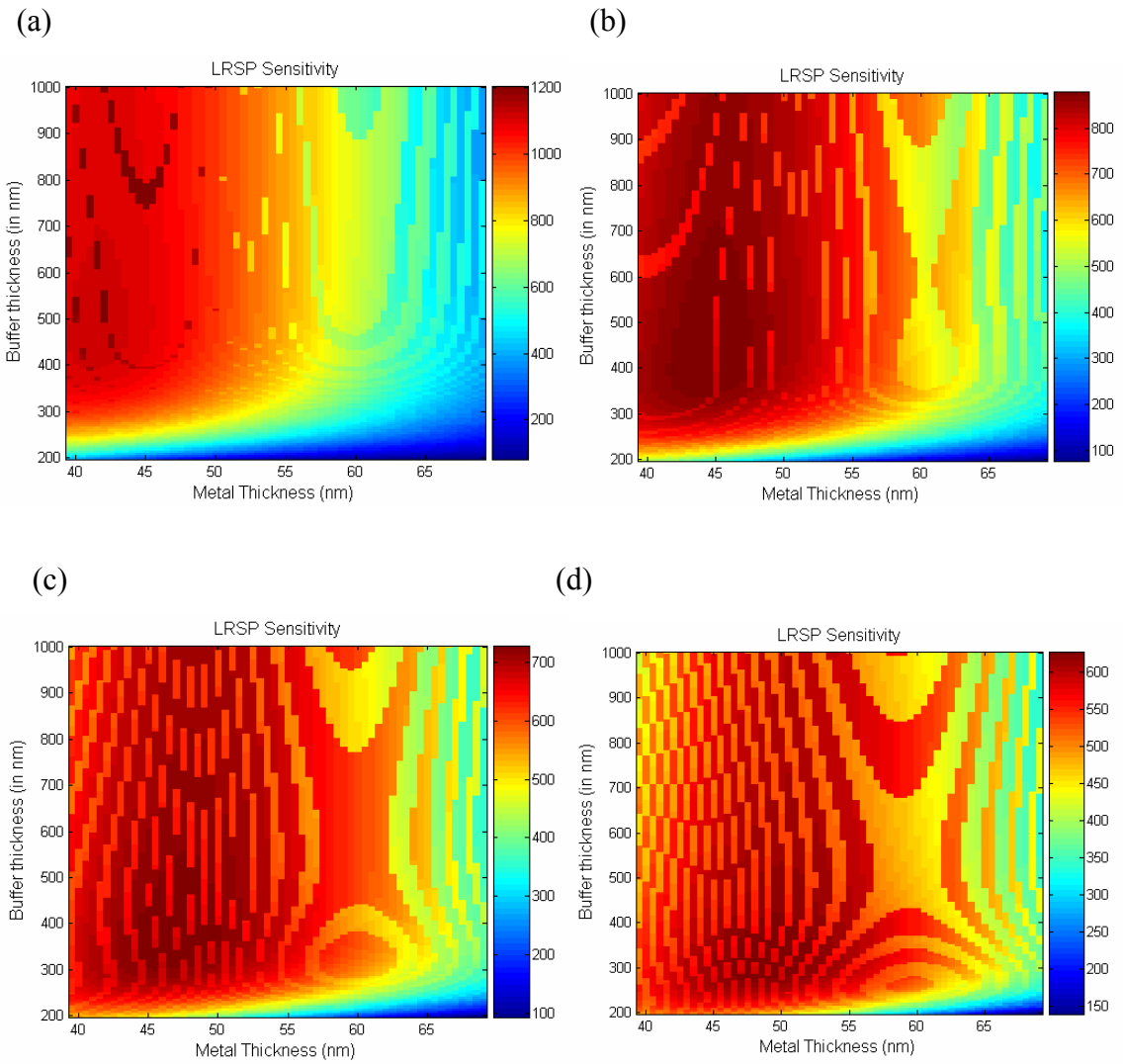

Figure 3.29 LRSP Bulk sensitivity for different gold and Teflon thicknesses for different angles using ethanol as the base solution – (a) θ = 67°, (b) θ = 68°, (c) θ = 69° and (d) θ = 70°

Note: If the resonance wavelength of any design is outside the range of the spectrometer, then the sensitivity, the reflectivity and the resonance wavelength were assigned a predefined value, i.e., Sensitivity = 0, Reflectivity = 1, Resonance wavelength = 0

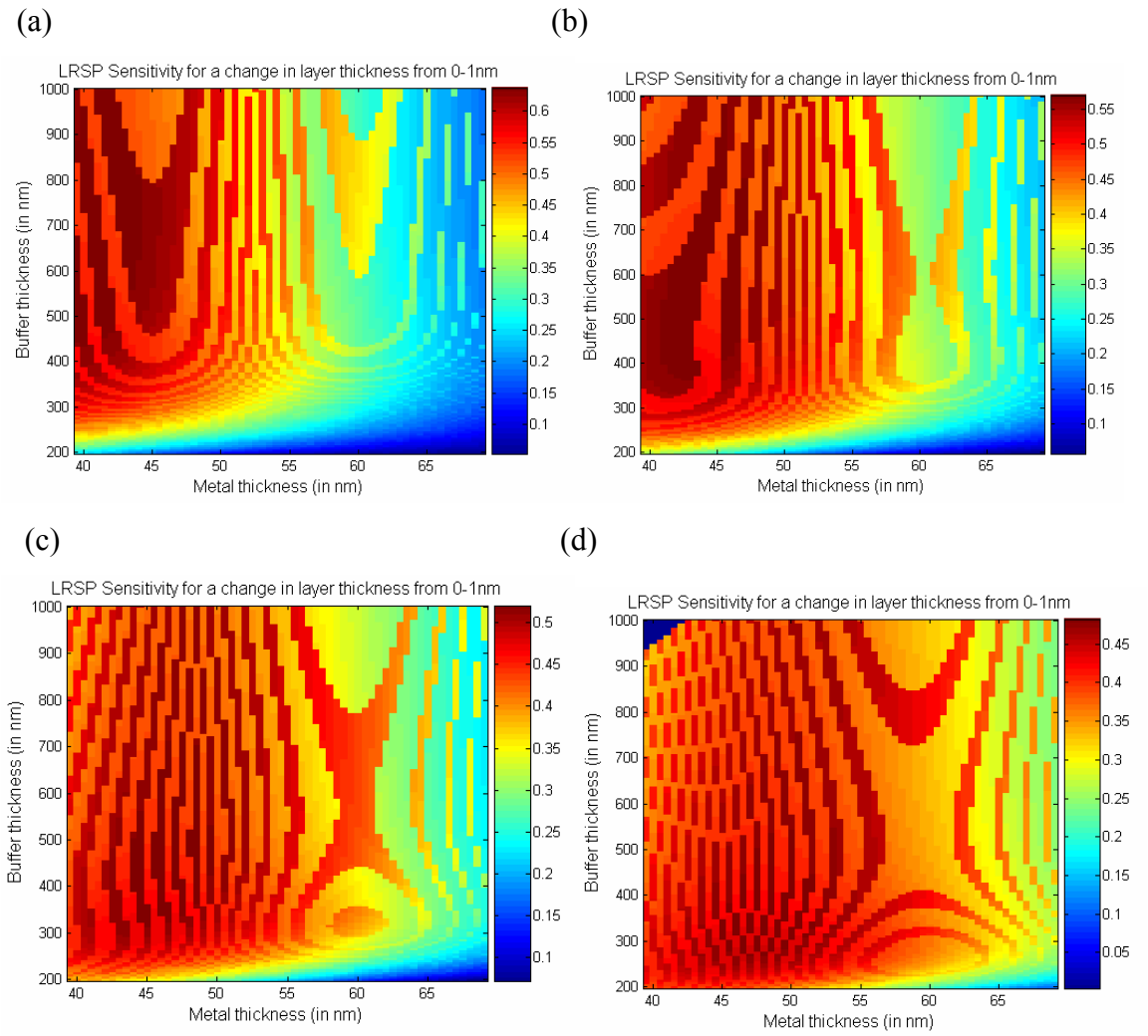

Figure 3.30 LRSP Surface sensitivity for different gold and Teflon thicknesses for different angles using ethanol as the base solution – (a) θ = 67°, (b) θ = 68°, (c) θ = 69° and (d) θ = 70°

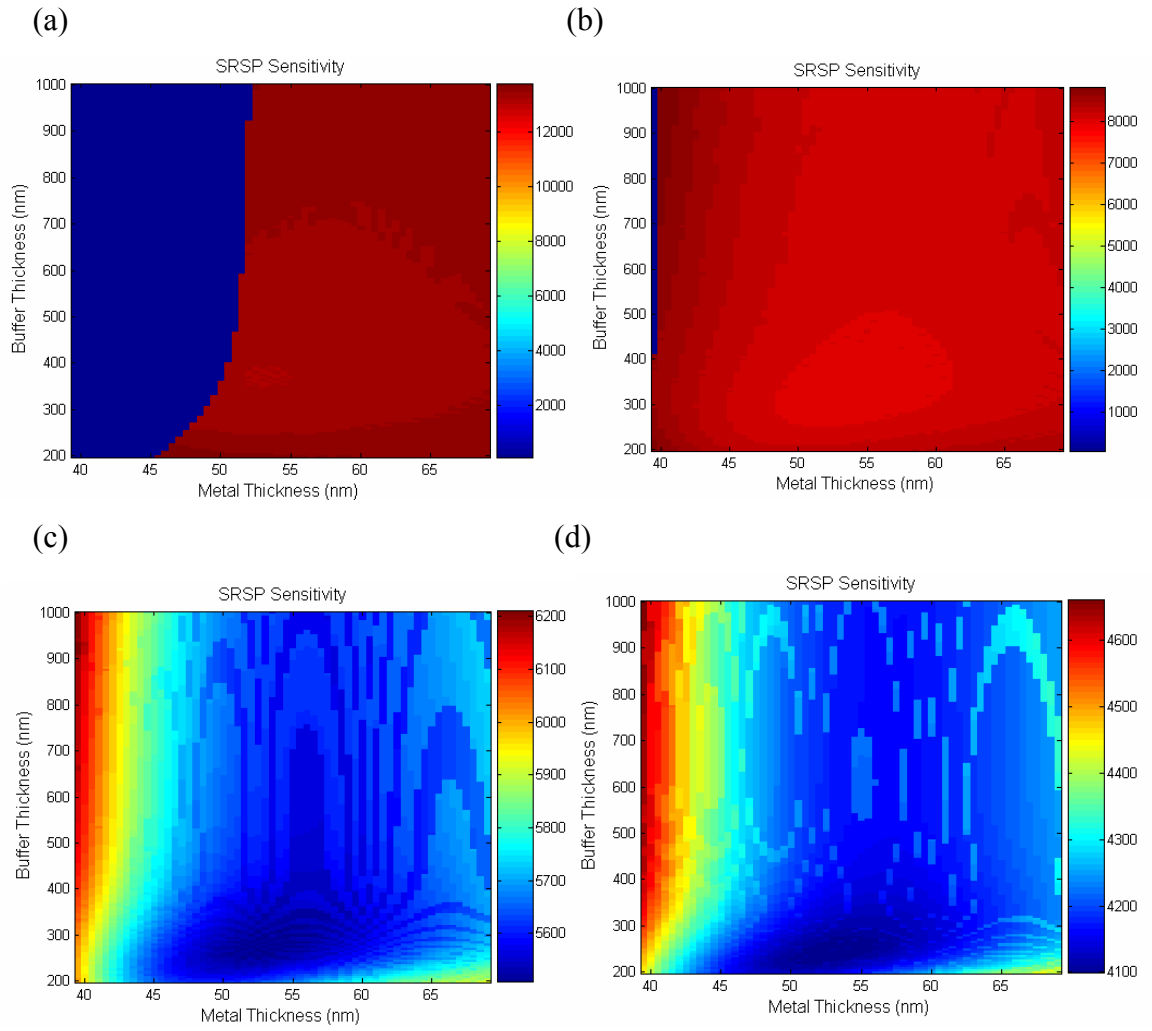

Figure 3.31 SRSP Bulk sensitivity for different gold and Teflon thicknesses for different angles using ethanol as the base solution – (a) θ = 67°, (b) θ = 68°, (c) θ = 69° and (d) θ = 70°

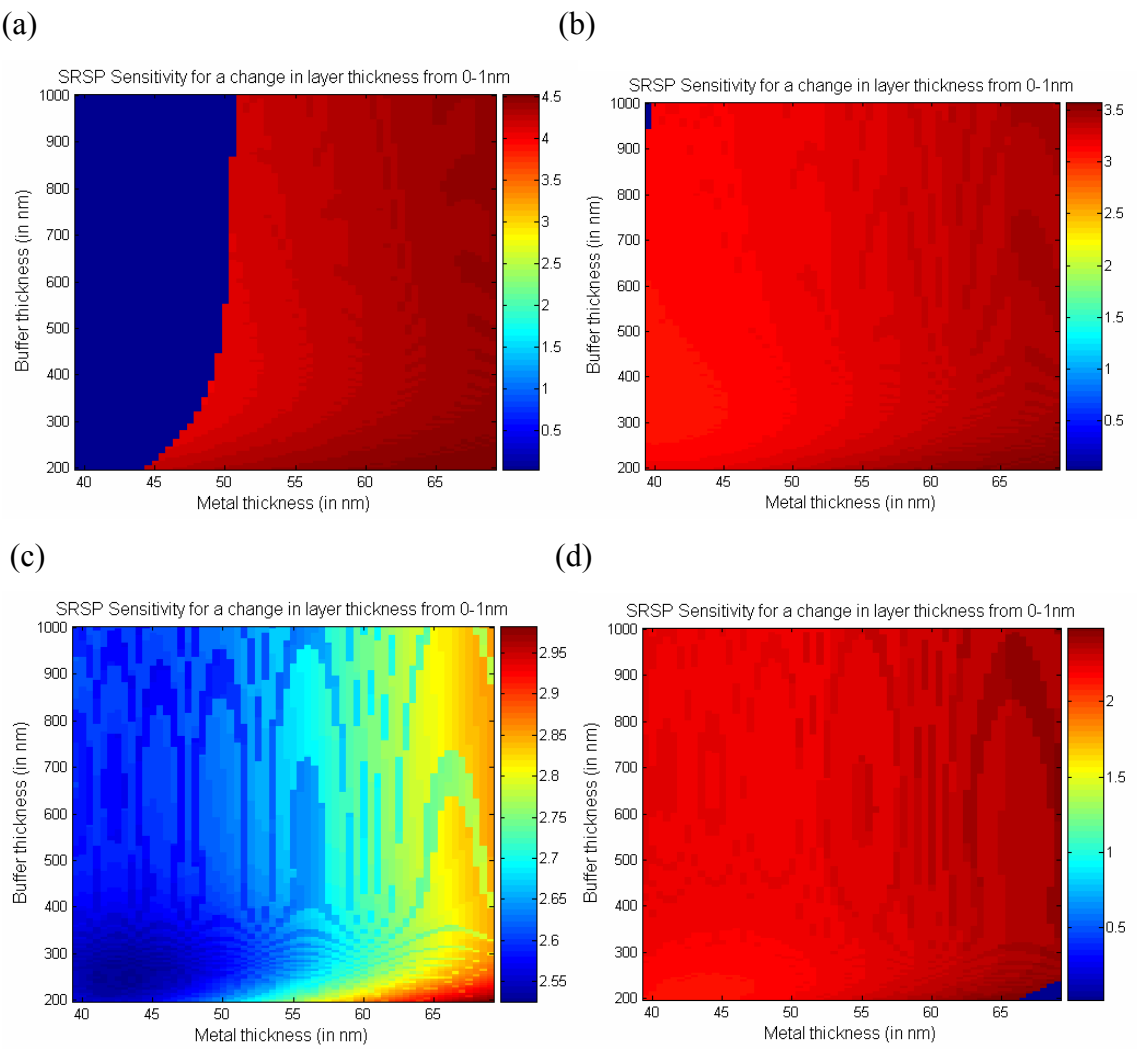

Figure 3.32 SRSP Surface sensitivity for different gold and Teflon thicknesses for different angles using ethanol as the base solution – (a) θ = 67°, (b) θ = 68°, (c) θ = 69° and (d) θ = 70°

As in the analysis for water we find the short range bulk and surface sensitivities remain fairly constant over the entire range of gold and Teflon thicknesses for the four different angles.

The range of gold and Teflon thicknesses needed to achieve maximum sensitivity (bulk and surface) is given in Table 3.7

	LRSP		SRSP	
	Thickness range (in nm)		Thickness range (in nm)	
Theta	Teflon	Gold	Teflon	Gold
67	275-1000	39.5-50	200-1000	50-69
68	250-1000	39.5-55	200-1000	39.5-69
69	200-1000	39.5-60	300-1000	39.5-41
70	200-1000	39.5-60	300-1000	39.5-42

Table 3.7 Range of gold and Teflon thicknesses needed to achieve maximum sensitivity for LRSP and SRSP using ethanol as the base solution for different incident angles

Since the SRSP bulk and surface sensitivities are invariant over different gold and Teflon thickness (the range of gold thickness for SRSP in Table 3.7 are for the maximum sensitivity, even though the spread of the overall sensitivity is not large), the deciding factor on the thickness of gold and Teflon is reflectivity.

The range of Teflon thicknesses having minimum reflectivity (<0.4) for the four different angles and for the entire range of Gold thickness

	Teflon thickness range (in nm)	
Theta	LRSP	SRSP
67	200-450	200-450
68	200-400	200-550
69	200-375	200-450
70	200-350	200-500

Table 3.8 Range of Teflon thickness needed to achieve minimum reflectivity for LRSP and SRSP using ethanol as the base solution for different incident angles

LRSP and SRSP reflectivity for the entire range of gold and Teflon thickness is given in Figure 3.33 and Figure 3.34

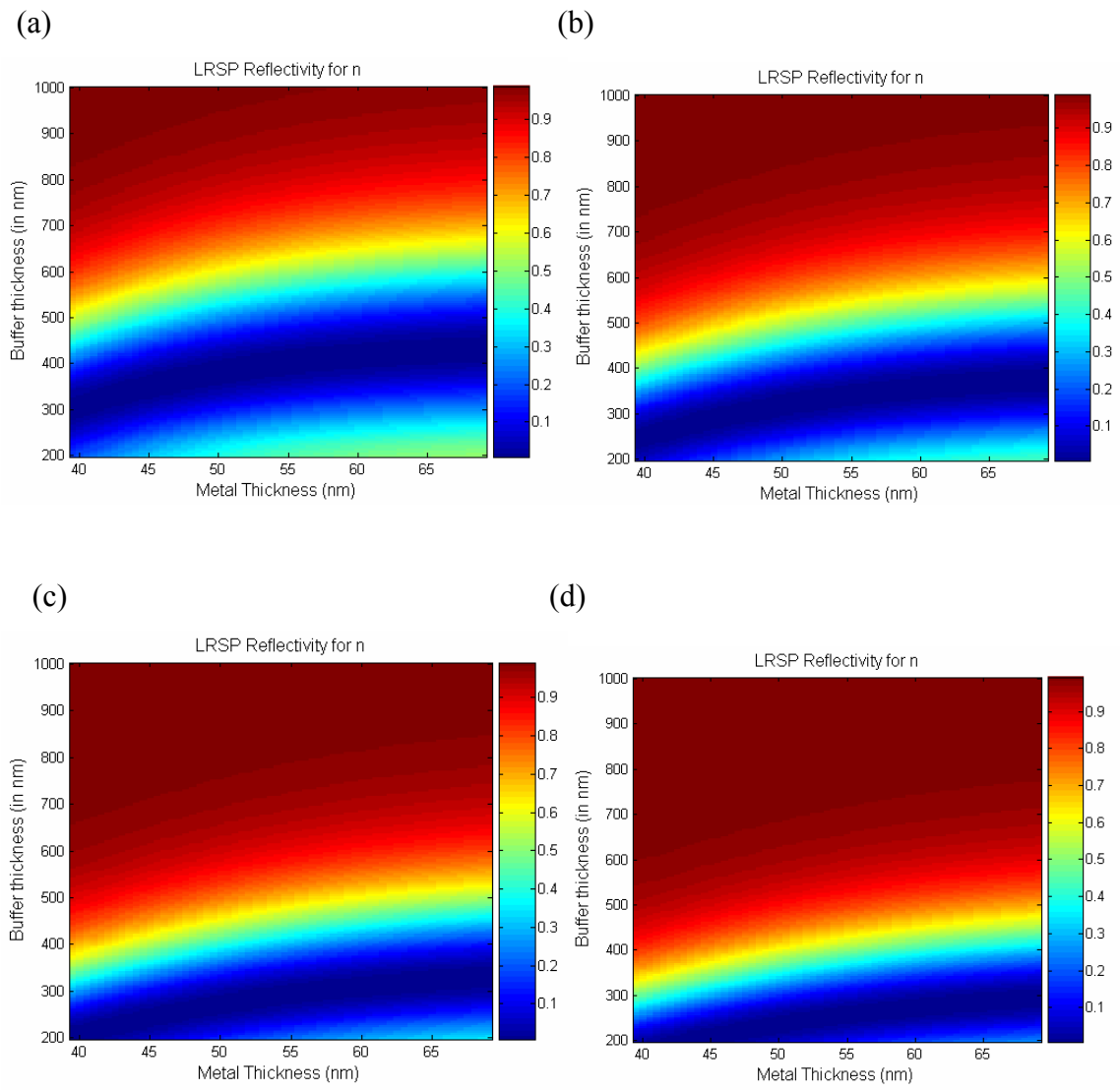

Figure 3.33 LRSP reflectivity for different gold and Teflon thicknesses for different angles using ethanol as the base solution – (a) θ = 67°, (b) θ = 68°, (c) θ = 69° and (d) θ = 70°

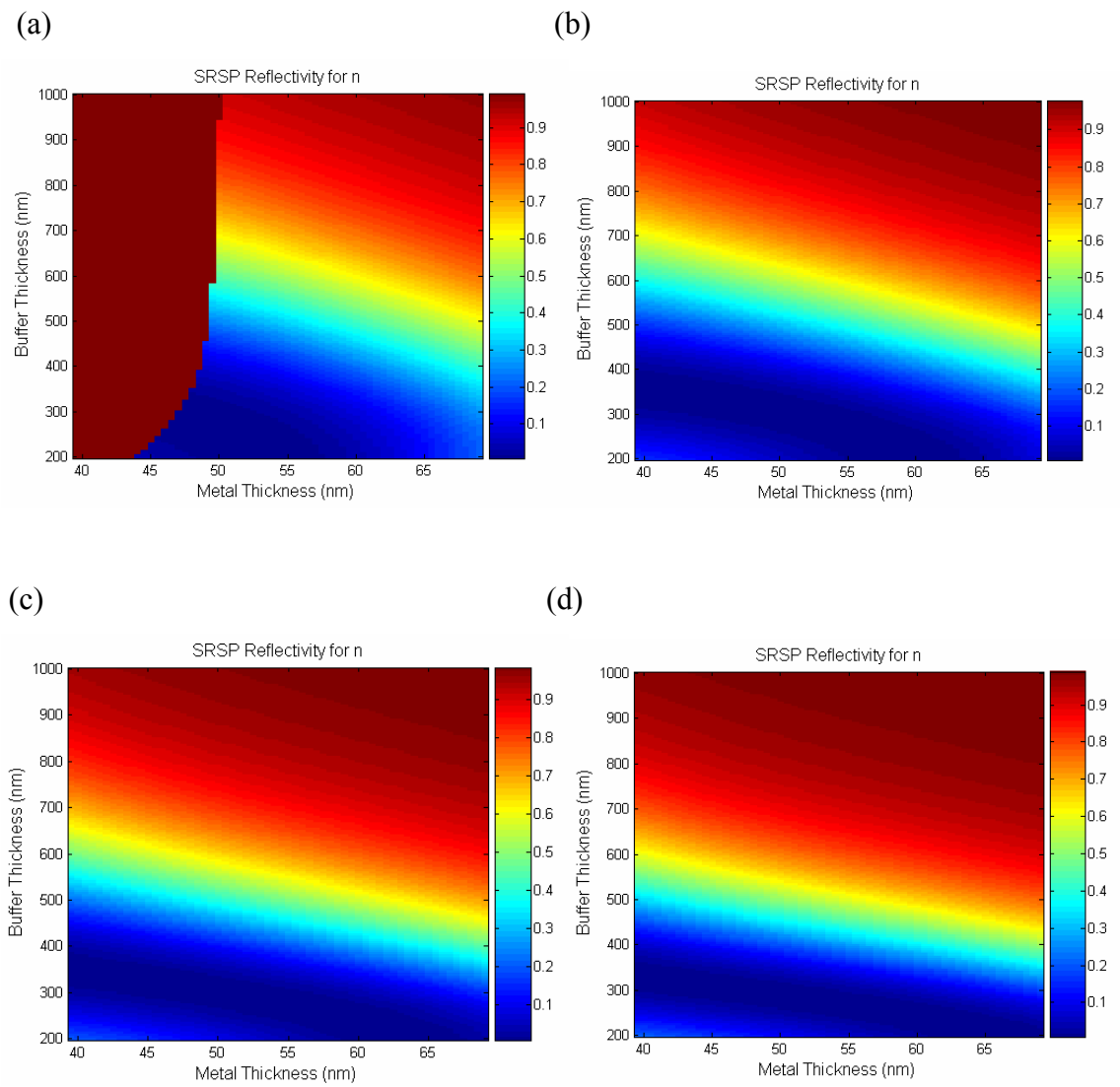

Figure 3.34 SRSP reflectivity for different gold and Teflon thicknesses for different angles using ethanol as the base solution – (a) θ = 67°, (b) θ = 68°, (c) θ = 69° and (d) θ = 70°

To obtain high sensitivity and low reflectivity, Table 3.9 provides the range of gold and Teflon thicknesses when each mode is considered individually, i.e. LRSP and SRSP are assumed to be independent and the thickness ranges are obtained to get the desired performance.

	LRSP		SRSP	
	Thickness range (in nm)		Thickness range (in nm)	
Theta	Teflon	Gold	Teflon	Gold
67	250-450	39.5-55	200-450	50-69
68	250-400	39.5-58	200-450	39.5-69
69	250-375	39.5-63	200-375	39.5-69
70	200-325	44-57	200-400	39.5-69

Table 3.9 Range of gold and Teflon thickness to achieve high sensitivity and low reflectivity using ethanol as the base solution with the two modes considered separately

From Table 3.9, the thickness ranges for LRSP and SRSP are not the same. Since the two modes propagate simultaneously, there is a need to modify Teflon and gold thicknesses to incorporate optimal performance from both modes.

	Thickness Range (in nm)		Reflectivity		Resonance wavelength Range (in nm)		
Theta	Teflon	Gold	LRSP	SRSP	LRSP	SRSP	Diff in λ
67	300-500	50-55	0-0.5	0-0.3	620-640	1050-1020	430-380
68	250-450	39.5-60	0-0.55	0-0.2	570-630	1040-910	470-280
69	250-350	39.5-62	0-0.5	0-0.15	560-620	980-850	420-230
70	250-325	39.5-57	0-0.5	0-0.1	550-600	920-810	370-210

Table 3.10 Range of gold and Teflon thicknesses along with LRSP and SRSP reflectivity and resonance wavelength range for optimal performance using ethanol as the base solution with the two modes considered simultaneously

This change in the thicknesses is shown in Table 3.10, where the two modes are considered together, when compared with Table 3.9, where the modes have been individually considered. As said earlier, the thickness range for Teflon and gold changed to produce optimal performance involving two modes.

Since the sensitivity of SRSP was relatively invariant, SRSP's reflectivity played a major part in deciding the range of thicknesses. One other factor affecting the thickness range is the reflectivity of LRSP. LRSP's low reflectivity range decreased as the angle (theta) increased, thereby providing a limit to the operating thickness range as evidenced in Table 3.9 and Table 3.10.

From Table 3.10, Teflon thickness from 250-500 nm and Gold thickness from 39.5 - 62 nm can be employed to provide optimal performance. The difference in LRSP and SRSP's resonance wavelength was the deciding factor in selecting the thickness of gold and the reflectivity determined the Teflon thickness. Since Teflon thickness around 300nm has lower reflectivity for all possible incident angles, this thickness was selected as the optimal thickness.

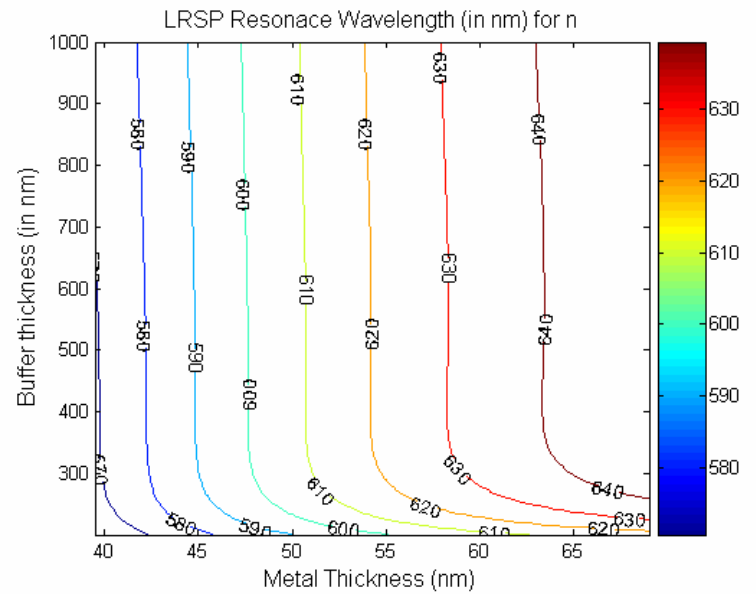

Figure 3.35 Resonance wavelength range for LRSP for θ = 68° using water as the base solution

As discussed in the optimization results for water, gold layers thicker than 39.5nm helped bring λ_{LRSP} to higher wavelengths and gold layers thinner than 62 nm brought λ_{SRSP} to lower wavelengths as shown in Figure 3.35 and Figure 3.36 respectively.

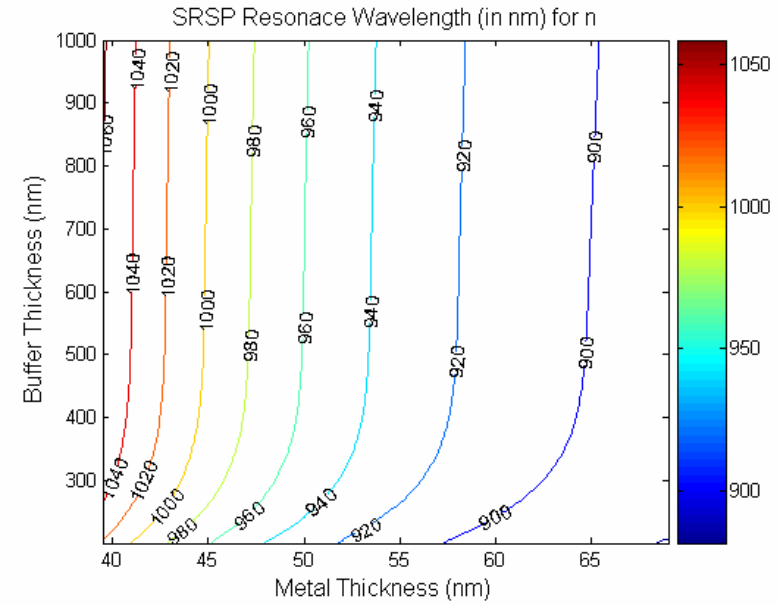

Figure 3.36 Resonance wavelength range for SRSP for θ = 66° using water as the base solution

3.6.2.1 Optimized thickness range for Teflon and gold

From the above results, Teflon thickness of 300nm and gold thickness of 50-55nm were considered to satisfy the requirements of optimal performance.

3.6.3 Using magnesium fluoride as the buffer layer and ethanol as the base solution

The optimization results were performed using ethanol as the base solution. The thickness of MgF2 was varied from 200-1000 nm and the thickness of Gold was varied from 39.5-69 nm.

a) A good spectrum involving both the modes was obtained for theta = 71° to 76° wherein the LRSP and SRSP had their resonance wavelength within the range of the spectrometer.
b) The maximum sensitivity for LRSP and SRSP for the different incident angles is given in Table 3.11

	Max. Bulk Sensitivity (nm/RIU)		Max. Surface Sensitivity (nm/nm)	
Theta	LRSP	SRSP	LRSP	SRSP
71	4000	2600	2.6	1
72	4100	2200	3.1	1
73	2900	1900	2.3	1
74	2300	1700	2	1
75	2000	1600	1.7	1
76	1700	1450	1.6	1

Table 3.11 Maximum bulk and surface sensitivity for LRSP and SRSP using ethanol as the base solution and magnesium fluoride as the buffer layer for different incident angles

Figure 3.37 through Figure 3.40 indicate the bulk and surface sensitivity of LRSP and SRSP for the entire range of gold and MgF2 thickness for different incident angles.

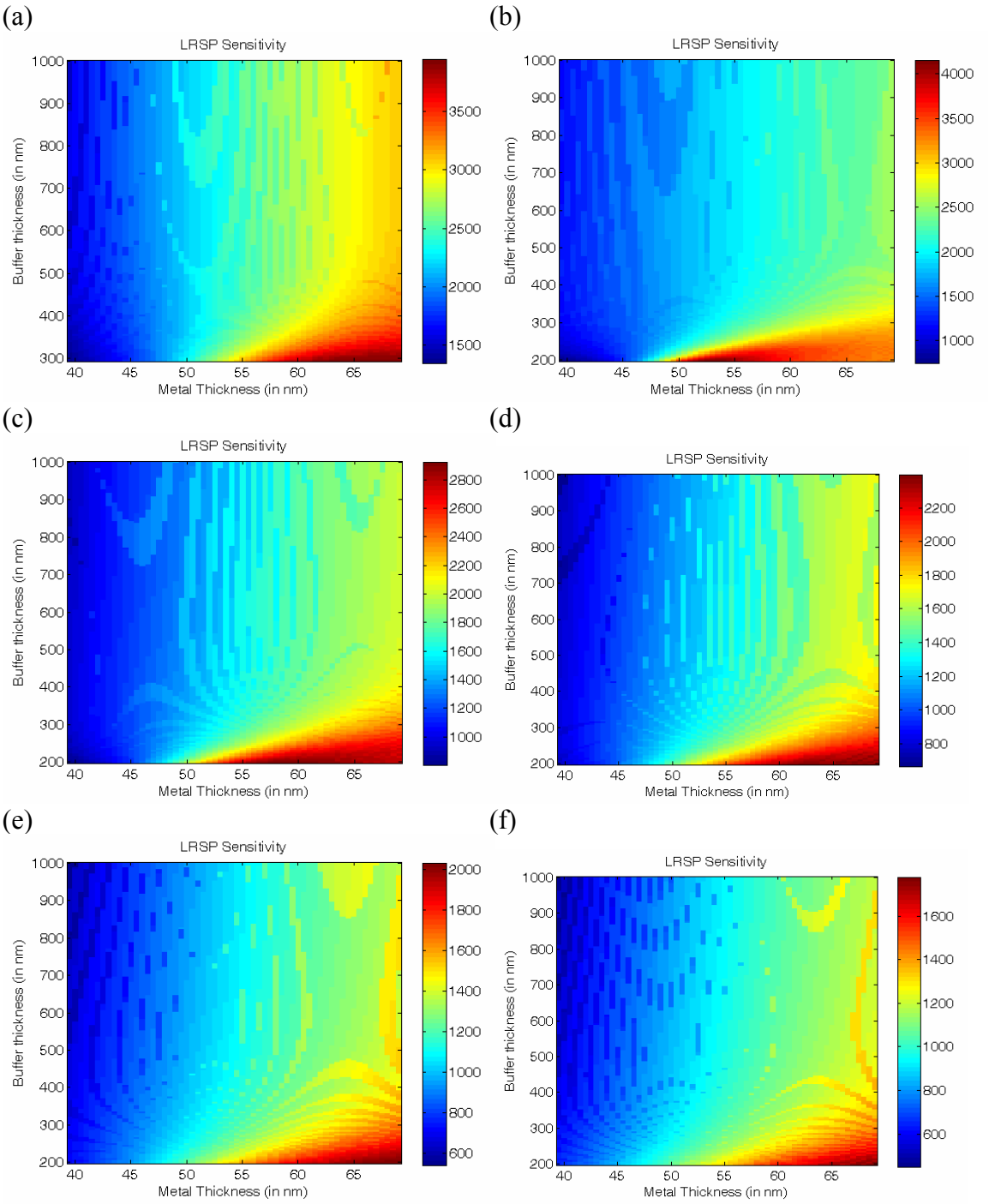

Figure 3.37 LRSP bulk sensitivity for different gold and magnesium fluoride thicknesses for different incident angles using ethanol as the base solution – (a) θ = 71°, (b) θ = 72°, (c) θ = 73° (d) θ = 74° (e) θ = 75° and (f) θ = 76°

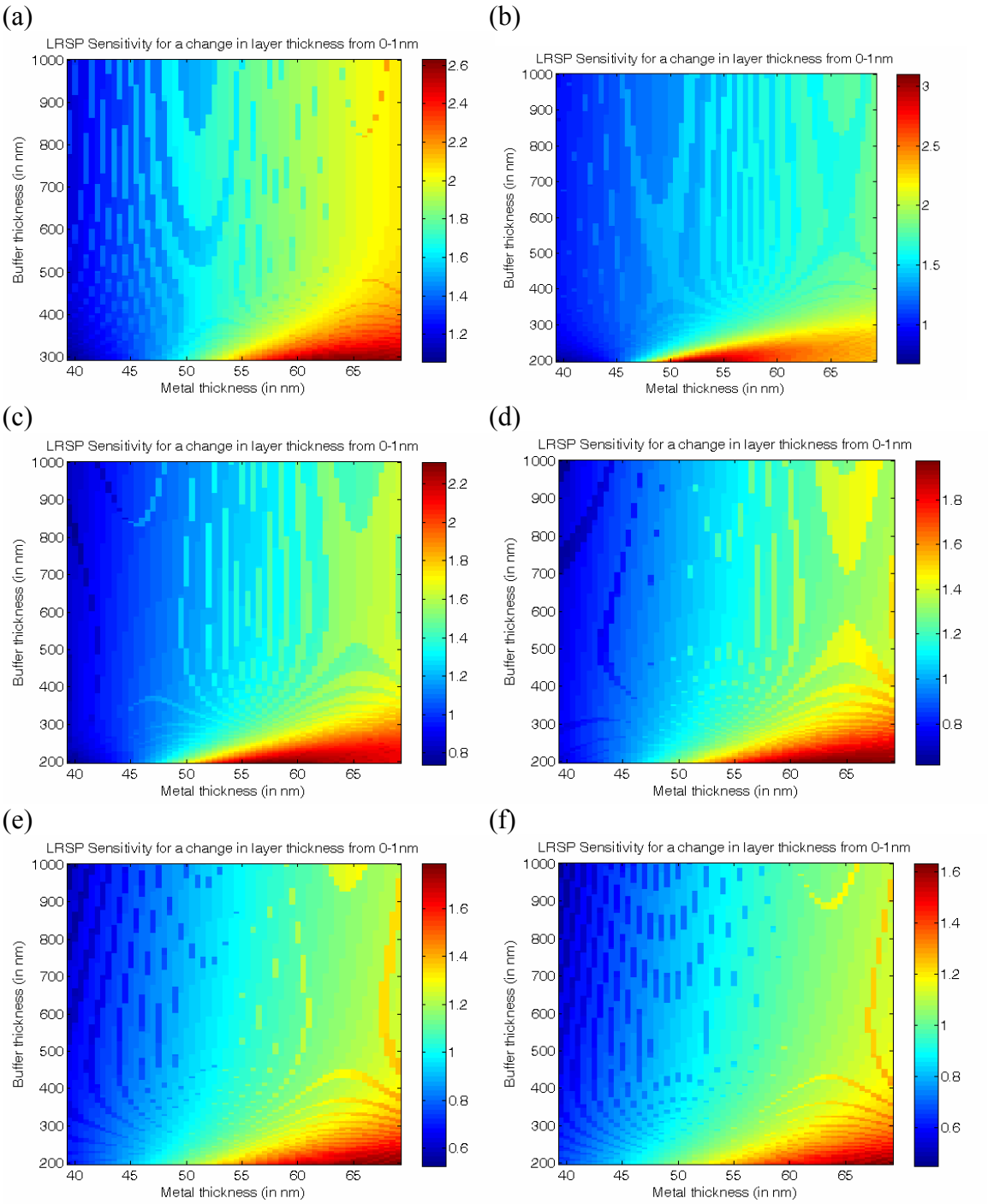

Figure 3.38 LRSP surface sensitivity for different gold and magnesium fluoride thicknesses for different incident angles using ethanol as the base solution – (a) θ = 71°, (b) θ = 72°, (c) θ = 73° (d) θ = 74° (e) θ = 75° and (f) θ = 76°

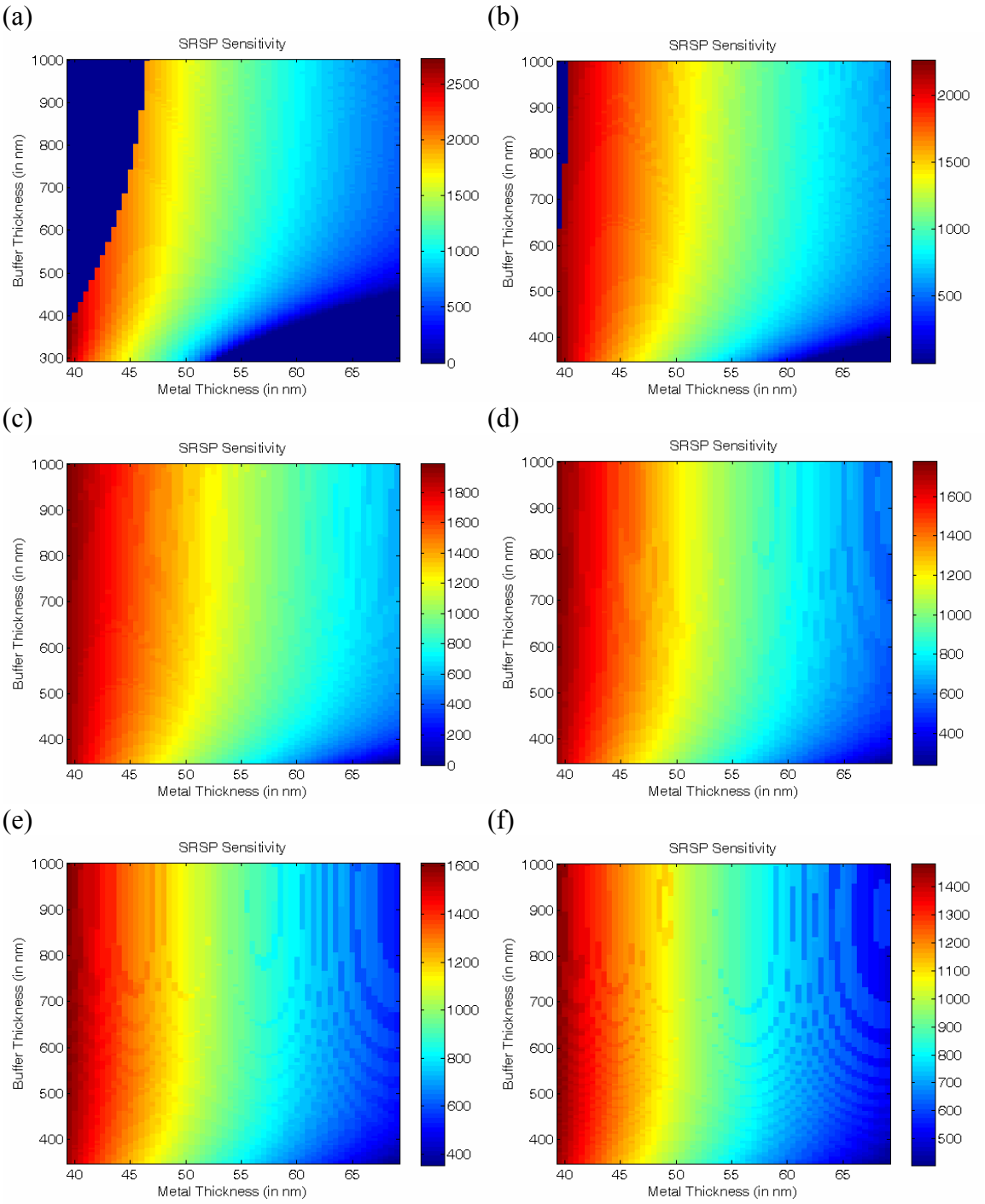

Figure 3.39 SRSP bulk sensitivity for different gold and magnesium fluoride thicknesses for different incident angles using ethanol as the base solution – (a) θ = 71°, (b) θ = 72°, (c) θ = 73° (d) θ = 74° (e) θ = 75° and (f) θ = 76°

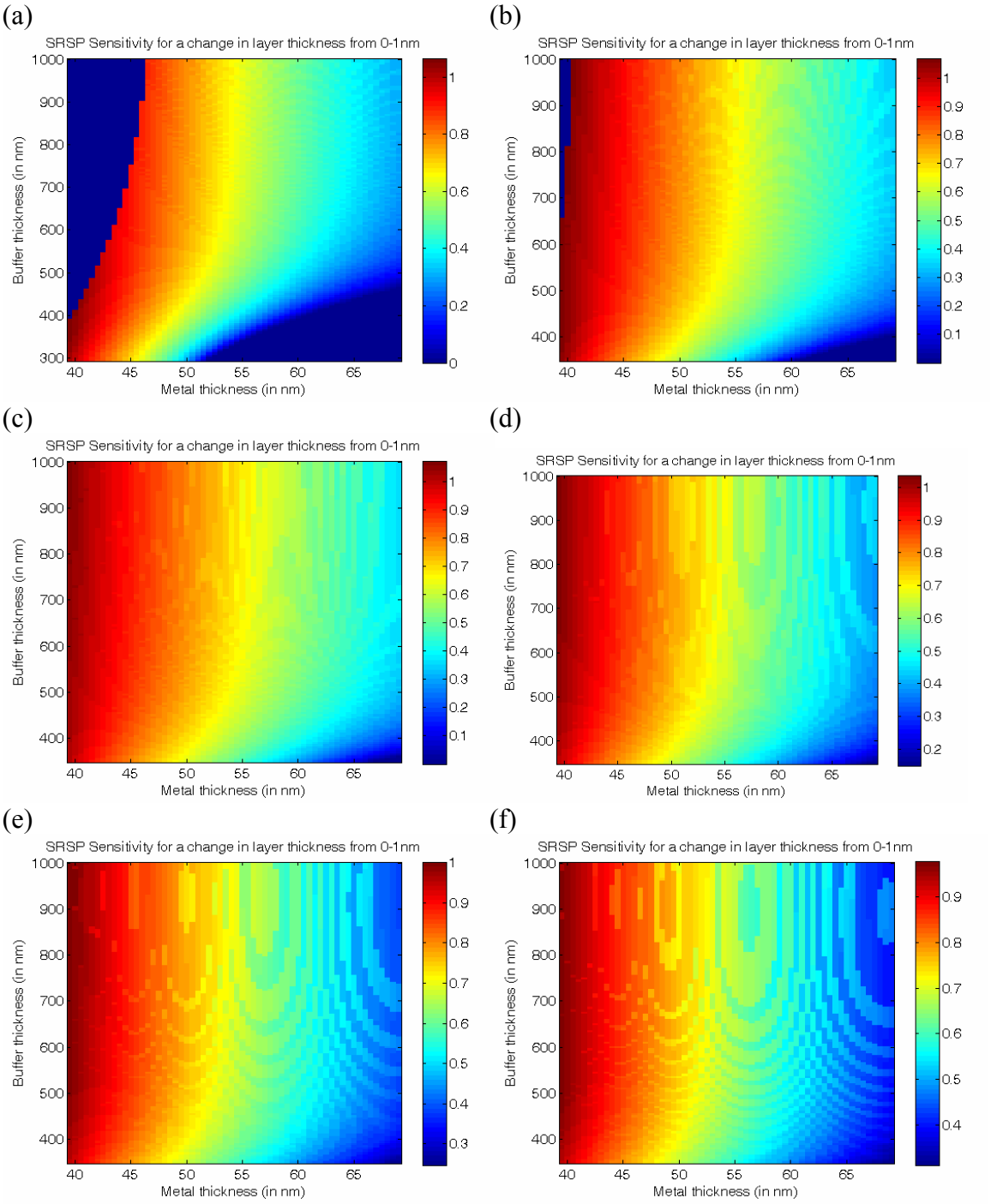

Figure 3.40 SRSP Surface sensitivity for different gold and magnesium fluoride thicknesses for different incident angles using ethanol as the base solution – (a) θ = 71°, (b) θ = 72°, (c) θ = 73° (d) θ = 74° (e) θ = 75° and (f) θ = 76°

The plots for SRSP shows reduced range for MgF2 layer as lower buffer thickness makes the resonance wavelength fall out of range. The SRSP surface sensitivities remain the same for each design value irrespective of the incident angle.

Based on the simulated sensitivities plot in Figure 3.37 - Figure 3.40, LRSP has higher sensitivity for designs with thicker gold layer whereas SRSP has higher sensitivity when the gold layer is thin.

When the gold layer is thin, SRSP resonance wavelength moves into the noisy region of the spectrometer used in the experiment.

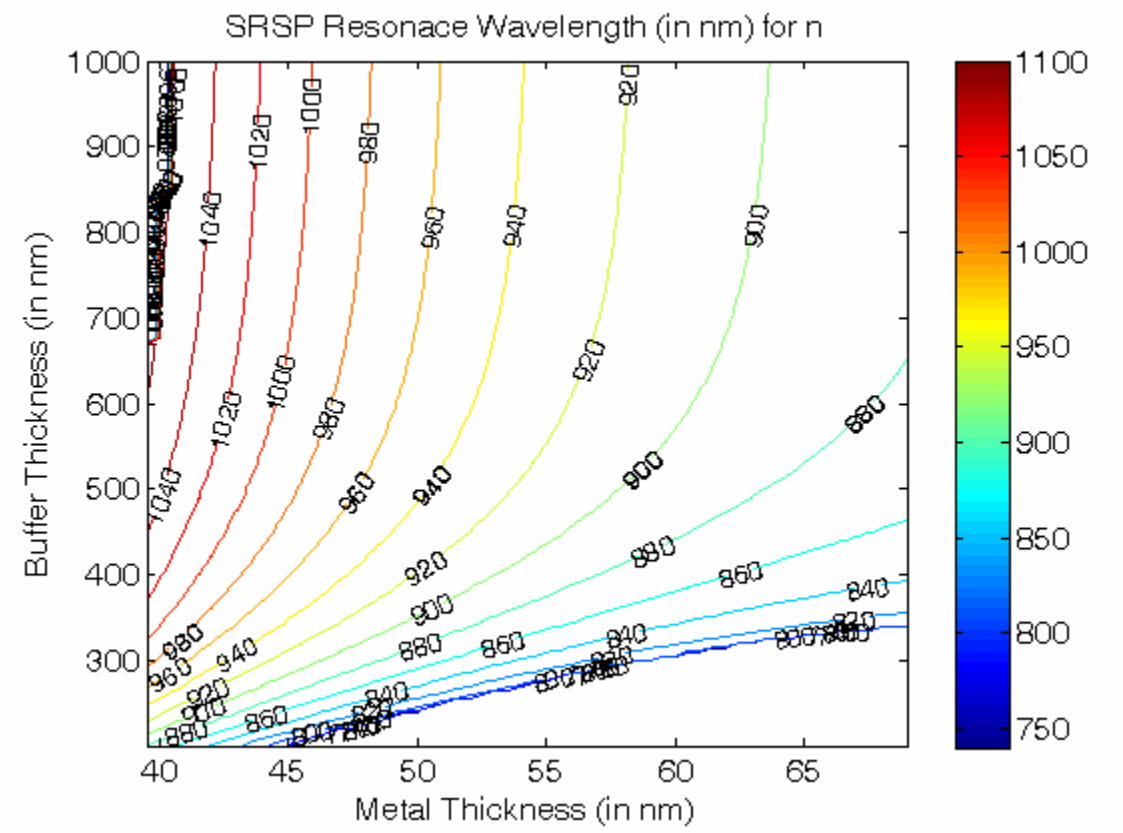

Figure 3.41 Resonance wavelength range for SRSP for θ = 72° using ethanol as the base solution and magnesium fluoride as the buffer layer

Thin gold layers also cause the propagation of LRSP waves at lower resonance wavelengths, shown in Figure 3.42, where the dielectric constant of gold is less negative.

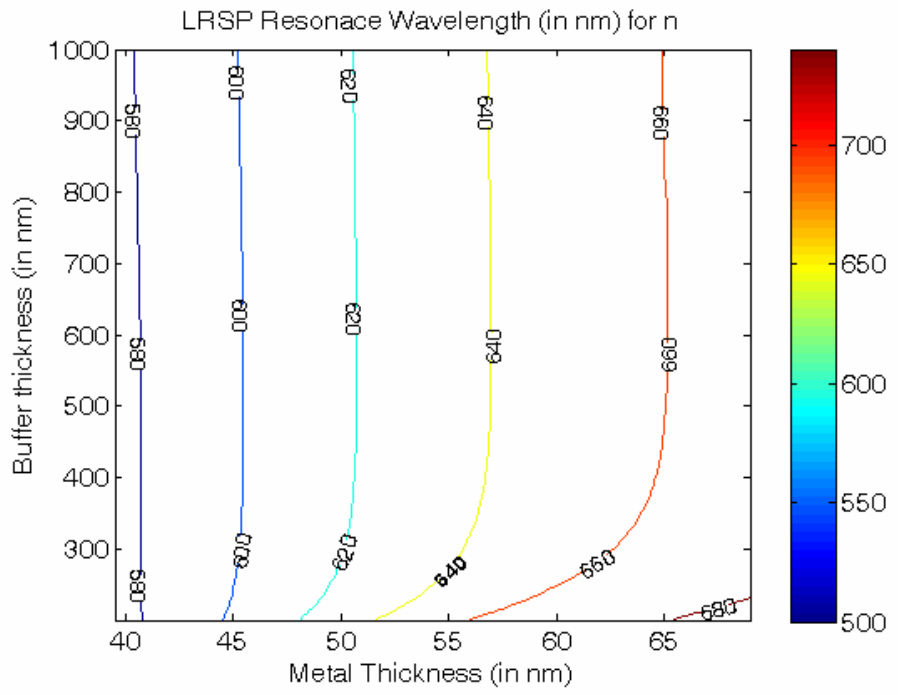

Figure 3.42 Resonance wavelength range for LRSP for θ = 72° using ethanol as the base solution and magnesium fluoride as the buffer layer

When the gold layer is thick, the two modes interact with each other indicated by the decrease in the difference between the resonance wavelengths of LRSP and SRSP, which affects the independent response of each mode.

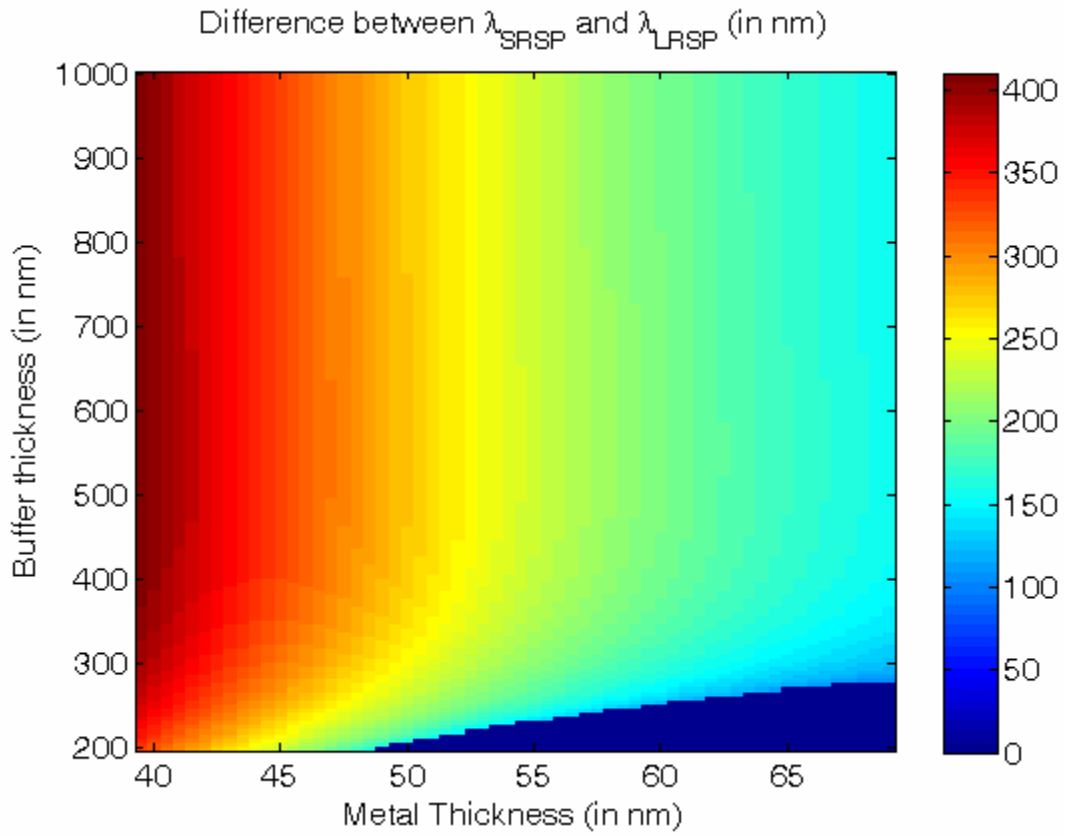

Figure 3.43 Difference in λ_{SRSP} and λ_{LRSP} for $\theta = 74°$

There is a need to select the optimized gold thickness.

a) Gold should be thick enough to couple the SRSP waves at the low noise zone of the spectrometer
b) Gold should be thin enough to allow independent propagation of two modes.

Hence gold is chosen to have thickness in the range of 52-58nm to give

a) better sensitivities in both LRSP and SRSP
b) independent coupling of both modes
c) resonance wavelengths lying within the noise-free zone of the spectrometer

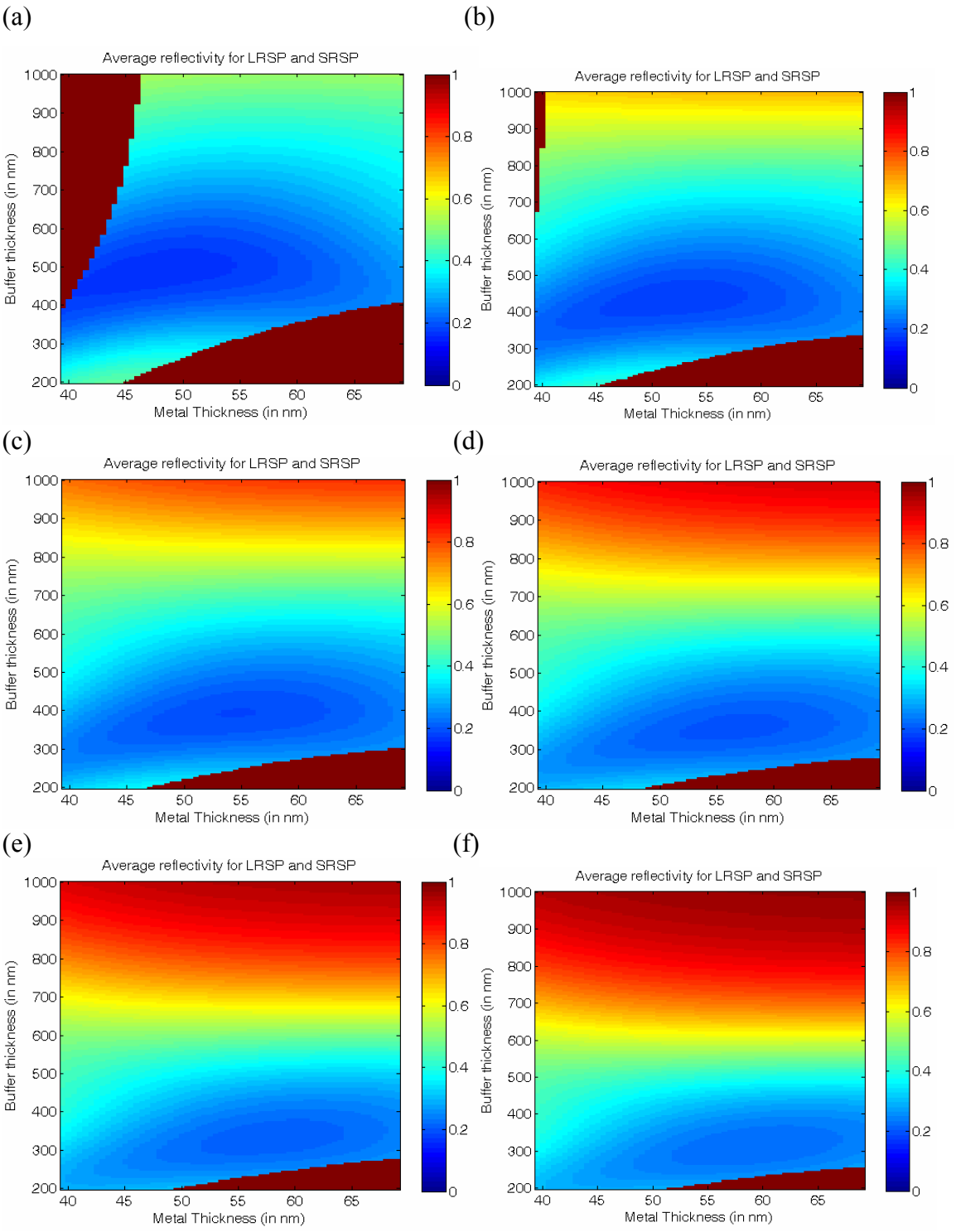

Figure 3.44 Average reflectivity LRSP and SRSP for – (a) θ = 71°, (b) θ = 72°, (c) θ = 73° (d) θ = 74° (e) θ = 75° and (f) θ = 76° for different gold and magnesium fluoride thicknesses using ethanol as the solution

The average reflectivity plot, shown in Figure 3.44, indicates the need to have a thinner magnesium fluoride layer to obtain lower reflectivity. A thickness range of 200-600nm enables maximal coupling into the two modes, indicated by decrease in reflectivity.

As per the maximum sensitivity in Table 3.11, lower theta values (71 and 72) yield higher sensitivities. Comparing with the reflectivity data in Figure 3.44 for those two incident angles, we get an optimized MgF2 thickness of 400-500nm

3.6.3.1 Optimized thickness range for magnesium fluoride and gold

From the above results, in order to obtain better performance, thickness of the magnesium fluoride has to be between 400-500nm and thickness of the gold has to be between 52-58nm.

4 CHAPTER 4 - SENSOR FABRICATION

The fabrication of the sensor involves sample selection, cleaning, deposition of a low refractive index buffer layer and deposition of gold. Either Teflon or magnesium fluoride is used as the buffer layer with gold as the metal layer. The buffer layer material is selected to achieve a closer refractive index matching with the solvent, water in the case of Teflon and ethanol in the case of magnesium fluoride.

4.1 Sample selection and Cleaning

BK7 glass substrates were used to make the SPR sensors. Initially, thinner BK7 substrates (Fisher Scientific, Inc) were used, but latter thicker BK7 substrates (Fisher Scientific, Inc) were used. The switch from thinner to thicker substrates was done due to the fragile nature of the thinner substrates. The sensors bind tightly to the prism due to the highly viscous index matching liquid and the tight assembly of the flow cell. As a result, safely unmounting the thin glass sensors from the prism proved difficult. Thus the reusability of the sensor was hindered with a thinner substrate. The switch to thicker substrates prevented the sensor from breaking.

The sample was cleaned with acetone and then with ethanol to remove any organic impurities.

4.2 Deposition of Teflon

4.2.1 Teflon

Teflon is a fluoropolymer whose chemical name is PTFE, polytetrafluoroethylene. The structure of Teflon is shown below:

$$(\text{-}CF_2\text{-}CF_2\text{-})_n$$

We specifically used Teflon-AF (Dupont Chemical Inc.) which is an amorphous form of Teflon engineered for optical applications. Compared to standard PTFE formulation, Teflon-AF has lower optical absorption and reduced light scattering. The refractive index of Teflon-AF ranges from 1.3173 to 1.3073 for the range of wavelength under consideration, i.e., from 400 to 1100nm. This range of index values matches relatively well with the index of water, 1.34 to 1.325, as shown in Figure 4.1.

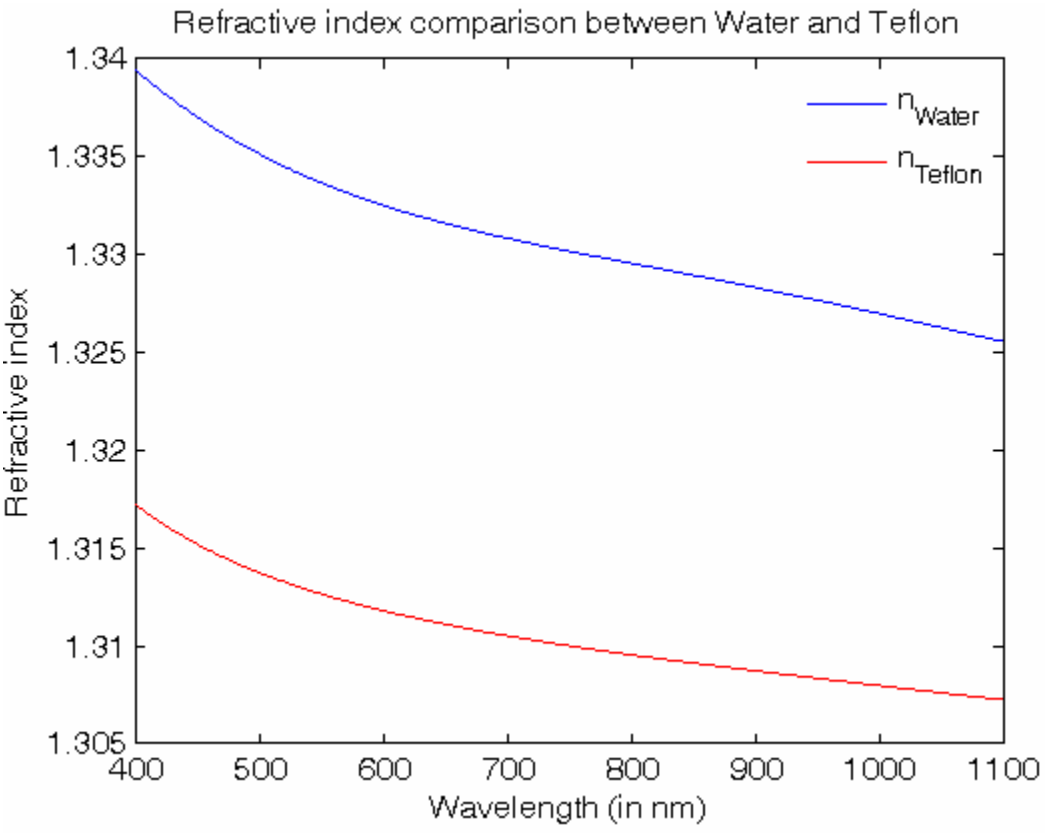

Figure 4.1 Refractive index comparison between water and Teflon-AF

4.2.2 Preparation of Teflon

Teflon AF-1600 (DuPont, Inc) solution (18% by weight in FC-40 Fluorinert solvent) was diluted with additional FC-40 (3 M, Inc) prior to spin coating to obtain the required Teflon thickness. Mixing the 18% Teflon solution and pure FC-40 in the ratio of 1:2.25 produces Teflon thickness of 660nm and a ratio 1:2.5 yields samples with 450nm thickness based on the coating condition described below. All the ratios are calculated by weight.

4.2.3 Preparation of the Adhesion Promoter

To improve adhesion of Teflon-AF to BK7 glass substrates, an adhesion promoter was used. A fluosilane molecule, 1H, 1H, 2H, 2H perfluorodecyltriethoxy silane (Lancaster Synthesis, Inc.) was used as the adhesion promoter. The adhesion promoter was prepared by mixing 2% solution of the fluorosilane with 95% ethanol+ 5% water.

4.2.4 Spin coating

The deposition of Teflon AF onto the BK7 substrate was done through spin coating. Adhesion promoter was first applied on the sample and spun at 2000 RPM (700 rpm/sec acceleration) for 35 seconds. The resultant adhesion promoter applied sample was baked at 110°C for 12 minutes.

Teflon AF solution was then spin coated at 500 RPM (850 rpm/sec acceleration) for 12 seconds to spread Teflon equally to all parts of the sample and spun at 3000 RPM (850 rpm/sec acceleration) for 30 seconds to achieve the required thickness. The sample was then baked at 165°C for 20 minutes to remove all the residual solvent.

4.3 Deposition of Magnesium Fluoride

4.3.1 Magnesium Fluoride

Magnesium Fluoride is a white crystalline salt with the formula MgF_2 with its refractive index in the range of 1.396 to 1.3845 for the wavelength range from 400-1100nm. This refractive index range matches with the index of ethanol which is 1.371 to 1.3535 for the same wavelength range as shown in Figure 4.2.

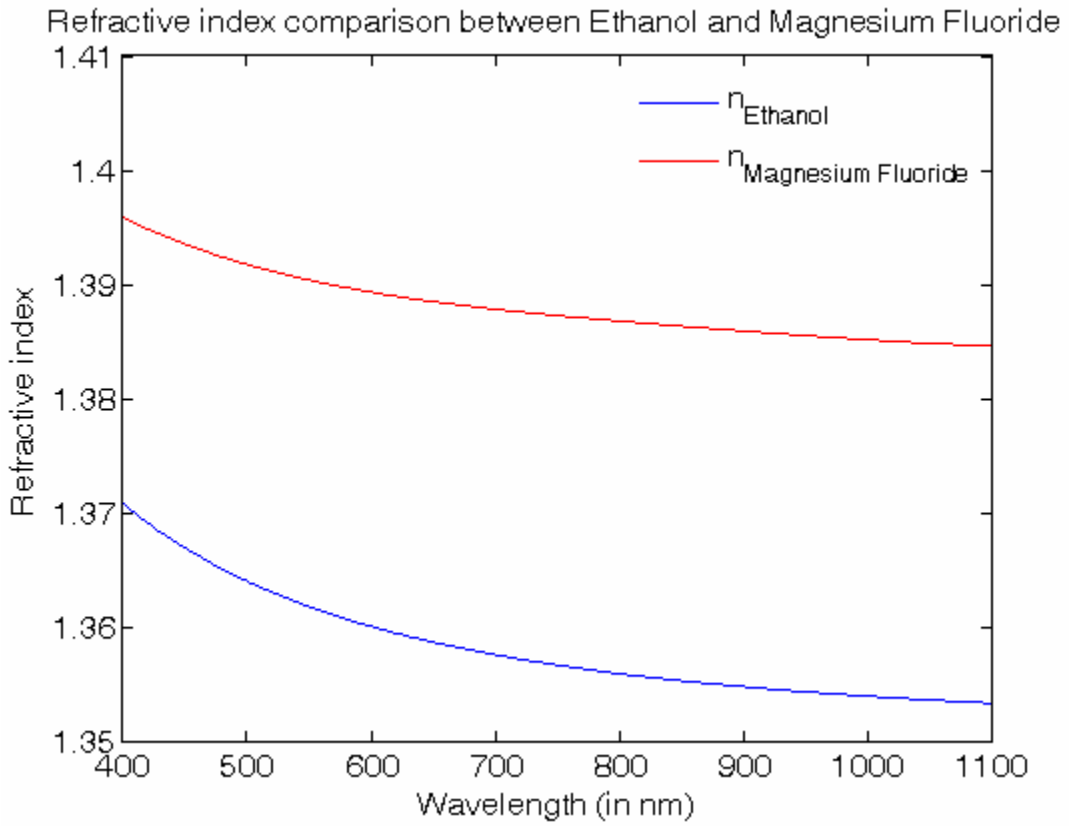

Figure 4.2 Refractive index comparison between ethanol and magnesium flouride

4.3.2 Deposition using electron- beam evaporation

Magnesium fluoride from (Kurt J. Lesker, Inc) which is 99.8% pure was evaporated using the e-beam evaporator at a base pressure of $4.1*10^{-6}$ torr. A constant electron acceleration voltage of 8KV was held throughout the process. The rate of deposition was between 11-12 Å/sec with the deposition pressure at $2.1*10^{-5}$ torr. The deposited film thickness was measured in-situ with a quartz crystal monitor. However, the measured

thickness was up to 40% lower than the actual thickness. As a result, the crystal monitor reading was compensated by proper calibration to achieve a final measured thickness of 480nm.

4.4 Deposition of Gold

Deposition of gold was initially done through electron beam evaporation and later through sputtering.

4.4.1 Deposition using electron- beam evaporation

Gold from (Kurt J. Lesker, Inc) which is 99.9% pure, was evaporated at the initial base pressure of approximately $5*10^{-6}$ torr. A constant acceleration voltage of 8KV was maintained throughout the process. During deposition, the rate of deposition varied from 1.8 to 2.2 Å/sec with the deposition pressure to around $5*10^{-5}$ torr. Since the crystal monitor was not accurate, optimal thickness of 55nm was obtained after careful calibration of the monitors' readings.

4.4.2 Deposition using sputtering system

Deposition of gold by sputtering rather than e-beam evaporation has the following advantages:

a) Thickness of the sputter deposited gold is more uniform than the electron-beam evaporated gold.
b) The entire process of sputter depositing gold takes 1/5 the time taken to deposit using the electron-beam evaporator.
c) The sample is not heated to as high a temperature during sputter as during electron-beam evaporation.

The last of these points proved especially important in this work. As the sample is kept at a relatively low temperature during sputter deposition of gold, the Teflon layer does not decompose and the thickness and the index of Teflon does not change greatly. The thickness of Teflon decreases by the order of few nms and the index increases by about 0.01 during gold sputtering. This compares favorably to a change of few hundreds of nms and index change of the order of 0.04 when using e-beam evaporation to deposit

gold. The index change was determined through curve fitting of the optical reflection spectrum.

Gold from (Kurt J. Lesker, Inc) which is 99.9% pure is used as the target. The sample is held at a base pressure of 0.10 mTorr and Argon gas is passed to the chamber at a flow rate of 15 scc/m. A constant power of 75W is supplied to the single target sputtering system and gold is deposited at a pressure of 3.55 mTorr.

4.5 Thickness measurement

The thickness of Teflon AF and Gold was measured using the DEKTAK 6M surface profilometer (Veeco, Inc). Inorder to measure the thickness of the Gold accurately, a similar sample (BK7 glass slide) without the Teflon/MgF2 layer was placed next to original sample in the sample holder of the e-beam evaporator/sputtering system and Gold was then deposited. From the thickness of the gold on glass, the thickness of the gold on the sample was determined accurately within 5 nm.

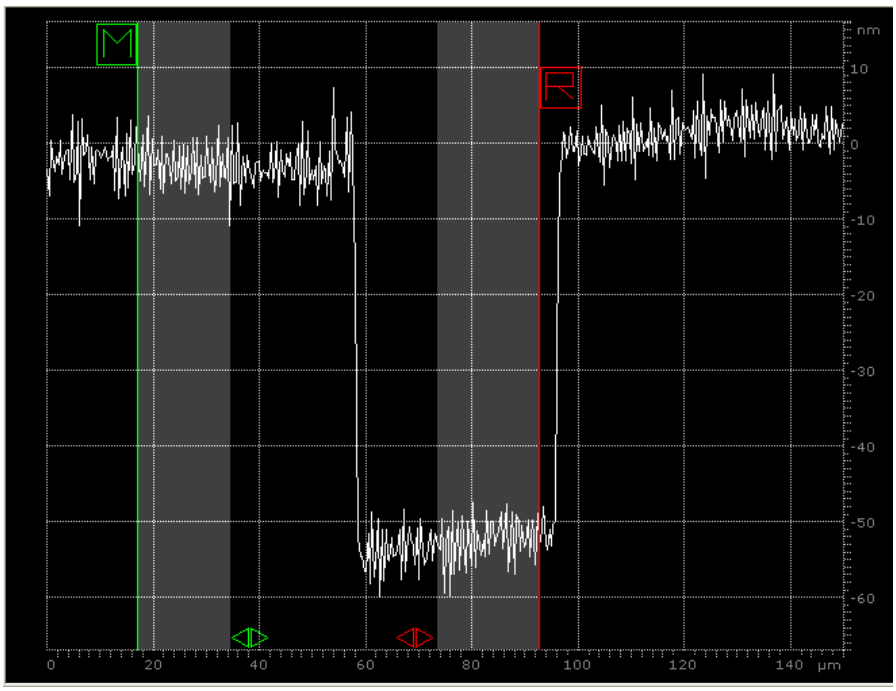

Figure 4.3 Example measurement of gold film thickness from the DEKTAK 6M profiler. The lower region in the center is the glass substrate, while the raised regions on the edges represent the gold.

5 CHAPTER 5 - EXPERIMENTAL DETAILS – ALKANETHIOL MONOLAYER FORMATION AND BIOSENSING

Two types of experiments were conducted to study the influence of background index change and surface layer thickness change. They were

1. Experiment with ethanol and different concentrations of methanol in ethanol, with octadecanethiol (ODT) as the surface binding layer on gold.
2. Experiment with different NaCl concentrations with streptavidin as the layer binding to biotin immobilized on the sensor.

5.1 Experimental setup

The experimental setup for both the experiments is shown in Figure 5.1. The fabricated sensor was placed in contact with a BK7 equilateral prism (Esco Products, Inc.) using a BK7 index matching fluid (Cargille, Inc.). The prism and the sensor were clamped in a custom made acrylic flow cell sealed with o-ring silicone gaskets (Small parts, Inc.). The flow cell had its geometry cutout to have three independent channels on the sensor. Different solutions used for testing the sensor were placed in a water bath to maintain a constant temperature, thus eliminating any possible refractive index changes due to temperature variations. Liquids were introduced to the sensor through Teflon (PTFE) tubing using a 12 roller peristaltic pump (Ismatec, Inc). In order to avoid air bubbles during the switching of one solution to another, a selection valve was used. This selection setup helped in easily changing between different solutions without the fear of introducing air bubbles. All tubings were primed either with their respective solutions or with their base solution in the case of solutions forming monolayers (e.g. ODT in exp.1 and streptavidin in exp.2).

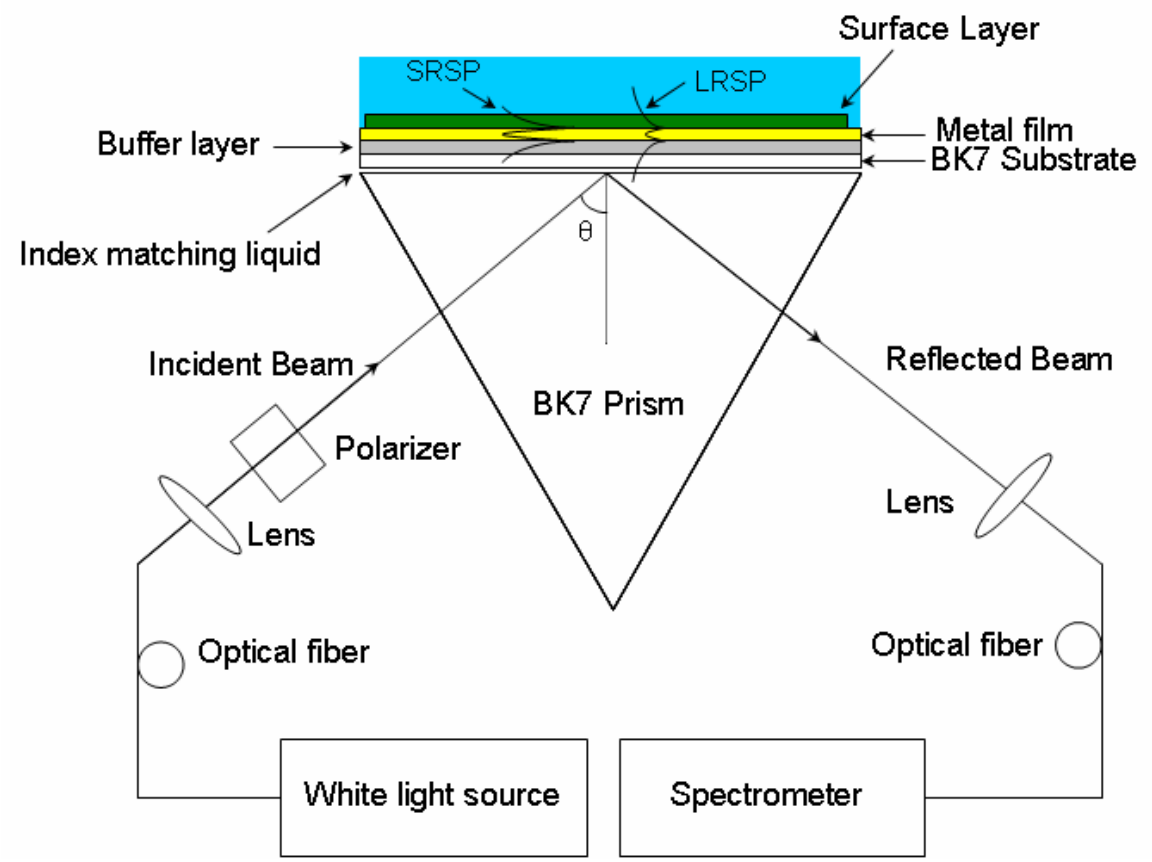

Figure 5.1 Optical configuration for the generation of surface plasmon waves

The flow-cell/sensor assembly was mounted on a custom designed variable angle optical reflection measurement system. Light from a halogen lamp (Model DH-2000, Ocean Optics, Inc.) was introduced into the reflection measurement apparatus using a 200 μm core multi-mode optical fiber. A collimating lens directed the light from the fiber through a calcite Glan-Taylor polarizer (ThorLabs, Inc.), into the prism. Light from the collimating lens had an approximate diameter of 4 mm. The polarizer was mounted in a rotation stage which can be adjusted to create either a TE or a TM polarized wave incident on the sensor. The reflected light was collected by another lens and coupled to a multimode fiber which routed it to a computer controlled spectrometer (Ocean Optics model HR-4000). Spectrum analysis was performed by custom software developed in LabView (National Instruments).

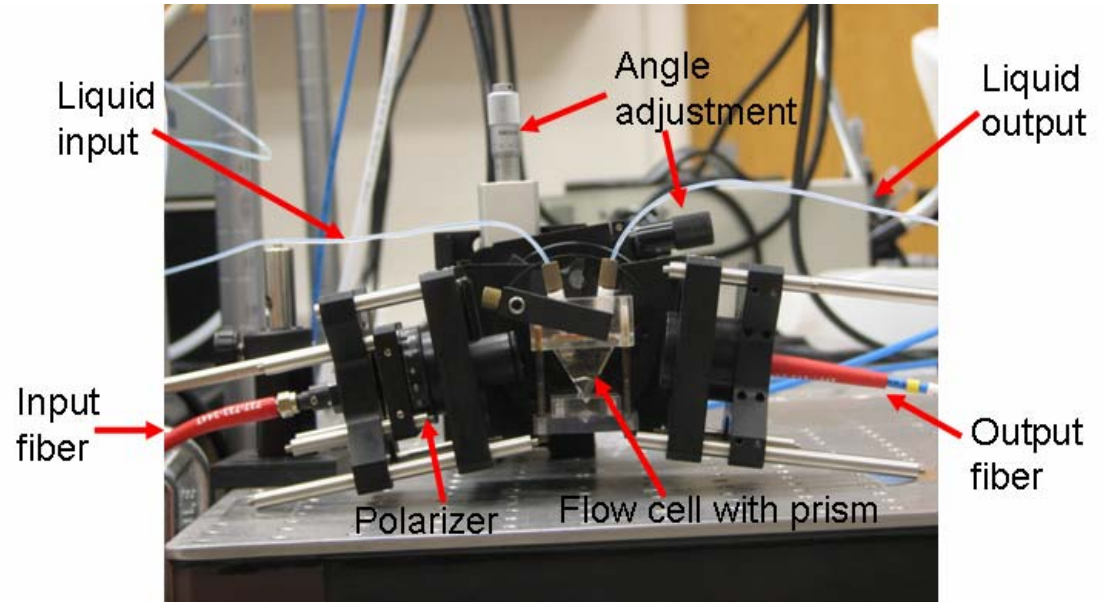

Figure 5.2 Experimental setup

5.2 Initial Experimental Steps

The flow cell was placed in the optical assembly for performing the sensing operation. The intensity of the light received could be varied by changing the fine or coarse angle adjustment. The assembly can also be adjusted to make the light incident on any one of the three independent channels, which are independent of one another. When the intensity of the light obtained from a particular channel was maximized, the flow cell and the optical assembly were clamped at that position to prevent any movement during the course of the experiment.

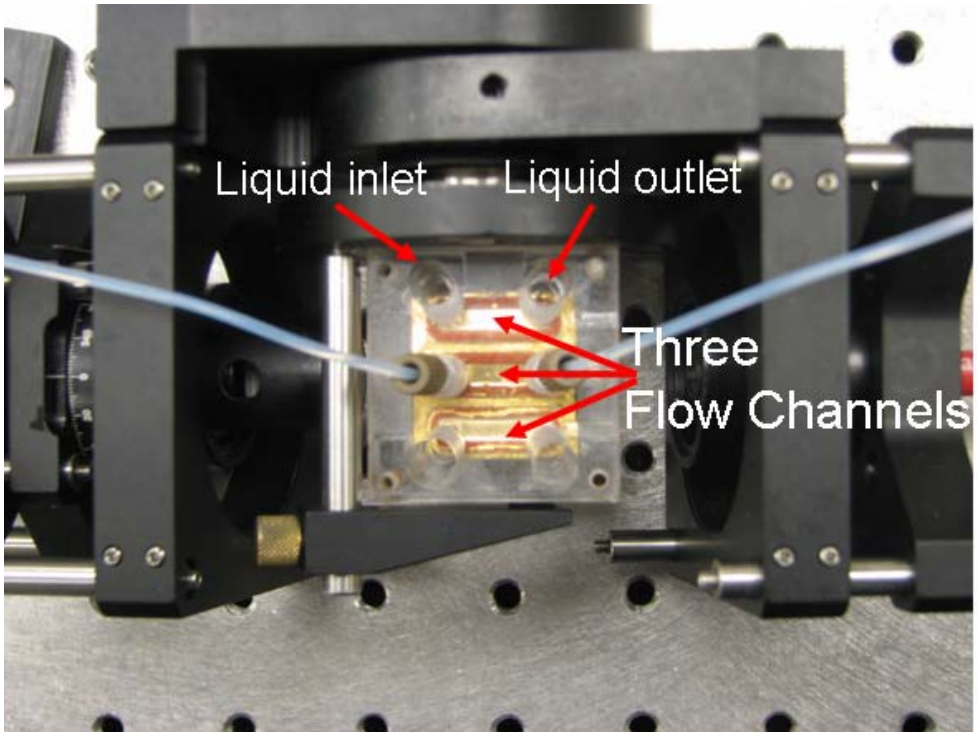

Figure 5.3 Flow cell setup showing three channels

After the flow cell was positioned, the input light was turned off and a dark spectrum was stored to account for background light and detector noise. The dark spectrum was subtracted from all future measurements. The light source was turned on and the TE reflection spectrum was taken as the reference. The polarizer was then turned to produce TM waves. The ratio of the TM to TE reflection spectra formed the basis for the sensing operation.

A custom labview program was executed which tracks the resonance wavelengths of both the long range and the short range surface plasmon modes.

5.3 ODT binding Experiment

5.3.1 Self-Assembled Monolayer (SAM)

Self-Assembled Monolayers (SAMs) are layers which are one molecule thick when deposited on a substrate. Instead of depositing the layers using conventional deposition methods such as Chemical Vapor Deposition, Molecular beam epitaxy or Electron beam evaporation, layers were formed by passing the solution containing the desired substance over the substrate.

A good example of the formation of the SAM was the reaction between alkanethiols with gold [40]. In our case, octadecanthiol was used to form a monolayer. The thickness of the layer formed was 2 nm [40]. Other notable SAM formation reactions include the reaction between alkyl silane molecules on silicon surfaces, e.g. octadecyltrichlorosilane [44].

5.3.2 Molarity Calculation of ODT solutions

For one of the experiments with Ethanol, a 3mM solution of Octadecanethiol was needed. Since there was an accurate way of finding weight than volume, the calculations were preceded by determining the relationship between weight and volume. This relationship helped to determine the accurate molarity.

$$\text{Density} = \frac{\text{Mass}}{\text{Volume}}$$

$$\text{Molarity} = \frac{\text{Number of Moles of a given substance}}{\text{one liter of solution}}$$

$$\text{Molality} = \frac{\text{Number of Moles of a given substance}}{\text{one kilogram of solvent}}$$

Density of water = 1 g/cm^3 = 1000 kg/m^3

Hence, Mass = Volume in the case of water

Therefore finding Molarity, which involves volume and Molality, which involves weight are the same, in the case of water. But it is not the case for ethanol.

Density of Ethanol = 0.789 g/cm^3 = 789 kg/m^3

$\Rightarrow$ Mass = 0.789 * Volume

$$\Rightarrow \text{ Volume (in cm}^3\text{)} = \frac{\text{Mass}}{0.789} = \text{ Volume (in ml)}$$

If the weight of Ethanol is X g,

then Volume of Ethanol = $\frac{X}{0.789} ml = Y\ ml \quad \left(where\ Y = \frac{X}{0.789} \right)$

Molecular weight of ODT = 286.56 g

$$\text{3mM of ODT} = \frac{\text{3 millimoles of ODT}}{\text{one liter of solution}} = \frac{3*10^{-3} * 286.56}{\text{one liter}}$$

$$\Rightarrow \text{ 3mM of ODT} = 0.86 \text{ g/liter}$$

Therefore,

$$\text{3mM of ODT in Y ml of Ethanol (or) 3mM of ODT in X g of Ethanol} = \left(\frac{0.86}{1000} * Y \right)$$

$$= \left(\frac{0.86}{1000} * \frac{X}{0.789} \right) \text{grams}$$

The result above indicates the amount of ODT (in grams) needed to be added to X grams of Ethanol solution to obtain 3mM concentrated solution of ODT in ethanol.

5.3.3 Formation of octadecanthiol monolayer

Octadecanthiol (ODT) is a long chained alkanethiol with the molecular formula

$$CH_3 (CH_2)_{17} SH$$

The sulphur present in the functional group of the molecule has a high affinity toward gold and helps in forming the monolayer. The bonding between ODT and gold is very strong and this monolayer cannot be removed by most solvents. The thickness of the layer formed ranges from 1.9-2.2 nm for incubation time of 10 min [40]. Even higher incubation time does not change the thickness of the layer formed [40].

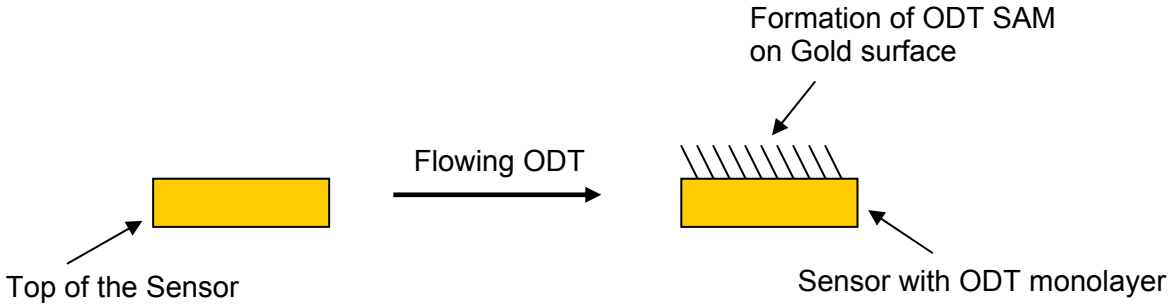

Figure 5.4 Formation of ODT layer on gold

5.3.4 Experimental Steps

The experiment was done by first varying the different background/bulk refractive index solutions and then by passing the ODT solution which forms the surface layer. This was followed by passing the different background index solutions again. The passage of different bulk index solutions before and after the surface layer formation was done to compare the change in bulk sensitivities due to the surface layer formation. The solutions were held at a constant temperature of 24°C in a water bath and the flow rate was held constant at 1ml/min.

The three different solutions used for background index changes are

1. Pure Ethanol
2. Ethanol + 2% Methanol
3. Ethanol + 4% Methanol

Solution	Refractive index	Index difference between 100%Ethanol
Ethanol	1.35931	---
Ethanol + 2% Methanol	1.3586	$7.76*10^{-4}$
Ethanol + 4% Methanol	1.3578	0.0015

Table 5.1 Comparison of Refractive indices between ethanol, 2% and 4% methanol solutions

Table 5.1 indicates the refractive index of ethanol and two different concentrations of methanol used in the experiment and the difference in their index with that of pure ethanol. The refractive index is calculated at 298.15K at the Sodium D line [45].The use of 2% and 4% Methanol instead of higher Methanol percentages is to avoid large index changes which will introduce relatively large nonlinearity in the measurements.

The experiment was performed by flowing the solutions given in the following order:

1. Ethanol
2. Ethanol + 2 % Methanol
3. Ethanol + 4% Methanol
4. Ethanol
5. Ethanol + ODT
6. Ethanol
7. Ethanol + 2% Methanol
8. Ethanol + 4% Methanol
9. Ethanol

Initially before passing any solution, the spectrum with air on top of the sensor looks as in Figure 5.5.

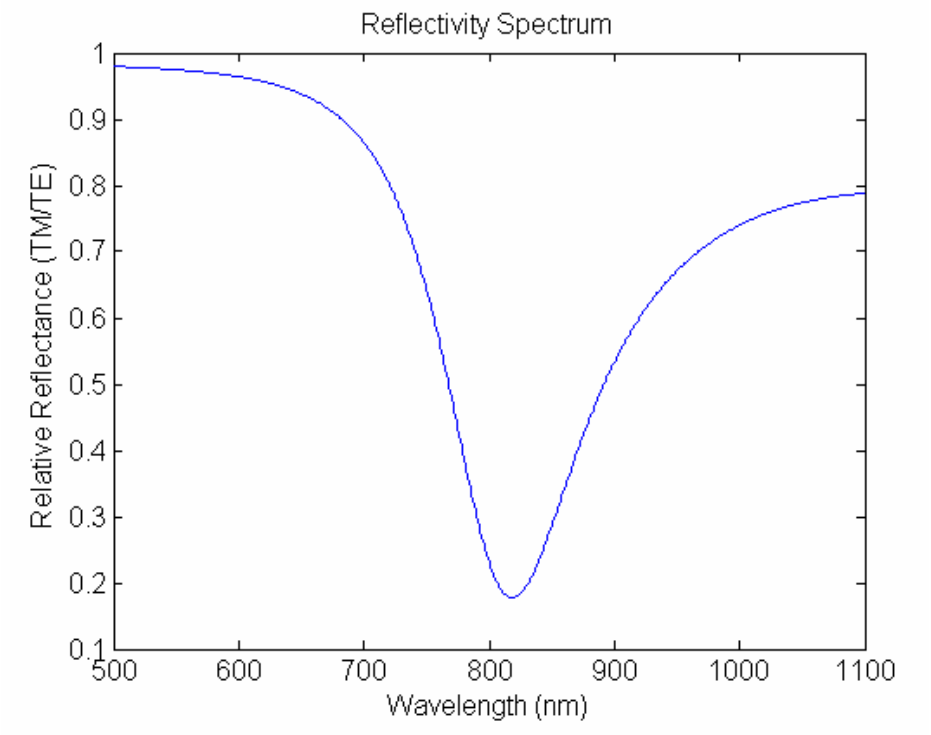

Figure 5.5 Simulated spectrum for θ=69°, gold = 50nm and Teflon=500nm with air on top of the sensor

When a solution, Ethanol in this case, was passed, there is almost an index matching of the two layers lying on either side of the gold layer –ethanol and Teflon-AF or MgF_2. This index matching helps in the coupling of two waves – the long range (LRSP) and short range (SRSP) surface plasmon waves, as indicated in Figure 5.6.

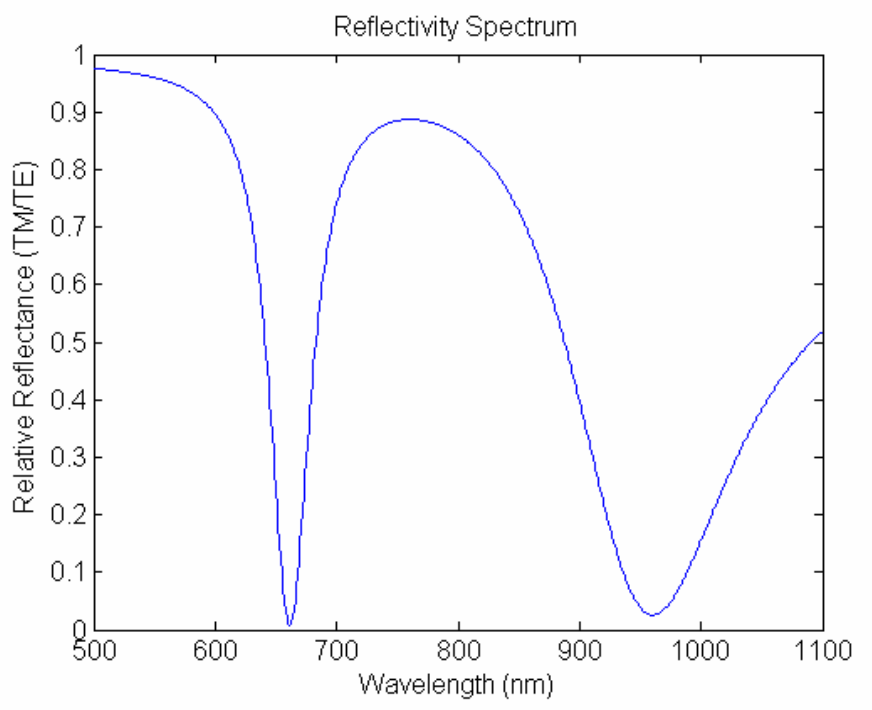

Figure 5.6 Simulated spectrum for θ=69°, gold=50nm and Teflon=500nm with ethanol flowing on top of the sensor. The long-range surface plasmon is excited at shorter wavelengths while the short range surface plasmon is excited at longer wavelengths.

Changes in background refractive indices were achieved by passing the 2% and the 4% methanol solutions, which was followed by passing ethanol once again to get a uniform baseline. The ODT solution was passed to the sensor surface to form a uniform surface layer. The ODT solution was flowed until a SAM is formed, which was indicated by the stabilization of the resonance wavelengths. This stabilization takes about 15-20 minutes and produce a 1.8 to 2.2 nm thick SAM [40].

After the ODT solution was passed, ethanol was once again introduced to get an accurate change in the resonance wavelength due to the binding of the surface layer. The 2% and the 4% methanol and the pure ethanol were passed in that order to demonstrate self-referencing.

5.4 Bio-sensing Experiment

Streptavidin – Biotin bonding is one of the strongest non-covalent biological interactions and hence its one of the most widely used recognition system [46]. Because of the extremely low dissociation constant (K_d) of ~10^{-14} mol/L, this bonding has its widespread Usage in the fields of immunology, biochemistry and cell-biology [47-51].

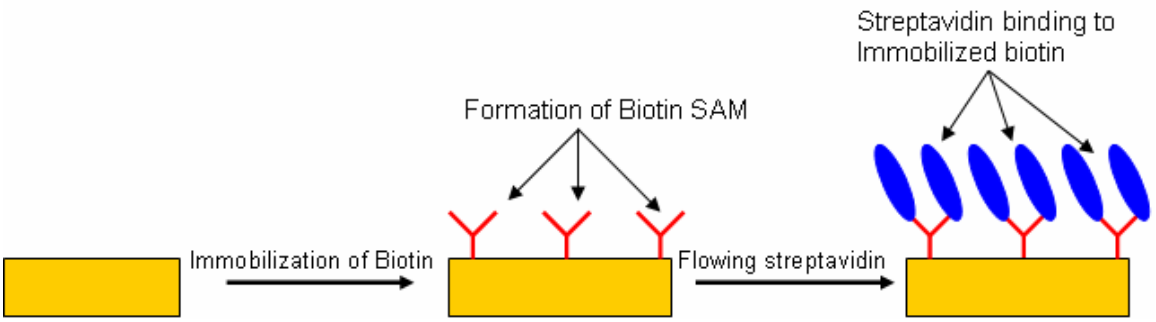

Figure 5.7 Formation of biotin SAM and binding of Streptavidin on the sensor's top surface

Our experiment involved immobilizing biotin on the sensor. The immobilization was performed by incubating the sensor overnight in an ethanol solution containing 10 mM 3-mercaptopropionic acid (3-MPA) and 10 mM 1-propanethiol. After that they were incubated for 4 h in a buffer solution (10 mM Tris, 50 mM NaCl, pH: 8.0) that contained 10 mg -Ethyl-3-(3-dimethylaminopropyl)-carbodiimide (EDC) and 1 mg of DSB-X biotin hydrazide. This sensor after immobilization was used to form a surface layer of streptavidin. Ideally, the formed SAM of streptavidin would be removed by passing another solution of biotin which has relatively stronger affinity toward Streptavidin than the immobilized biotin. But, in the experiments conducted, the second biotin solution could not remove the streptavidin and hence 10mM HCl was used to break the bonding between streptavidin and the immobilized biotin layer.

5.4.1 Using different NaCl concentrations as bulk index solutions

To provide background index changes, solutions of 50mM, 0.15M and 0.25M salt (NaCl) concentrations were used as different bulk index solutions to produce a concentration

change of 0.001 [52]. Solutions were kept at a constant temperature of 24°C and all the solutions except streptavidin and biotin solutions were flowed at a rate of 1ml/min. Streptavidin was flowed at a rate of 0.4ml/min and biotin at a rate of 0.1ml/min. The experiment was done in the following order:

Solution	Refractive index	Index difference between 50mM NaCl
50mM Nacl	1.331	----
0.15M Nacl	1.332	0.001
0.25M Nacl	1.333	0.002

Table 5.2 Comparison of Refractive indices between different salt (NaCl) solutions

To provide background index changes, solutions of 50mM, 0.15M and 0.25M NaCl solutions are used. The experiment was done in the following order:

1. 50mM NaCl
2. 0.15M NaCl
3. 0.25M NaCl
4. 50mM NaCl
5. streptavidin
6. 50mM NaCl
7. 0.15M NaCl
8. 0.25M NaCl
9. 50mM NaCl
10. Biotin
11. 50mM NaCl
12. 0.15M NaCl
13. 0.25M NaCl
14. 50mM NaCl
15. 2M HCl
16. 50mM NaCl

17. 0.15M NaCl
18. 0.25M NaCl
19. 50mM NaCl

As in the first experiment, the background index was changed by flowing solutions with different salt concentrations. Flowing streptavidin solution resulted in the formation of a surface layer due to the binding between the flowed streptavidin and the immobilized biotin. The different bulk index solutions are then passed to demonstrate self-referencing. Flowing a solution of biotin, which has a higher affinity toward streptavidin than the immobilized biotin, was expected to remove the streptavidin. Since the streptavidin did not seem to dissociate (as seen from the absence in resonance wavelength changes), a 2M HCl solution was passed to break the SAM formed. The acid solution breaks the bonds in biotin and streptavidin which helps in removing the surface layer. Different bulk index solutions were passed to determine the effect of surface layer on the bulk sensitivities.

5.4.2 Using different glycerol concentrations as bulk index solutions

This experiment is performed in the same way as the previous bio-sensing experiment with the only difference being the different bulk index solutions. 0%, 0.5% and 1% glycerol solutions having an index difference of $5.65*10^{-4}$ between each solution were employed as the bulk solutions. The buffer solution is prepared with trishydroxy methylaminomethane (or) 2-amino-2-hydroxymethyl-1,3-propanediol, referred to as TRIS. From this buffer solution, the other two bulk index variant solutions were prepared with 0.5% and 1% Glycerol. Solutions were kept at a constant temperature of 24°C and all the solutions except streptavidin and biotin solutions were flowed at a rate of 1ml/min. Streptavidin was flowed at a rate of 0.4ml/min and biotin at a rate of 0.1ml/min.

Solution	Refractive index	Index difference between buffer
buffer	1.3305	----
buffer + 0.5% glycerol	1.331	$5.65*10^{-4}$
buffer + 1% glycerol	1.3316	0.00113

Table 5.3 Comparison of Refractive indices between buffer, 0.5% and 1% glycerol solutions

As in the first bio-sensing experiment, the background index was changed by flowing solutions with different glycerol concentrations. Following the formation of a streptavidin monolayer on the immobilized biotin, different bulk index solutions are flowed once again to demonstrate the self-referencing capability of the sensor. Flowing a solution of biotin, which has a higher affinity toward streptavidin than the immobilized biotin, was expected to remove the streptavidin. Since the streptavidin did not seem to dissociate (as seen from the absence in resonance wavelength changes), a 10mM HCl solution was passed to break the SAM formed. The concentration of the HCl solution was diluted from 2M to 10mM to prevent the silicone tubing, used in the experiment, from getting damaged. The acid solution breaks the bonds in biotin and streptavidin which helps in removing the surface layer. Different bulk index solutions were once again passed for self-referencing.

6 CHAPTER 6 - RESULTS AND DISCUSSION

6.1 ODT experiment

The octadecanethiol (ODT) experiment was conducted with ethanol and different concentrations of methanol. The change in index between each of these different solutions is $7.76*10^{-4}$. ODT is flowed over the sensor for 23 minutes to form a 2nm thick surface layer. The raw wavelength plot of the LRSP and SRSP resonance wavelengths is shown in Figure 6.1.

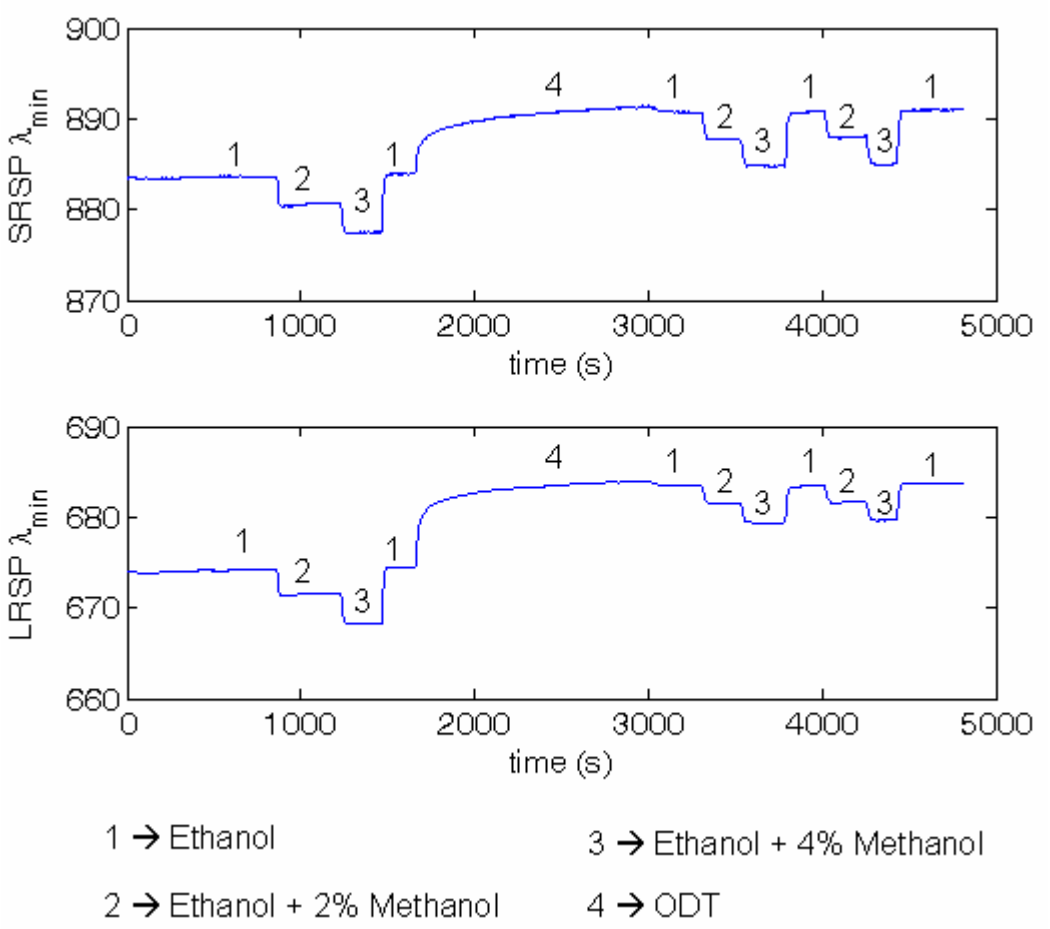

Figure 6.1 Raw wavelength plot of SRSP (top) and LRSP (bottom) vs time for ODT experiment

Analyzing the above data using linear model, we obtain the plots of

a) Change in background index (Δn_B) Vs time

b) Change in surface layer thickness (Δt) Vs time

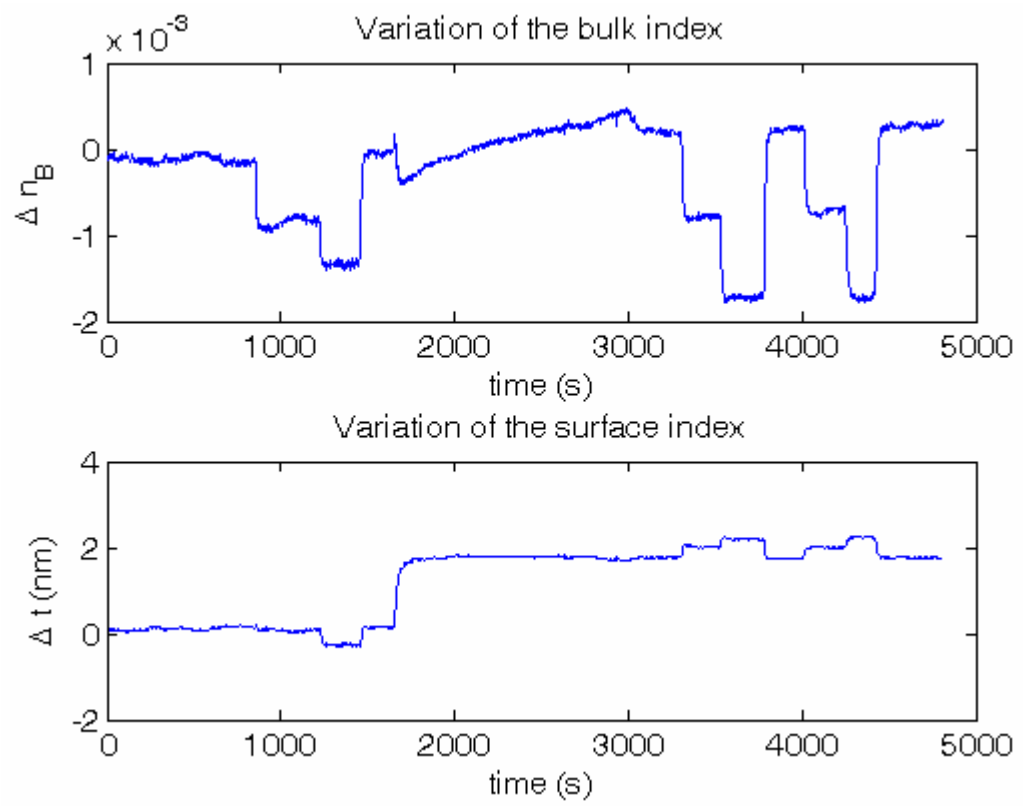

Figure 6.2 Change in bulk index, Δn_B and surface thickness, Δt vs time. Values were calculated from the measured resonance wavelengths shown in Figure 6.1

Figure 6.2 indicates the change in bulk index, Δn_B and surface layer thickness, Δt for the measurements shown in Figure 6.1. The different bulk index solutions were introduced first, followed by the ODT solution. After a surface layer was formed, the different bulk index solutions were flowed twice to find the change in their sensitivity after the formation of a surface layer.

Figure 6.3 shows the variation in bulk index, Δn_B when the different bulk solutions are passed before and after the surface layer formation. The figure also shows the surface layer binding indicated by a sharp rise in the thickness in the bottom plot of Figure 6.3 when the ODT solution is flowed. From these two plots, we can confirm the self-referencing capability of the sensor.

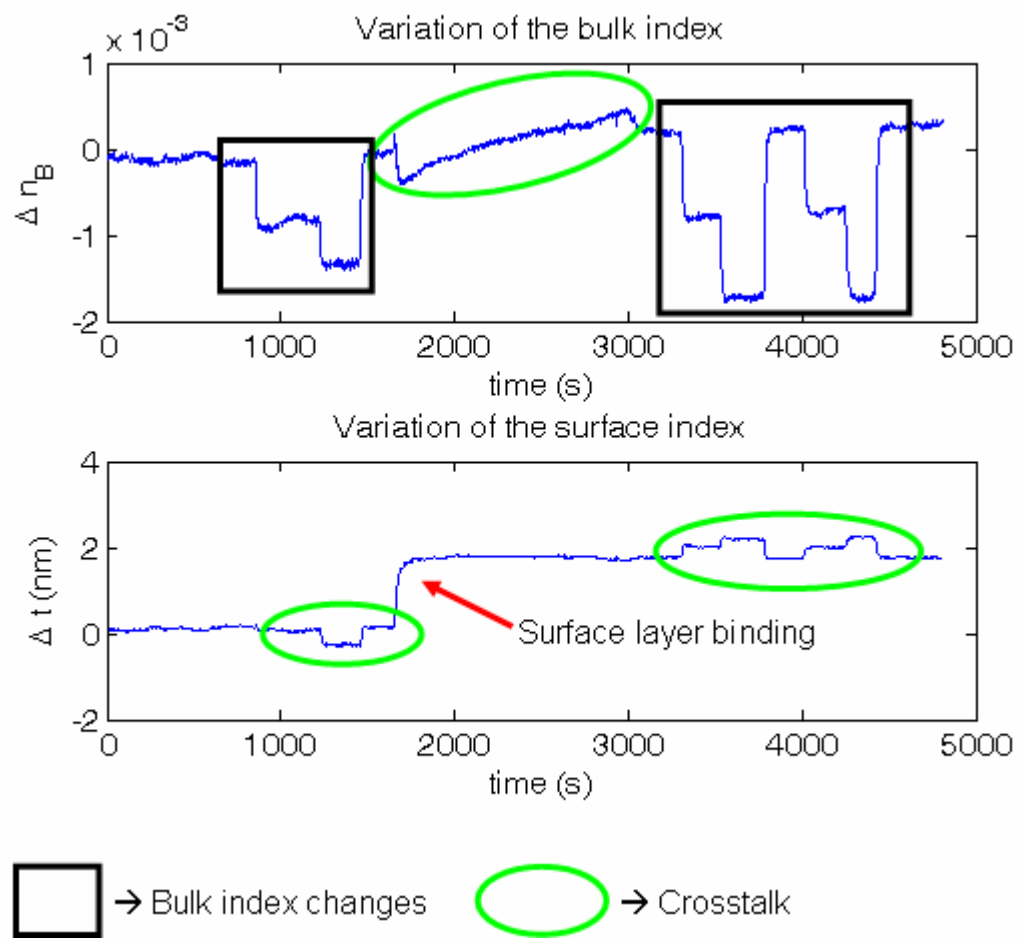

Figure 6.3 Change in bulk index, Δn_B and surface thickness, Δt Vs time with the changes highlighted

We can also see a slight change in both Δn_B and Δt during the formation of the surface layer and change in bulk index respectively. These unwanted changes are referred as crosstalk, which is defined as a change in Δn_B affecting Δt or vice-versa. These changes are illustrated in Figure 6.3. This crosstalk is made worse due to the similar sensitivities of both the modes to bulk and surface index changes for the particular sensor used in this experiment.

6.2 Biosensing experiment

The biosensing experiment was performed using three different salt concentration solutions, 50mM, 0.15M and 0.25M NaCl solutions, having a index difference of 0.001 between each solutions [52]. The surface layer is formed by flowing streptavidin which binds onto the immobilized biotin and forms a surface layer. After the formation of the surface layer, three different bulk index solutions are flowed to check the self-referencing capability of the sensor. The formed surface layer is then removed. Initially, a second set of biotin solution, having higher affinity to streptavidin than the immobilized biotin was employed to remove the surface layer. Failure of this method led to the usage of 2M HCl solution to break the bond between streptavidin and biotin and remove the surface layer. After the removal of the layer, the above steps are repeated twice to check for the sensor's sensitivity.

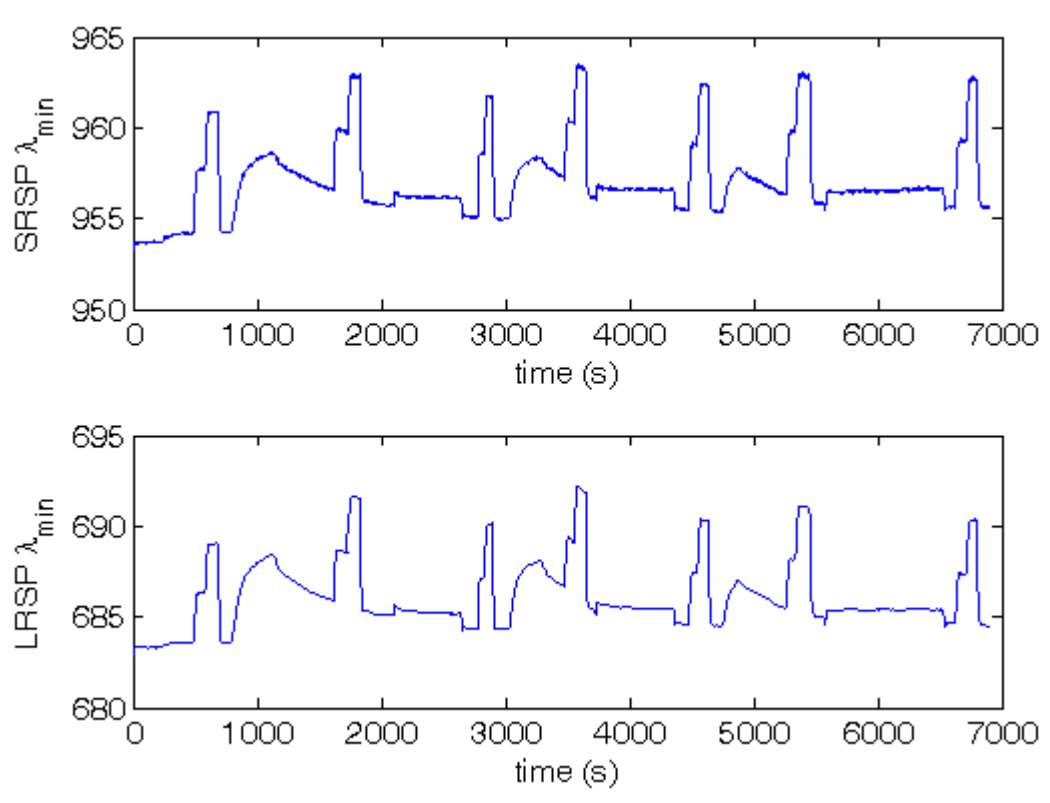

Figure 6.4 Raw wavelength plot of SRSP (top) and LRSP (bottom) vs time for the bio-sensing experiment

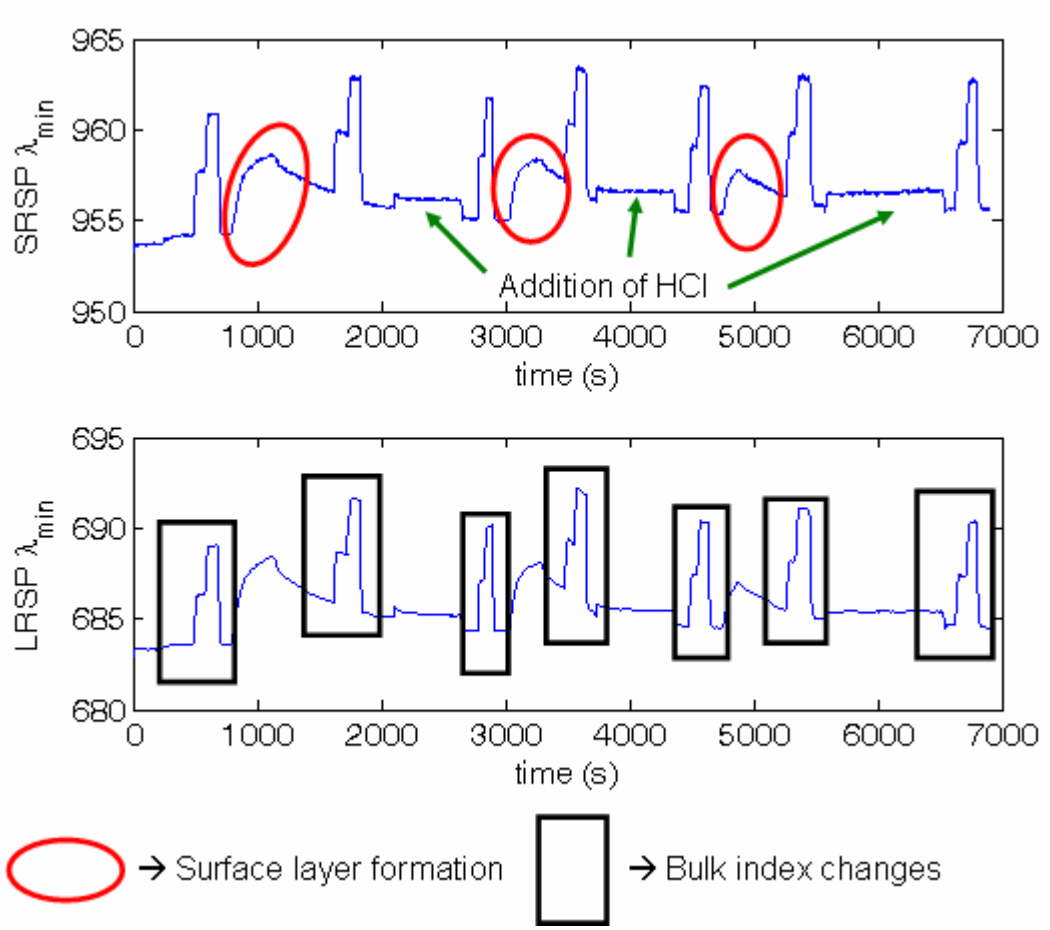

Figure 6.5 Raw wavelength plot of SRSP (top) and LRSP (bottom) vs time for the bio-sensing experiment with the bulk changes and surface layer formation indicated

The raw wavelength data plot with the bulk changes and the formation of the surface layer is shown in Figure 6.5. The binding and the unbinding of the surface layer is shown in Figure 6.6. Also shown in the top plot of Figure 6.6 is the variation in bulk index.

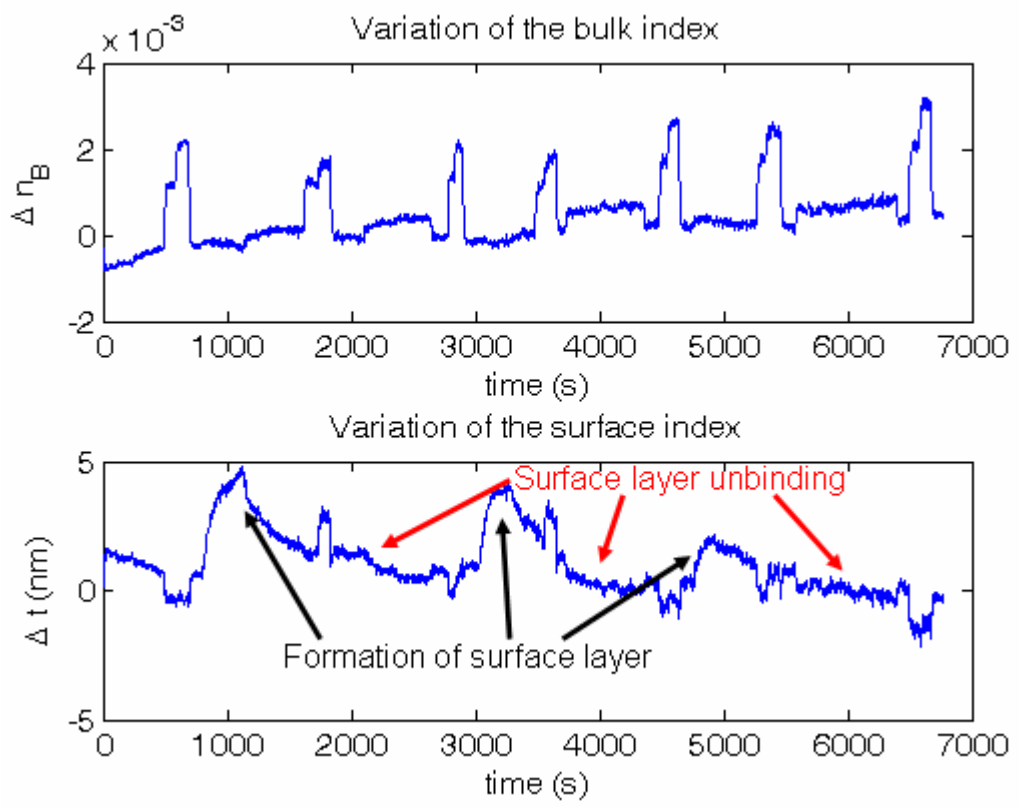

Figure 6.6 Change in bulk index, Δn_B and surface thickness, Δt Vs time

6.3 Problems encountered

Several experimental problems occurred during the course of this thesis. Most of them were rectified but some of them still remain.

6.3.1 Drift

The resonance wavelengths of either or both modes seem to drift during some of the experiments. This drift is not constrained to just one mode. To eliminate other variables, experiment was conducted at constant temperature with only ethanol flowing on top of the sensor for 40 minutes. Two sets of experiments were carried out and their raw wavelength plot is shown in Figure 6.7 and Figure 6.8. Although both the experiments were carried out with the same sensor and all other factors being same, there seemed to be a disparity in the drift. In Experiment 1, drift in LRSP was ~0.2nm and SRSP ~1nm whereas in experiment2, LRSP had a drift of ~1nm and SRSP ~1.5nm.

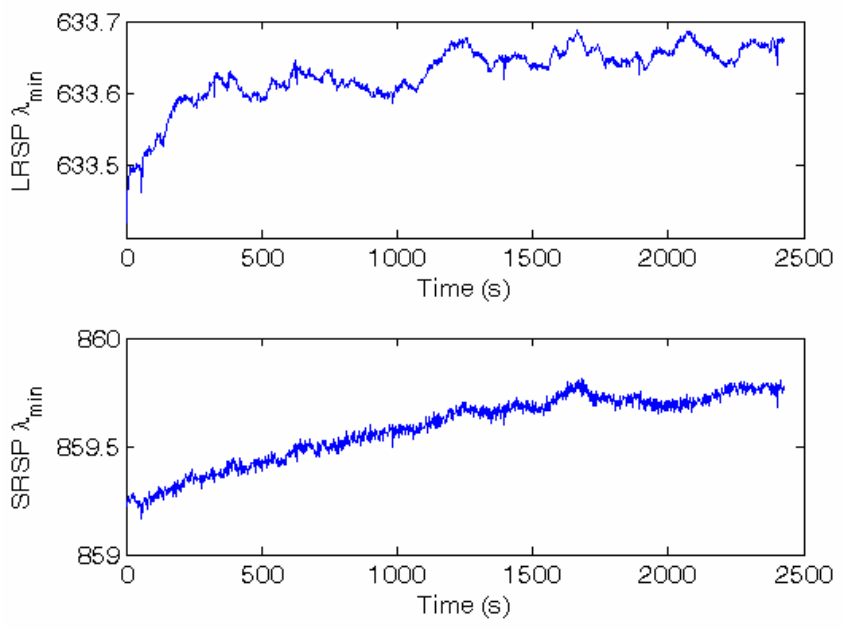

Figure 6.7 Ethanol only experiment-1

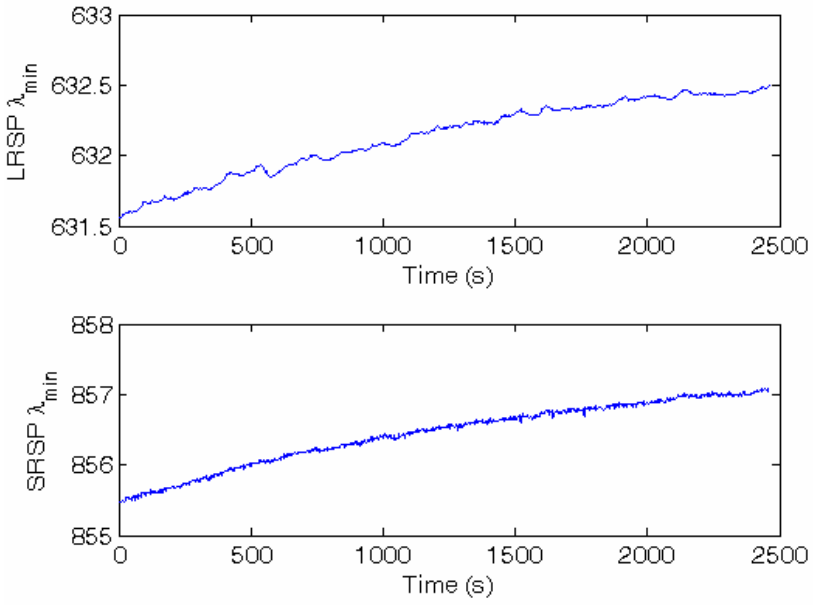

Figure 6.8 Ethanol only experiment-2

The possible reasons for drift are addressed in the following two sections.

6.3.1.1 Thermal instability

Though the experiments were carried out at constant temperature by employing a water bath, the solutions might not be at the same temperature, which can lead to drift in resonance wavelengths.

The thermal co-efficient of water at 600nm is 10^{-4} RIU/°C and that of BK7 prism is $3*10^{-6}$ RIU/°C [53].

Assuming sensitivity = 1000 nm/RIU,

Change in resonance wavelength due to change in temperature $= 10^{-4} \frac{RIU}{°C} * 1000 \frac{nm}{RIU}$

$$= 10^{-1} \frac{nm}{°C} = 0.1\ nm/°C$$

We have a change of 0.1nm for one degree change in temperature.

Therefore, for 0.2nm, 1nm and 1.5nm drift in resonance wavelength, there has to be 2°C, 10°C and 15°C change in temperature, which is highly improbable.

Assuming sensitivity to be higher i.e. 5000nm/RIU, the corresponding change in resonance wavelength for a change in temperature = 0.5nm/°C

Hence the changes for 0.2nm, 1nm and 1.5nm drifts, the corresponding change in temperature has to be 0.4°C, 2°C and 3°C respectively. A change of 0.4°C in solution's temperature cannot be strictly ruled out, but we have to consider the fact that higher sensitivities were obtained for SRSP and this 0.2nm change in detected in LRSP cannot use higher sensitivity model to describe LRSP drifts.

There can be a consideration that drift in λ can be due to the change in temperature inside the prism. Applying the same calculations as above using the prism's coefficient, we get

a) For lower sensitivities of the order of 1000nm/RIU,

Change in λ for a change in temperature = 0.003 nm/°C

b) For higher sensitivities of the order of 5000nm/RIU

Change in λ for a change in temperature = 0.015nm/°C

These two changes are lower than the changes for that of water, implying the higher change in prism's temperature of the order of 65-330°C, which is not possible.

Hence thermal instability cannot be the reason for drift in resonance wavelength.

6.3.1.2 Increase in Teflon thickness

During some of our experiments, the spectrum changed over the course of the experiment. We observed an increase in minimum reflectivity and a broadening of the resonance dip. This could be explained by an increase in thickness of the Teflon layer which may be the result by swelling. This increase in Teflon thickness can be considered as a reason for drift in resonance wavelength; however, this effect was not consistent enough to warrant a closer look into this effect.

6.3.2 Air-bubbles

Air bubbles affected the experiment much more than any other factor. A new flow cell was designed and both the input and the output port had Teflon tape on them to produce a tight seal with the flow cell. But in spite of all these efforts, there were air-bubbles during the course of some experiments which could not be explained.

6.3.3 Cross-sensitivity

This problem deals mainly with the design of the sensor. When the sensor is designed to operate in a region where the cross-sensitivity is high, in other words, the response of both the modes are same for bulk index change and surface layer index change, then the task of differentiating the two effects becomes difficult. As a result, the self-referencing sensor is similar in operation to a conventional SPR sensor. Our general design procedure to maximize sensitivity and minimize reflectivity does not guarantee low cross-sensitivity, and this should be accounted for in the future.

6.3.4 Lack of agreement between theoretical and observed sensitivities

The following is our hypothesis for the lack of agreement between theoretical and observed sensitivities. The following is our hypothesis for the lack of agreement between theoretical and observed sensitivities. In the ODT experiment described in this work, gold was deposited using e-beam evaporation which caused the Teflon layer to shrink and its index to increase by about 0.04. As a result, the field profiles are no longer the same as in Figure 2.11. The increased index causes the LRSP's field profile to be more concentrated in the solution and the SRSP's field more concentrated in the buffer layer. This effect will increase the LRSP's sensitivity and decrease the SRSP's sensitivity compared to the theoretical predictions, and this is consistent with our experimental observations.

7 CHAPTER 7 - CONCLUSION

A dual-mode SPR sensor was optimized for sensitivity and dual mode sensors were fabricated according to the optimization results. Resonance wavelengths were accurately predicted; however, sensitivities of the two modes were in error by as much as 25%. Because of their different responses of the LRSP and SRSP to bulk index changes and surface binding changes, we were able to differentiate both effects.

From the optimization data, the design parameters for the fabrication of the sensor were not rigid. The simulations gave us design boundaries to work with which greatly helped in the fabrication process, as getting the layers exactly to their required thickness is a nearly impossible job. The optimization of the sensor gave us a leeway in the thickness of the buffer and metal layers, so that an operating range of ±5-10nm for gold (metal) and ±50-80nm for Teflon/magnesium fluoride (buffer) was obtained.

Several areas for further investigation arose during the course of this work:

a) The optimization of the sensor was done with major emphasis on the sensitivities of the modes involved. When the sensitivities were constant over the entire design values, reflectivity and resonance wavelengths of the two modes were taken into account to determine the optimal operation range. Extending this optimization to include lower cross-sensitivity is a major task needed to be taken. Ultimately, optimization based on the limit of detection (LOD) for the target analyte will be the preferred technique.

b) For real-world biosensing both bulk index changes and non-specific binding can interfere with effective sensing. To compensate for the effects of non-specific binding in addition to bulk index changes, the sensor could be redesigned to couple to three modes in the same region.

c) Instead of operating using wavelength interrogation, angular interrogation can be employed. Since the wavelength remains constant in angular interrogation, the two

modes are excited at the same wavelength. This can eliminate the need for a broad bandwidth spectrometer/detector. In addition, we expect angular interrogation to further differentiate the response of the LRSP and SRSP modes and thus reduce cross sensitivity.

REFERENCES

[1] I. Pockrand, J. D. Swalen, J. G. Gordon, and M. R. Philpott, "Surface-Plasmon Spectroscopy of Organic Monolayer Assemblies," *Surface Science,* vol. 74, pp. 237-244, 1978.

[2] J. G. Gordon and S. Ernst, "Surface-Plasmons as a Probe of the Electrochemical Interface," *Surface Science,* vol. 101, pp. 499-506, 1980.

[3] C. Nylander, B. Liedberg, and T. Lind, "Gas-Detection by Means of Surface-Plasmon Resonance," *Sensors and Actuators,* vol. 3, pp. 79-88, 1982.

[4] B. Liedberg, C. Nylander, and I. Lundstrom, "Surface-Plasmon Resonance for Gas-Detection and Biosensing," *Sensors and Actuators,* vol. 4, pp. 299-304, 1983.

[5] B. Liedberg, C. Nylander, and I. Lundstrom, "Biosensing with Surface-Plasmon Resonance - How It All Started," *Biosensors & Bioelectronics,* vol. 10, pp. R1-R9, Fal 1995.

[6] J. Homola, S. S. Yee, and G. Gauglitz, "Surface plasmon resonance sensors: review," *Sensors and Actuators B-Chemical,* vol. 54, pp. 3-15, Jan 1999.

[7] J. Dostalek, H. Vaisocherova, and J. Homola, "Multichannel surface plasmon resonance biosensor with wavelength division multiplexing," *Sensors and Actuators B (Chemical),* vol. 108, pp. 758-64, 2005.

[8] J. Homola, J. Dostalek, and J. Ctyroky, "A novel approach to surface plasmon resonance multichannel sensing," Yokohama, Japan, 2001, pp. 86-9.

[9] G. G. Nenninger, J. B. Clendenning, C. E. Furlong, and S. S. Yee, "Reference-compensated biosensing using a dual-channel surface plasmon resonance sensor system based on a planar lightpipe configuration," *Sensors and Actuators B-Chemical,* vol. 51, pp. 38-45, Aug 1998.

[10] J. Homola, H. B. Lu, and S. S. Yee, "Dual-channel surface plasmon resonance sensor with spectral discrimination of sensing channels using dielectric overlayer," *Electronics Letters,* vol. 35, pp. 1105-6, 1999.

[11] J. Homola, H. B. Lu, G. G. Nenninger, J. Dostalek, and S. S. Yee, "A novel multichannel surface plasmon resonance biosensor," Basel, 2001, pp. 403-410.

[12] S. Lofas, M. Malmqvist, I. Ronnberg, E. Stenberg, B. Liedberg, and I. Lundstrom, "Bioanalysis with Surface-Plasmon Resonance," *Sensors and Actuators B-Chemical,* vol. 5, pp. 79-84, Aug-Dec 1991.

[13] C. E. H. Berger, T. A. M. Beumer, R. P. H. Kooyman, and J. Greve, "Surface plasmon resonance multisensing," *Analytical Chemistry,* vol. 70, pp. 703-706, Feb 1998.

[14] R. Slavik, J. Homola, and H. Vaisocherova, "Advanced biosensing using simultaneous excitation of short and long range surface plasmons," *Measurement Science and Technology,* vol. 17, pp. 932-938, 2006.

[15] R. Slavik and J. Homola, "Simultaneous excitation of long and short range surface plasmons in an asymmetric structure," *Optics Communications,* vol. 259, pp. 507-12, 2006.

[16] http://www.protein.iastate.edu/seminars/BIACore/TechnologyNotes/TechnologyNote1.pdf.

[17] C. Mouvet, R. D. Harris, C. Maciag, B. J. Luff, J. S. Wilkinson, J. Piehler, A. Brecht, G. Gauglitz, R. Abuknesha, and G. Ismail, "Determination of simazine in water samples by waveguide surface plasmon resonance," *Analytica Chimica Acta,* vol. 338, pp. 109-117, Feb 1997.
[18] T. T. Goodrich, H. J. Lee, and R. M. Corn, "Direct detection of genomic DNA by enzymatically amplified SPR imaging measurements of RNA microarrays," *Journal of the American Chemical Society,* vol. 126, pp. 4086-4087, Apr 2004.
[19] J. Dostalek, J. Ctyroky, J. Homola, E. Brynda, M. Skalsky, P. Nekvindova, J. Spirkova, J. Skvor, and J. Schrofel, "Surface plasmon resonance biosensor based on integrated optical waveguide," *Sensors and Actuators B-Chemical,* vol. 76, pp. 8-12, Jun 2001.
[20] J. Homola, J. Dostalek, S. F. Chen, A. Rasooly, S. Y. Jiang, and S. S. Yee, "Spectral surface plasmon resonance biosensor for detection of staphylococcal enterotoxin B in milk," *International Journal of Food Microbiology,* vol. 75, pp. 61-69, May 2002.
[21] V. Koubova, E. Brynda, L. Karasova, J. Skvor, J. Homola, J. Dostalek, P. Tobiska, and J. Rosicky, "Detection of foodborne pathogens using surface plasmon resonance biosensors," *Sensors and Actuators B-Chemical,* vol. 74, pp. 100-105, Apr 2001.
[22] J. Homola, "Present and future of surface plasmon resonance biosensors," *Analytical and Bioanalytical Chemistry,* vol. 377, pp. 528-539, Oct 2003.
[23] G. Margheri, A. Mannoni, and F. Quercioli, "A new high-resolution displacement sensor based on surface plasmon resonance," Besancon, France, 1996, pp. 211-20.
[24] J. K. Schaller, R. Czepluch, and C. G. Stojanoff, "Plasmon spectroscopy for high resolution angular measurements," Munich, Germany, 1997, pp. 476-86.
[25] M. N. Weiss, R. Srivastava, and H. Groger, "Experimental investigation of a surface plasmon-based integrated-optic humidity sensor," *Electronics Letters,* vol. 32, pp. 842-843, Apr 1996.
[26] J. Homola, G. Schwotzer, H. Lehmann, R. Willsch, W. Ecke, and H. Bartelt, "A new optical fiber sensor for humidity measurement," Prague, Czech Republic, 1995, pp. 245-8.
[27] B. Chadwick and M. Gal, "An optical temperature sensor using surface plasmons," *Japanese Journal of Applied Physics, Part 1 (Regular Papers & Short Notes),* vol. 32, pp. 2716-17, 1993.
[28] Kretschm.E and H. Raether, "Radiative Decay of Non Radiative Surface Plasmons Excited by Light," *Zeitschrift Fur Naturforschung Part a-Astrophysik Physik Und Physikalische Chemie,* vol. A 23, pp. 2135-&, 1968.
[29] A. Otto, "Excitation of Nonradiative Surface Plasma Waves in Silver by Method of Frustrated Total Reflection," *Zeitschrift Fur Physik,* vol. 216, pp. 398-&, 1968.
[30] G. S. Agarwal, "New Method in Theory of Surface Polaritons," *Physical Review B,* vol. 8, pp. 4768-4779, 1973.
[31] A. Otto, "A New Method for Exciting Nonradiant Plasma Surface Vibration," *Physica Status Solidi,* vol. 26, pp. K99-&, 1968.

[32] J. D. Swalen, "Optical properties of Langmuir-Blodgett films," *Journal of Molecular Electronics,* vol. 2, pp. 155-81, 1986.
[33] H. Raether, "Surface-Plasmons on Smooth and Rough Surfaces and on Gratings," *Springer Tracts in Modern Physics,* vol. 111, pp. 1-133, 1988.
[34] A. D. Boardman, "Electromagnetic Surface Modes," 1982.
[35] M. A. Ordal, L. L. Long, R. J. Bell, S. E. Bell, R. R. Bell, R. W. Alexander, and C. A. Ward, "Optical-Properties of the Metals Al, Co, Cu, Au, Fe, Pb, Ni, Pd, Pt, Ag, Ti, and W in the Infrared and Far Infrared," *Applied Optics,* vol. 22, pp. 1099-1119, 1983.
[36] J. H. Lowry, J. S. Mendlowitz, and N. S. Subramanian, "Optical Characteristics of Teflon Af(R) Fluoroplastic Materials," *Optical Engineering,* vol. 31, pp. 1982-1985, Sep 1992.
[37] G. G. Nenninger, M. Piliarik, and J. Homola, "Data analysis for optical sensors based on spectroscopy of surface plasmons," *Measurement Science & Technology,* vol. 13, pp. 2038-2046, Dec 2002.
[38] J. Ctyroky, J. Homola, P. V. Lambeck, S. Musa, H. Hoekstra, R. D. Harris, J. S. Wilkinson, B. Usievich, and N. M. Lyndin, "Theory and modelling of optical waveguide sensors utilising surface plasmon resonance," *Sensors and Actuators B-Chemical,* vol. 54, pp. 66-73, Jan 1999.
[39] J. J. Burke, G. I. Stegeman, and T. Tamir, "Surface-Polariton-Like Waves Guided by Thin, Lossy Metal-Films," *Physical Review B,* vol. 33, pp. 5186-5201, Apr 1986.
[40] C. D. Bain, E. B. Troughton, Y. T. Tao, J. Evall, G. M. Whitesides, and R. G. Nuzzo, "Formation of Monolayer Films by the Spontaneous Assembly of Organic Thiols from Solution onto Gold," *Journal of the American Chemical Society,* vol. 111, pp. 321-335, Jan 1989.
[41] J. Chilwell and I. Hodgkinson, "Thin-Films Field-Transfer Matrix-Theory of Planar Multilayer Waveguides and Reflection from Prism-Loaded Waveguides," *Journal of the Optical Society of America a-Optics Image Science and Vision,* vol. 1, pp. 742-753, 1984.
[42] R. S. Quimby, "Photonics and Lasers: An Introduction," pp. 12-14, 2006.
[43] L. A. Coldren and S. W. Corzine, "Diode Lasers and Photonic Integrated Circuits," pp. 71-77, 1995.
[44] S. Y. Song, S. L. Ren, J. Q. Wang, S. R. Yang, and J. Y. Zhang, "Preparation and tribological study of a peptide-containing alkylsiloxane monolayer on silicon," *Langmuir,* vol. 22, pp. 6010-6015, Jul 2006.
[45] L. Albuquerque, C. Ventura, and R. Goncalves, "Refractive indices, densities, and excess properties for binary mixtures containing methanol, ethanol, 1,2-ethanediol, and 2-methoxyethanol," *Journal of Chemical and Engineering Data,* vol. 41, pp. 685-688, Jul-Aug 1996.
[46] G. T. Hermanson, "Bioconjugate Techniques," pp. 570-580, 1996.
[47] M. R. Bonen, A. A. Garcia, and S. A. Hoffman, "A comparison of silver ion to streptavidin coated microplates," *Journal of Microbiological Methods,* vol. 44, pp. 113-120, Mar 2001.
[48] S. Y. Kim and M. J. Choi, "Preparation and characterization of digoxin antibody and its application to immunoassays: comparison of performance characteristics

between enzyme immunoassay and immunostrip test," *Microchemical Journal,* vol. 65, pp. 209-219, Oct 2000.
[49] G. Houen and K. Hansen, "Interference of sugars with the binding of biotin to streptavidin and avidin," *Journal of Immunological Methods,* vol. 210, pp. 115-123, Dec 1997.
[50] I. Cordiano, A. Steffan, M. L. Randi, P. Pradella, A. Girolami, and F. Fabris, "Biotin-Avidin Immobilization of Platelet Glycoproteins (Baipg) - a New Capture Assay for the Detection of Antiplatetlet Antibodies," *Journal of Immunological Methods,* vol. 178, pp. 121-130, Jan 1995.
[51] S. Y. Kim, Y. A. Jo, J. Choi, and M. J. Choi, "Characterization of s-triazine antibodies and comparison of enzyme immunoassay and biotin-avidin enzyme immunoassay for the determination of s-triazine," *Microchemical Journal,* vol. 68, pp. 163-172, Mar 2001.
[52] G. J. Daviero, P. J. W. Roberts, and K. Maile, "Refractive index matching in large-scale stratified experiments," *Experiments in Fluids,* vol. 31, pp. 119-126, Aug 2001.
[53] M. J. Weber, "Handbook of Optical Materials," 2002.

VITA

The author was born in Madurai, Tamil Nadu, India on December 4, 1982. In 2000, he completed his under-graduation in India at Bharathidasan University, in the department of Electronics and Communication Engineering. In August 2004, he joined Louisiana State University, before transferring to the University of Kentucky in January 2005 to continue his Master's degree in Electrical Engineering. He was awarded the Kentucky Graduate scholarship for the entire duration of his Master's program. He worked as a Research Assistant from January 2006 to March 2007 at the Center for Nanoscale Science and Engineering (CeNSE).